Department of Signal Processing and Acoustics

Spectral and Power Efficient Modulation Methods in Presence of Nonlinear Distortions

Markku Kiviranta

Aalto University

DOCTORAL DISSERTATIONS

Aalto University publication series
DOCTORAL DISSERTATIONS 56/2017
VTT SCIENCE 149

Spectral and Power Efficient Modulation Methods in Presence of Nonlinear Distortions

Markku Kiviranta

A doctoral dissertation completed for the degree of Doctor of Science (Technology) to be defended, with the permission of the Aalto University School of Electrical Engineering, at a public examination held at the lecture hall TUAS/AS1 of the school on 1st June 2017 at 12.

Aalto University
School of Electrical Engineering
Department of Signal Processing and Acoustics

Supervising professors
Professor Risto Wichman, Aalto University, Finland

Thesis advisor
Research Professor Aarne Mämmelä, VTT Technical Research Centre of Finland

Preliminary examiners
Professor Hanna Bogucka, Poznan University of Technology, Poland
Professor Giorgio M. Vitetta, University of Modena and Reggio Emilia, Italy

Opponent
Professor Markku Renfors, Tampere University of Technology, Finland

Aalto University publication series
DOCTORAL DISSERTATIONS 56/2017

VTT SCIENCE 149

ISBN 978-952-60-7356-9 (printed)
ISBN 978-952-60-7355-2 (pdf)
ISSN-L 1799-4934
ISSN 1799-4934 (printed)
ISSN 1799-4942 (pdf)
http://urn.fi/URN:ISBN:978-952-60-7355-2

ISBN 978-951-38-8526-7 (printed)
ISBN 978-951-38-8525-0 (pdf)
ISSN-L 2242-119X
ISSN 2242-119X (printed)
ISSN 2242-1203 (pdf)
http://urn.fi/URN:ISBN:978-951-38-8525-0

Unigrafia Oy
Helsinki 2017

Finland

NORDIC ECOLABEL
441 697
Printed matter

Aalto University

Abstract

Aalto University, P.O. Box 11000, FI-00076 Aalto www.aalto.fi

Author
Markku Kiviranta

Name of the doctoral dissertation
Spectral and Power Efficient Modulation Methods in Presence of Nonlinear Distortions

Publisher School of Electrical Engineering

Unit Department of Signal Processing and Acoustics

Series Aalto University publication series DOCTORAL DISSERTATIONS 56/2017

Field of research Digital signal processing

Manuscript submitted 22 November 2016 **Date of the defence** 1 June 2017

Permission to publish granted (date) 16 March 2017 **Language** English

☐ **Monograph** ☒ **Article dissertation** ☐ **Essay dissertation**

Abstract

This thesis presents a state-of-the-art review and brings new contributions to the waveform design for 5G systems in the presence of analog nonlinearities. A system model for the typical analog impairments at each stage of the transmitter and the receiver with a channel is first presented. The highlighted nonlinearities are power amplifier (PA), phase noise, and DC offset.

In this thesis, the further development of the orthogonal frequency division multiplexing (OFDM) is considered since the evolutionary approach from the 4G to the 5G is assumed to be more mature for technology demonstrations. In particular, the constant envelope OFDM (CE-OFDM) where phase modulation creates a constant envelope is studied, and the results indicate that CE-OFDM has an advantage compared to OFDM when the PA efficiency is taken into account in the simulations. Since the phase noise transforms just into an additive noise term after the phase detector, CE-OFDM is very resistant to phase noise unlike OFDM. CE-OFDM can be seen as an interesting candidate for the 5G scenarios when the power efficiency is a more important parameter than the spectral efficiency.

This thesis presents also new findings and results for the constant envelope tamed frequency modulation (TFM) and trellis-coded modulation (TCM) that is a traditional combined coding and modulation technique for spectral and power limited systems. In phase or frequency modulation spectral spreading and detection performance are controlled using a modulation index. In a simple analog implementation of TFM, the modulation index deviates during the transmission and generates time varying phase jitter. In this work a modulation index estimator in conjunction with per-survivor processing (PSP) carrier phase estimation is presented for the TFM which has also very small spectral out-of-band radiation compared to other known CPM methods. A novel scheme based on multiple TCM, PSP and Reed–Solomon (RS) coding is proposed and shown to prevent the trellis-code to become a catastrophic code in the presence of phase noise. In general, the TCM and CPM modulations can complement the future adaptive OFDM based 5G systems.

Keywords continuous phase modulation (CPM), constant envelope orthogonal frequency division multiplexing (CE-OFDM), nonlinearity, tamed frequency modulation (TFM), trellis-coded modulation (TCM)

ISBN (printed) 978-952-60-7356-9 **ISBN (pdf)** 978-952-60-7355-2

ISSN-L 1799-4934 **ISSN (printed)** 1799-4934 **ISSN (pdf)** 1799-4942

Location of publisher Helsinki **Location of printing** Helsinki **Year** 2017

Pages 122 **urn** http://urn.fi/URN:ISBN:978-952-60-7355-2

Aalto-yliopisto

Tiivistelmä

Aalto-yliopisto, PL 11000, 00076 Aalto www.aalto.fi

Tekijä
Markku Kiviranta

Väitöskirjan nimi
Spektri- ja energiatehokkaat modulaatiomenetelmät epälineaaristen vääristymien läsnä ollessa

Julkaisija Sähkötekniikan korkeakoulu

Yksikkö Signaalikäsittelyn ja akustiikan laitos

Sarja Aalto University publication series DOCTORAL DISSERTATIONS 56/2017

Tutkimusala Signaalinkäsittely

Käsikirjoituksen pvm 22.11.2016 **Väitöspäivä** 01.06.2017

Julkaisuluvan myöntämispäivä 16.03.2017 **Kieli** Englanti

☐ **Monografia** ☒ **Artikkeliväitöskirja** ☐ **Esseeväitöskirja**

Tiivistelmä

Väitöskirja sisältää kirjallisuuskatsauksen ja esittää uusia tuloksia tulevaisuuden 5G-järjestelmien aaltomuodon suunnitteluun analogia osien aiheuttamien vääristymien läsnä ollessa. Tyypillisille epälineaarisuuksille lähettimessä ja vastaanottimessa esitetään järjestelmämalli, joka sisältää myös kanavan. Erityistä huomiota kiinnitetään epälineaariseen tehovahvistimeen, vaihekohinaan ja DC offset.

Väitöskirjassa keskitytään 4G-järjestelmissä käytettävän OFDM (orthogonal frequency division multiplexing) monikantoaalto tekniikan jatkokehittämiseen, koska 4G-evoluution oletetaan olevan riittävän kypsä tulevaisuuden 5G-järjestelmien demonstroinneille. Erityistä huomiota kiinnitetään vaihemodulaation avulla saavutettavaan vakioverhokäyräiseen OFDM-modulaatioon. Suorituskyky tulokset osoittavat, että vakioverhokäyräisellä OFDM-järjestelmällä on etu vastaavaan OFDM-järjestelmään nähden, kun lähettimen tehovahvistimen hyötysuhde otetaan huomioon simuloinneissa. Vakioverhokäyräinen OFDM sietää myös paremmin vaihekohinaa, koska vaihekohina muuttuu summa termiksi vaiheilmaisen lähdössä. Vakioverhokäyräinen OFDM on mielenkiintoinen vaihtoehto 5G-järjestelmille, kun energiatehokkuus on tärkeämpi kriteeri kuin spektrin tehokkuus.

Väitöskirjassa esitetään myös uusia tuloksia vakioverhokäyräiselle TFM-modulaatiolle (tamed frequency modulation), jonka kaistan ulkopuolinen säteily on pieni verrattuna muihin tunnettuihin CPM-modulaatiomenetelmiin (continuous phase modulation). Vaihe- ja taajuusmodulaatiossa kaistanleveyttä ja ilmaisun suorituskykyä säädetään modulaatioindeksin avulla. TFM-modulaation yksinkertaisessa analogiatoteutuksessa modulaatioindeksi poikkeaa kuitenkin asetetusta nimellisarvosta lähetyksen aikana aiheuttaen vaihevärinää. Ilmaisun suorituskyvyn parantamiseksi tässä työssä esitetään uusi modulaatioindeksin estimaattori vastaanottimessa yhdistettynä selviytyjäkohtaista käsittelyä (per-survivor processing, PSP) hyödyntävään kantoaallon vaiheen estimointiin.

Väitöskirjassa esitetään myös uusia tuloksia TCM-modulaatiolle (trellis-coded modulation), joka on yhdistetty koodaus- ja modulaatiomenetelmä teho- ja kaistarajoitetuille järjestelmille. Työssä osoitetaan, että hyödyntämällä niin sanottua moni-trelliskoodattua modulaatiota (multiple trellis-coded modulation), PSP-kantoaallon vaihesynkronointia ja Reed–Solomon (RS) koodausta voidaan TCM-modulaatio estää tulemasta katastrofaaliseksi koodiksi vaihekohinan yhteydessä. TCM- ja CPM-menetelmät voivat täydentää tulevaisuuden OFDM pohjaisia 5G-järjestelmiä.

Avainsanat continuous phase modulation (CPM), constant envelope orthogonal frequency division multiplexing (CE-OFDM), nonlinearity, tamed frequency modulation (TFM), trellis-coded modulation (TCM)

ISBN (painettu) 978-952-60-7356-9 **ISBN (pdf)** 978-952-60-7355-2

ISSN-L 1799-4934 **ISSN (painettu)** 1799-4934 **ISSN (pdf)** 1799-4942

Julkaisupaikka Helsinki **Painopaikka** Helsinki **Vuosi** 2017

Sivumäärä 122 **urn** http://urn.fi/URN:ISBN:978-952-60-7355-2

Preface

The research for this dissertation was conducted at the VTT Technical Research Centre of Finland in Oulu, Finland in the years 2001–2016. The work was also carried out at the Berkeley Wireless Research Center (BWRC), California, USA from August 2004 to August 2005. In fact, the dissertation is a continuation on my Licentiate Thesis “Trellis-coded modulation and per-survivor processing” (Kiviranta 2000) where the effects of phase noise in non-constant envelope trellis-coded modulation (TCM) were studied. On the other hand, the dissertation is based on published novel articles.

I would like to express my gratitude to Mr Kyösti Rautiola for providing me with the opportunity to carry out the research at VTT and giving me some free time to finalize this thesis. I am grateful to my daily supervisor and mentor Research Professor Aarne Mämmelä for his comments and support during the project. He has patiently taught me since the year 1993. I thank very much my supervisor Professor Risto Wichman at the Aalto University. I greatly appreciate Professors Hanna Bogucka and Giorgio M. Vitetta for the pre-examination of this dissertation and their valuable comments. I would also like to thank all my colleagues and co-authors. Special acknowledgements go to Dr Antti Anttonen, Dr Marko Höyhtyä, Mr Mika Lasanen, Mr Ilkka Moilanen, Mrs Sandrine Boumard and Mr Pertti Järvensivu. The author was privileged to receive personal grants for doctoral studies from the Jenny and Antti Wihuri Foundation and the Riitta and Jorma J. Takanen Foundation. They are gratefully acknowledged.

Finally, I thank very much my wife Terhi being for there always and pushing me forward. My sporty daughters Kirsikka, Katariina and Kiia have helped me to forget the business when needed. We are a family! I would also like to thank my parents Toini and Paavo for their care. Thank you also my parents-in-law Olli and Tellervo.

Question of Time

Oulu, March 2017 Markku Kiviranta

Contents

List of publications

This thesis is based on the following original publications which are referred to in the text as I–VI. The publications are reproduced with kind permission from the publishers.

I Kiviranta M., Mämmelä A., Zhang Y., Moilanen I., Boumard S., Sarkkinen T., & Jämsä T. 2005. A real-time simulation of impairments in the analog parts of the transmitter-receiver. In Proc. IEEE VTC, pp. 968-972.

II Kiviranta M., Mämmelä A., Cabric D., Sobel D., & Brodersen R. W. 2005. Constant envelope multicarrier modulation: Performance evaluation in AWGN and fading channel. In Proc. IEEE MILCOM, pp. 807-813.

III Kiviranta M., Mämmelä A., Paaso H., Höyhtyä M., & Moilanen I. 2009. Digital signal design and nonlinear distortions in antenna array beamforming. In Proc. WCNC, pp. 1-6.

IV Kiviranta M. & Mämmelä A. 2014. Receiver structure and estimation of the modulation index for tamed frequency modulated (TFM) signals. Physical Communication, vol. 10, pp. 61-71.

V Kiviranta M. & Mämmelä A. 2015. Multiple trellis-coded modulation, per-survivor processing and Reed-Solomon coding in the presence of phase noise. Physical Communication, vol. 17, pp. 86-93.

VI Kiviranta M. Mämmelä A., & Apilo O. 2017. Power efficiency, phase noise, and DC offset in constant envelope OFDM transceivers. Transactions on Emerging Telecommunications Technologies, vol. 28, pp. 1-11.

Author's contributions

The author had the main responsibility for developing the original ideas in Publications II–VI. The author was the first writer in all Publications I-VI. The roles of author and other contributors are summarized as follows:

I The author had the main responsibility for making the state-of-the art review of nonideal analog parts and developed the high level block diagrams for the selected nonlinear models for implementation. Ilkka Moilanen made the MATLAB scripts and floating point simulations. Sandrine Boumard and Yan Zhang were responsible for the complexity analyses and hardware implementation with testing. Timo Sarkkinen and Tommi Jämsä provided guidance as well as criticism. Aarne Mämmelä was the supervisor.

II The author had the main responsibility for the studying and simulating the constant envelope orthogonal frequency division multiplexing (CE-OFDM). Danijela Cabric and David Sobel helped with the theory of algorithms and fading channel. Aarne Mämmelä and Robert Brodersen supported the overall work and provided guidance as well as criticism.

III The author had the main responsibility for making the state-of-the art review and selecting the nonlinearities to be studied. Henna Paaso and Marko Höyhtyä made the MATLAB scripts and simulations for the beamforming. Ilkka Moilanen carried out the peak-to-average power ratio (PAPR) simulations. Aarne Mämmelä gave guidance and criticism.

IV The principle of the modulation index estimator was originally described in author's patent (Kiviranta 2003). The author had also the main responsibility for the performance simulations. Johannes Peltola helped with the MATLAB scripts. Aarne Mämmelä supported the work and provided guidance as well as criticism.

V The author had the main responsibility for the studying and simulating the effects of phase noise and developing the compensation method for that. Aarne Mämmelä supported the work and provided guidance as well as criticism.

VI The author had the main responsibility for the studying and simulating the effects of phase noise. The idea of the direct current (DC) offset compensation was developed together with Aarne Mämmelä who also supported the overall work and provided guidance as well as criticism. Olli Apilo and Mika Lasanen helped with the MATLAB code for the power consumption analysis and spectrum simulations.

Publications I-III have been published in conference proceedings. Publications IV-VI are journal articles. The Publications are summarized in more detail in Chapter 3 after presenting the background for this thesis.

List of symbols and abbreviations

b	filter coefficient
B	channel bandwidth
E_0	energy per bit
h	modulation index
k	number of bits
l	number of symbols in codeword
N	length of FFT
N_0	noise power spectral density
r	roll-off factor
R	information rate in bit per second
s	number of symbols
θ	phase noise
v	constraint length
σ	standard deviation
ϕ	phase
4G	fourth generation
5G	fifth generation
ACI	adjacent channel interference
AM	amplitude modulation
AOF	asymptotically optimum filter
ARMA	autoregressive moving average
AWGN	additional white Gaussian noise
BER	bit error rate
BPSK	binary phase shift keying
ceCPM	constrained envelope continuous phase modulation
CE-OFDM	constant envelope orthogonal frequency division multiplexing

CORDIC	coordinate rotation digital computer
CP	cyclic prefix
CPM	continuous phase modulation
D2D	device-to-device
DA	data-aided
DC	direct current
DCT	discrete cosine transform
DD	decision directed
DFT	discrete Fourier transform
DSL	digital subscriber loop
DVB	digital video broadcasting
DVB- NGH	digital video broadcasting — next generation handheld
DVB-S2X	digital video broadcasting — forward link second generation extension
DVB-T	digital video broadcasting — terrestrial
ECC	Electronic Communications Committee
ECMA	European Computer Manufacturers Association
FBMC	filter bank multicarrier
FFT	fast Fourier transform
FHT	fast Hartley transform
FM	frequency modulation
f-OFDM	filtered orthogonal frequency division multiplexing
FSK	frequency shift keying
GEO	geostationary orbit
GFDM	generalized frequency division multiplexing
GMSK	Gaussian minimum shift keying
GSM	Global System for Mobile Communications
GTFM	generalized tamed frequency modulation
HF	high frequency
HPA	high power amplifier
ICI	intercarrier interference

IEEE	Institute of Electrical and Electronics Engineers
IFFT	inverse fast Fourier transform
ISI	intersymbol interference
ITU-R	International Telecommunication Union Radiocommunication Sector
ITU-T	International Telecommunication Union Telecommunication Standardization Sector
JDCE	joint data and channel estimation
LNA	low noise amplifier
LOS	line of sight
LTE	Long Term Evolution
M2M	machine-to-machine
MIMO	multiple-input multiple-output
ML	maximum likelihood
MLSE	maximum likelihood sequence estimation
MPSK	*m*-ary phase shift keying
MQAM	*m*-ary quadrature amplitude modulation
MRC	maximum-ratio combiner
MSK	minimum shift keying
MTC	machine type communication
MTCM	multiple trellis-coded modulation
NIST	National Institute of Standards and Technology
OFDM	orthogonal frequency division multiplexing
OOB	out-of-band
OQAM	offset quadrature amplitude modulation
PA	power amplifier
PAE	power added efficiency
PAPR	peak-to-average power ratio
PCS	personal communications services
PHY	physical layer
PM	phase modulation

PMP	point-to-multipoint
PMR	private mobile radio
PSP	per-survivor processing
QAM	quadrature amplitude modulation
QPSK	quadrature phase shift keying
RF	radio frequency
RS	Reed–Solomon
RSSS	reduced state sequence detector
SC-FDMA	single carrier frequency division multiple access
SNR	signal-to-noise ratio
TCM	trellis-coded modulation
TFM	tamed frequency modulation
UDN	ultra-dense network
UFMC	universal filtered multicarrier
UAV	unmanned aerial vehicle
VLF	very low frequency
WAN	wide area networks
WiMAX	Worldwide Interoperability for Microwave Access
WLAN	wireless local area network
WOLA	weighted overlap and add
WPAN	wireless personal area network
WRAN	wireless regional area network
WRC	World Radiocommunication Conference

1. Introduction

1.1 Motivation of the thesis

In telecommunications the performance is normally measured in terms of spectral efficiency and energy or power efficiency since frequency and energy are seen as the most important resources. In single-criterion optimization either spectral efficiency or energy efficiency is maximized. When the spectral efficiency is increased, the energy or power efficiency is decreased and vice versa (Chen 2011). Therefore, the spectral and power efficiency cannot be optimized independently, and this challenge is the theoretical motivation for the thesis. Multi-criteria optimization (Marler & Arora 2004) of both spectral efficiency and energy efficiency implies some trade-off since the optimum is not unique. In theory, Pareto optimum (Björnson et al. 2014) is a state in which it is not possible to make any criterion better without making at least one criterion worse. In general, the energy or power is a good measure of the complexity of digital electronics (Wu 1987) but it must be traded-off against the spectral efficiency. An ideal AWGN channel is a good and simple starting point for system planning, especially because it gives us very important information about the theoretical performance boundaries of a given communication system. Since both the physical channel itself and the analog parts of the transmitter and receiver are sources of noise and distortions, it is crucial to take the impairments into account in comparing different air interface technologies and when developing robust high data-rate products (Fettweis et al. 2007).

1.2 Contributions of the thesis

In this Section the contributions of the whole thesis are presented and compared to the literature. The thesis is based on Publications I-VI. The detailed contributions of each Publication I-VI are explained in the introduction part of the corresponding Publication. The main results of Publications are presented in Section 3, too.

The thesis considers spectral and power efficient modulations by taking into account analog impairments in the transmitter and the receiver. Good text books for orientation of the thesis are (Proakis 2001) for digital communications and (Jeruchim

2000) for nonlinearities. There is also a new textbook for bridging nonlinearities and digital communications (Baudin 2015). Overall, this thesis supports the maximization of technology commonalities which is a key factor for the rapid uptake of new systems and standards. Satellite and terrestrial system integration is already a trend (Kim et al. 2015) and this will continue with the development of interoperability specifications (ITU-R M.2047, 2013). A similar process is ongoing for commercial and public safety systems (ECC 199, 2013). The fifth generation (5G) is envisioned (Demestichas et al. 2013) to be the integration of new mobile and wireless access networks seamlessly with legacy networks in order to use deployed investments as long as such systems will be in operation (NetWorld2020 2015). The hybrid fiber-copper integration will even complement the development enabling a cost-effective multi-gigabit backhaul networks (Coomans et al. 2015). All these systems should cooperate and interwork seamlessly at the same time reducing costs (Osseiran et al. 2014). Use-cases originating from verticals such as Factories of the Future, Automotive, Health, Energy and Media & Entertainment (5G PPP 2016) should be considered as drivers of 5G. The requirements for the systems vary by applications but will include data rates ranging from very low sensor data to very high video content delivery, stringent low latency requirements, low energy consumption (Fettweis 2014), and high reliability (ITU-R M.2083, 2015). There is a consensus that these goals cannot be met with one single technological solution and the 5G infrastructures need to be flexible and adaptable to diverse use cases and scenarios (Liu et al. 2011, NGMN 2015). The World Radiocommunication Conference (WRC) in 2015 set directions for the next 5G standard and final decisions on new spectrum allocations towards higher frequency bands will most likely be made in the following WRC in 2019. The advantage of the mm-wave frequencies is the higher bandwidth availability. Also the small wavelength allows a larger number of antenna elements to be integrated into the devices. On the other hand, the mm-wave communications suffer from propagation loss, and the analog components are subject to radio frequency (RF) impairments (Qiao et al. 2015, Niu et al. 2015). Therefore, the modulation and waveform design for 5G systems in the presence of nonlinearities is the focused context in which this thesis makes the state-of-the-art review and develops and brings contributions.

Spectral efficient orthogonal frequency division multiplexing (OFDM) (Van Nee & Prasad 2000) is an adopted multicarrier (Bingham 1990) waveform in several terrestrial wireless standards (Stuber et al. 2004) such as the Long Term Evolution (LTE) for the 4G. The conventional OFDM system is designed for severe multipath channels. However, the application scenarios (Boccardi et al. 2014, Fettweis & Alamouti 2014) predicted for 5G systems such as low power machine-to-machine (M2M) or machine type communication (MTC) (Kim et al. 2014), real time Tactile Internet (Fettweis 2014, Simsek et al. 2016) and dynamic spectrum access (Haykin 2005) present challenges for the OFDM (Andrews et al. 2014, Michailow et al. 2014, Farhang-Boroujeny & Moradi 2016). The technical drawbacks of the OFDM include among others high peak-to-power ratio (PAPR), out-of-band (OOB) radiation, and length of cyclic prefix (CP) (Andrews et al. 2014). Transition from the existing OFDM based systems to the next generation radio access technologies may follow two

paths where 1) the current multicarrier OFDM structure is maintained via evolution and the shortcomings are improved by ensuring backward compatibility, or 2) a revolutionary framework for totally new schemes is adopted (Sahin et al. 2014). This thesis concentrates on the further development of the OFDM, since the evolutionary approach from the 4G to the 5G is assumed to be more mature for technology demonstrations. On the other hand, this thesis presents new findings and results for tamed frequency modulation (TFM) (Jager & Dekker 1978) and trellis-coded modulation (TCM) (Ungerboeck 1982) which is a traditional combined coding and modulation technique for spectral and power limited systems. TFM has a very small spectral OOB radiation compared to other known continuous phase modulation (CPM) methods. The two treated modulations can complement the future adaptive OFDM based 5G systems. Concerning the OFDM evolution a special attention is given to the constant envelope OFDM (CE-OFDM) where a phase modulation (PM) creates a constant envelope (Thompson et al. 2008). Therefore, a power amplifier (PA) can operate at or close to the saturation point, and it is shown here to maximize average transmitter power which is good for range and PA efficiency which is good for battery life. A novel 5G transceiver would include both more spectral efficient OFDM and more power efficient CE-OFDM modes. Adaptive radio might select the more applicable mode. Concerning the nonlinear PA, the predistortion is beyond the scope of this thesis but it is studied by Hekkala in his doctoral dissertation in 2014 (Hekkala 2014), and therefore, these two theses complement each other. This thesis shows that the CE-OFDM has a significant advantage compared to phase noise sensitive OFDM since the phase noise transforms just into an additive noise term after the phase detector. This work is also the first to illustrate that there are no impairments in the RF phase shifters beamforming (Doan et al. 2004) if there is phase noise at the input of the antenna array. The simulations show that CE-OFDM with assumption of nearly ideal beamforming outperforms OFDM in a typical 60 GHz channel. In addition to phase noise and nonlinear power amplifier, I/Q imbalance and direct current (DC) offset are other expected major analog impairments in the future OFDM based systems. Particularly, a novel DC offset removal is developed and it is shown to enhance spectral flatness and performance of channel estimation in CE-OFDM. The spectral flatness is one quality parameter in LTE (ETSI TS 36.101, 2008), and the measurement compares the power variations of a subcarrier to the average power of all subcarriers, in decibels (dB).

In phase modulation, spectral spreading and detection performance are controlled using a modulation index (Sundberg 1986). In a simple and low cost analog implementation (Bockelmann et al. 2016), the modulation index, however, deviates during the transmission and generates time varying phase jitter. As a novelty a modulation index estimator in conjunction with per survivor processing (PSP) carrier phase estimation is presented for the inherently constant envelope TFM. In general, the PSP provides a general framework for the approximation of the maximum likelihood sequence estimation (MLSE) algorithms whenever the presence of unknown parameters prevents the precise use of the classical Viterbi algorithm (Raheli et al. 1995). Concerning the PSP this thesis provides also new contributions for the TCM that is shown to become a catastrophic code (Viterbi & Omura 1979) in the presence

of phase noise. A novel combination of multiple trellis-coded modulation (MTCM) (Biglieri et al. 1991) with Reed–Solomon (RS) coding (Oh et al. 2013) is proposed in a simple manner. A semianalytical approach (Nordman & Mämmelä 1998) is applied to verify the simulation results.

The research methods of this Thesis include state of the art reviews, theoretical analysis and simulations. The discussion and conclusion part includes also recommendations for future research. The basic approach in analysis and simulations has been reduction: The system model is first divided into simple sub-blocks and the effects of different parameters are considered separately and the results are generalized inductively and special cases are found deductively. For the simulations MATLAB, Simulink and CoCentric System Studio have been used.

1.3 Organization of the thesis

The thesis is organized as follows: Chapter 2 reviews the relevant literature and background on the considered spectral and power efficient modulations and typical analog impairments at each stage of the transmitter and the receiver. Then Chapter 3 presents new results of this thesis summarizing the original papers. Chapter 4 discusses the main findings, limitations and recommendations for future work. Finally, Chapter 5 provides a summary.

Table 1 summarizes the relation of the original Publications to the spectral and power efficient modulations and the discussed nonlinearities in Chapter 2. In more detail, Publication I introduces typical analog impairments at each stage of the transmitter and the receiver with a system model. The prioritized classification for the distortions includes nonlinear PA, phase noise, I/Q imbalance and DC offset. Publication III discusses the effects of nonlinearities in more detail. Especially, the distortions in beamforming are illustrated, and a system model for the antenna array system is presented. Publications II and VI consider CE-OFDM which allows PA to operate near saturation levels thus maximizing power efficiency. Publication II presents a system model for CE-OFDM in a fading channel with bit error rate (BER) simulation results. Transceiver power efficiencies in OFDM and CE-OFDM systems are compared in Publication VI by measuring the BER as a function of average PA input signal-to-noise ratio (SNR) so that the effects of the PA nonlinearities are taken into account in the performance evaluation. Publication IV presents a TFM receiver with a modulation index estimator who has an acquisition and tracking ability. Finally, Publication V presents a novel receiver structure for TCM in the presence of phase noise.

Table 1. Relation of the original Publications to the Thesis.

Publication	**I**	**II**	**III**	**IV**	**V**	**VI**
Modulation efficiency						
• Power		x				x
• Spectral	x		x			
• Both				x	x	
Nonlinearity						
• nonlinear PA	x	x	x			x
• phase noise	x		x	x	x	x
• I/Q imbalance	x		x			
• DC offset	x		x			x

2. Nonlinearities and modulation methods

2.1 Waveform design challenges

According to the Shannon law (Shannon 1948), the capacity of an ideal additive white Gaussian noise (AWGN) channel in bit/s can be given as

$$C = B\log_2\left(1 + \frac{E_0}{N_0} \cdot \frac{R}{B}\right) \quad (1)$$

where B is the channel bandwidth in Hz, E_0 is the energy per bit in J, R is the information rate in bit/s and N_0 is the noise power spectral density in W/Hz. According to the law the basic resources of the transmission system are the transmitted power, which determines the SNR at the receiver, and the bandwidth. The resources are tried to economise according to the transmission conditions and strategies such as the transmission distance, modulation, and coding scheme, and resource management algorithms (Chen 2011). In power limited systems error control coding is used to obtain better performance results at the expense of increased bandwidth. In a bandwidth limited system amplitude or phase modulation with a higher alphabet size of *M* is used to transmit more bits per symbol, but at the cost of increased power requirements (Proakis 2001). Spectral and power efficiencies with average bit error rate are measured in terms of bit/s/Hz and bit/J or equivalently bit/s/W, respectively. The system efficiency can be measured as bits per second and energy efficiency as number of bits per energy unit (Hubka & Eder 1988). When the efficiency is improved, the performance will be improved. In power-limited systems we can have essentially an infinite amount of energy, as in the case of the base stations, although the power is limited because of thermal and cooling problems and safety requirements (Mämmelä et al. 2010). Mobile terminals are both power and energy-limited systems where the energy is carried in a battery that must be recharged every now and then.

Developing next generation wireless systems not only requires to approach physical limits in means of the theoretical Shannon law, but it also calls for techniques to approach so called “engineering Shannon bounds” – the technological limits set by analog RF front-ends (Fettweis et al. 2007). The circuit power consumption has also an impact on the energy-efficient communication (Miao et al 2009). The practical performance simulations of the any communication system take also into account the impairments of analog RF components (Gardner & Baker 1997, Jeruchim et al. 2000). Historically, the nonlinear phenomena were touched by Lucky (Lucky 1973) in his survey of the communication theory in the early seventies. Shortly afterwards, Bello presented a channel simulator system with a discussion of its nonideality (Bello 1978).

2.1.1 Nonlinear distortions

Both the physical channel itself and the analog parts of the transmitter-receiver are sources of noise and distortions (Gardner & Baker 1997, Jeruchim et al. 2000). The typical analog impairments at each stage of the transmitter and the receiver with the channel are presented in Figure 1. The order of the blocks can be changed depending on the current application, and the number of the required filters depends on the performance requirements. The only error mechanism present in an ideal analog-to-digital (A/D) converter is quantization. This error arises because the analog input signal may assume any value within the input range of the A/D while the output data is a sequence of finite precision samples (Proakis & Manolakis 1996). In practice, the main issues limiting converter performance are thermal noise, aperture jitter and comparator ambiguity (Walden 1999). The aperture jitter refers to uncertainty in sampling time, and it is the most critical parameter in fast conversion. When the A/D-converter processes unknown signals in the receiver, the digital-to-analog converter (D/A) converter processes known signals in the transmitter. Therefore, state-of-the-art D/Cs can have significantly better resolutions than ADCs achieving same sample rate. The jitter is a critical parameter also in the D/As.

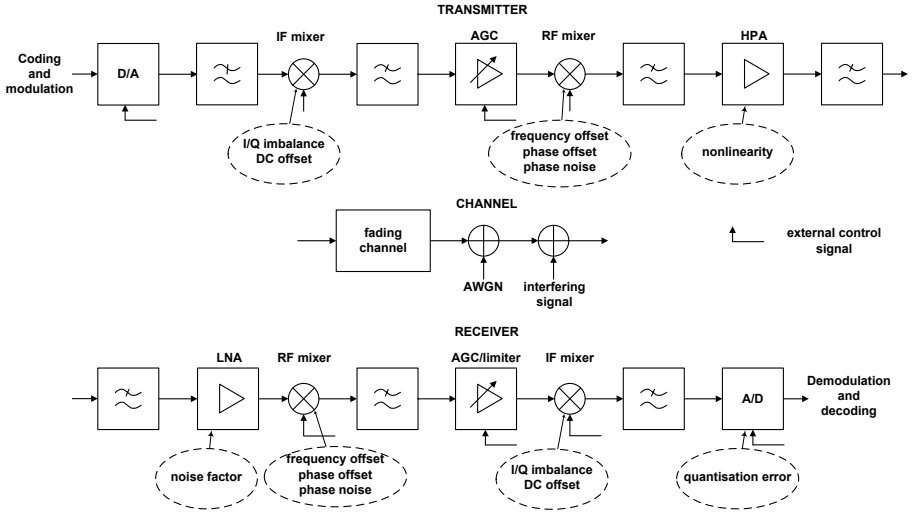

Figure 1. System model with a channel. Redrawn from Publication I ©[2005] IEEE.

In a direct conversion receiver, only one RF mixer is needed since the band of interest is directly translated to zero frequency. In general, receivers' mixers can be adjustable, and the control signal for the intermediate frequency (IF) mixer is provided by automatic frequency control (AFC). The automatic gain control circuit (AGC) operates in a receiver where the power control command for the transmitter is also generated. An alternative to an AGC circuit in the receiver is a limiter. The ideal mixer can be modeled by a multiplier and this is a linear operation (Haykin

2001). However, practical mixers are nonlinear (Schetzen 2006). The local oscillator (LO) leakage results in a DC offset at the output of a mixer. In the case of the quadrature frequency translations, shifting either the input signal or the LO output by 90° is required. In binary modulation a phase shift of 180° must be performed. Differences in gain factors and errors in the phase shift cause a mismatch between the in-phase and quadrature-phase branches which is called an I/Q imbalance (Razavi 1997). Oscillators exhibit phase noise θ of two different types: finite power or asymptotically infinite power (Piazzo & Mandarini 2002). When the system is only frequency locked, the resulting phase noise is slowly varying but not limited, and it is modeled as a zero mean, nonstationary, asymptotically infinite power Wiener process. If the system is phase locked, the phase noise is small and it can be modeled as a zero mean, stationary, finite power autoregressive moving average (ARMA) process. When the phase noise causes a multiplicative disturbance $e^{j\theta}$ on the input signal, the spectrum of sinusoid is Lorentzian when the phase noise is nonstationary Wiener process. In the case of the stationary ARMA process there is spectrum of phase noise itself plus the impulse in origin. In practice, the spectrum of $e^{j\theta}$ is specified in standards such as the National Institute of Standards and Technology (NIST) through a phase noise mask consisting of decibels relative to the carrier (dBc) per Hz values (Glase 1970). The Institute of Electrical and Electronics Engineers (IEEE) defines for one the spectral density of the phase θ fluctuations in radians squared per Hz.

All amplifiers are nonlinear if driven hard enough; they all exhibit saturation effects, whereby the output is not linearly proportional to the input at the high input signal levels. In the transmitter high power amplifier (HPA) is typically operated close to saturation, or even saturated. In the receiver low noise amplifier (LNA) can be usually assumed to operate in a linear region. The required backoff increases with respect to the PAPR of the modulation (Li & Stuber 2006). The drive power at which the output saturation occurs is called the input saturation power. The ratio of input saturation power to the actual input power is called the amplifier input backoff. Increasing the input backoff decreases input drive power and produces less output power but improves the linearity. The maximum output power available from the amplifier is the output saturation power. The ratio of the output saturation power to actual output power is called the output backoff. An increase in the input backoff causes an increase in the output backoff (Gagliardi 1984). The required backoff increases with respect to the PAPR of the modulation (Li & Stuber 2006). In the literature (e.g., Van Nee & Prasad 2000), the PAPR is usually determined as the ratio between the maximum power and the average power of the complex signal. A constant envelope 0 dB PAPR modulation such as minimum shift keying (MSK) (Pasupathy 1979) is a common method to avoid distortions caused by the nonlinear amplifier. However, the analog filtering distorts the constant envelope nature of the transmitted signal. After filtering the envelope fluctuation depends on the bandwidth and type of filter (Spilker 1977), and thus an additional backoff may be required in the amplifiers. Filtering may also contribute significant intersymbol interference (ISI), and an equaliser is needed if the performance degradation is large. The pulse shape

filtering destroys the constant envelope property also in linear modulations. For example, if binary phase shift keying (BPSK) or quadrature phase shift keying (QPSK) signal with a rectangular pulse and sudden instantaneous phase shifts is filtered with a square root raised cosine filter, its envelope is no more constant (Ziemer and Peterson 1985).

Efficiency is a critical factor in the PA design and several definitions are given in the literature (Ochiai. 2013). When amplifying signals with time-varying amplitudes or in power-adaptive systems (Neuvo 2004), a useful measure is the average efficiency, which is defined (Raab et al. 2002) as

$$\eta = \frac{E[P_{\text{out}}]}{E[P_{\text{DC}}]}. \quad (2)$$

where P_{out} is the output power and P_{DC} is the DC power consumption of the PA. The power $(1-\eta)E[P_{\text{DC}}]$ not converted to the RF signal is wasted as heat. For the OFDM the average efficiencies have been considered in (Ochiai. 2013). Power added efficiency (PAE) takes also into account the input power by subtracting it from the output power. In most practical applications, however, the power from other inputs than DC power supply is negligible. The efficiency of the PA is an important measure of the battery life of the wireless transceiver. The instantaneous efficiency is usually optimized for the maximum output power and the efficiency decreases when output power is decreased. In general, common PAs can be classified into A, B, AB and C classes (Bahl 2009), and the class B amplifiers have higher maximum efficiency of 78.5% than the class A amplifiers of 25-50 % efficiency and better linearity than the class C amplifiers which have 99% efficiency. The constant envelope modulation allows using of the very nonlinear but very power efficient class C amplifiers (Anderson & Sundberg 1991). The transmitted and received powers are equal if the channel attenuation is normalized to unit. The BER performance is usually measured in an AWGN channel as a function of the average SNR at the receiver. The PA input SNR is defined as the ratio of PA input energy to the receiver noise spectral density, and measuring BER as a function of that takes into account the PA (Apilo et al. 2013).

The changes in the nonlinear properties are usually slow and caused by, e.g., component aging and temperature changes (Ziemer & Peterson 1985). In general, models for amplifiers can be divided into 1) memoryless nonlinear systems represented by amplitude modulation to amplitude modulation (AM/AM), 2) quasi-memoryless nonlinear systems represented by AM/AM and amplitude modulation to phase modulation (AM/PM) or 3) nonlinear systems with memory (Jeruchim et al. 2000). If the nonlinear amplifier has memory, the system response depends not only on the input amplitude but also on its frequency (Saleh 1981). In general, block oriented separable nonlinear systems are preferred due to complexity reasons (Mämmelä et al. 2008). For example, in Hammerstein model we have first the memoryless nonlinearity and then a linear filter with memory. In the Wiener model the blocks are in reverse order. If the models cannot be divided into subsystems, we can use Volterra series (Schetzen 2006) models, which are a generalization of the Taylor series.

Nonlinearities cause in-band and OOB distortions to the transmitted signal. Nonlinear systems typically create spectral components (harmonic and intermodulation distortions) that are totally absent from the input spectrum (de Coulon 1986). The same phenomenon is also possible in linear time variant systems (Bello 1963). Spectral spreading causes adjacent channel interference (ACI). If the nonlinear amplifier has memory, each point of the signal constellation becomes a cluster showing ISI. Constellation warping refers to the situation where the constellation points are not on a rectangular grid as in the original constellation (Karam & Sari 1991). Other usual changes in the constellation are attenuation, rotation, spreading, origin offset as well as I/Q amplitude and phase error (Kenington 2000). On the left Figure 2 shows a 16-ary QAM constellation warping with clusters and DC offset on the right.

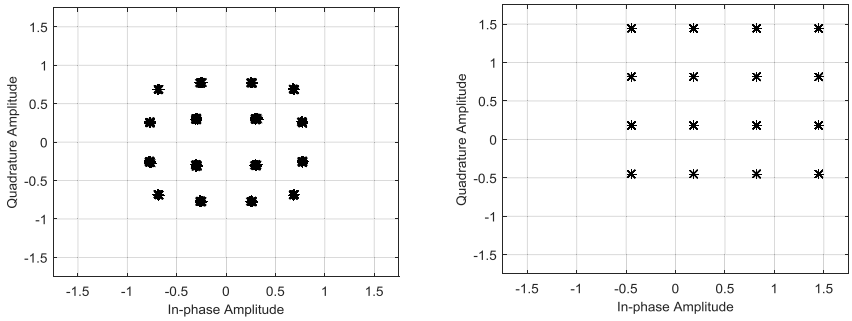

Figure 2. QAM constellation warping with clusters (left) and DC offset (right).

2.1.2 Antenna arrays

The large bandwidth at mm-wave spectrum from 30 GHz to 300 GHz is an attractive choice for high data rate transmissions (Qiao et al. 2015). However, due to the high carrier frequency, the mm-wave communications suffer from high propagation loss, and directional beamforming with antenna array (Litva 1996) gain has been adopted as an essential compensation technique. The small wavelength allows larger number of antenna elements to be integrated into the devices. While additional antenna elements are usually inexpensive and the additional digital signal processing becomes even cheaper, the RF elements are expensive and are more challenging to follow Moore's law (Molisch & Win 2004). This is a problem especially in digital beamforming where for each antenna element at the transmitter or the receiver, a complete dedicated RF chain is required. Therefore, realizing digital beamforming, especially for massive MIMO systems appears to be impractical (Bogale & Le 2014). From an implementation point of view, digitally controlled RF phase shifter architecture in Figure 3 is simple since only one DA converter and RF mixer is needed in the transmitter and the receiver. Vector modulator phase shifter is considered as the most practical solution, especially with integrated circuit technology (Doan et al.

2004). However, and as in the case of I/Q modulator of RF mixers, dc offset, I/Q amplitude and phase are introduced in practice.

In a hybrid beamforming, RF phase shifter beamforming is used to obtain array gain, and baseband digital precoding is used to obtain spatial multiplexing gain. With highly directional beams, there is a shortage of multipath in the mm-wave bands, and the diversity gain is low for the baseband precoding. Finally, the high performance digital beamforming is usually used in base station downlink transmitters. The low complex analog beamforming structure is for one mainly used in the mm-wave short-range communication scenarios. The hybrid beamforming structure is proposed for the 5G to achieve the trade-off between performance and complexity (Niu et al. 2015). Two dimensional or three dimensional array factor represents the far-field radiation pattern of an array of isotropically radiating elements. In general, the isotropic antenna element antenna is a mathematical fiction, and it can radiate or receive energy uniformly in all directions. However, all practical antenna elements have nonuniform radiation patterns. The nonlinearities include, for example, conductor loss, dielectric loss, surface wave excitation as well as losses due to feed lines and associated feed circuitry (Litva 1996). The left-hand and right-hand 2D array factor graphs in Figure 4 show the impairments in the level and direction of the main beam, respectively. For a linear array the array factor is rotationally symmetric about the axis it is placed. The main beam of an antenna radiation pattern is the lobe containing the direction of maximum radiation power. The errors are generated by the amplitude and phase errors in the input of the antenna element and between the antenna elements. If the antenna element spacing is too large compared to the wavelength, a second main lobe can appear in the antenna array factor. The other usual impairments include distortions in beamwidth, sidelobe level, null depth, and null direction (Ucci & Petroit 1989, Xue et al. 1994).

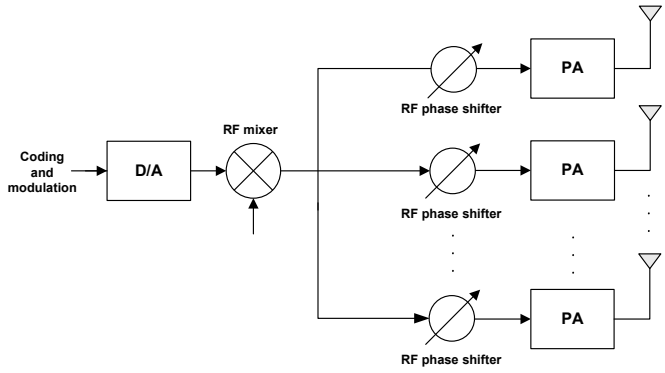

Figure 3. RF phase shifter antenna array.

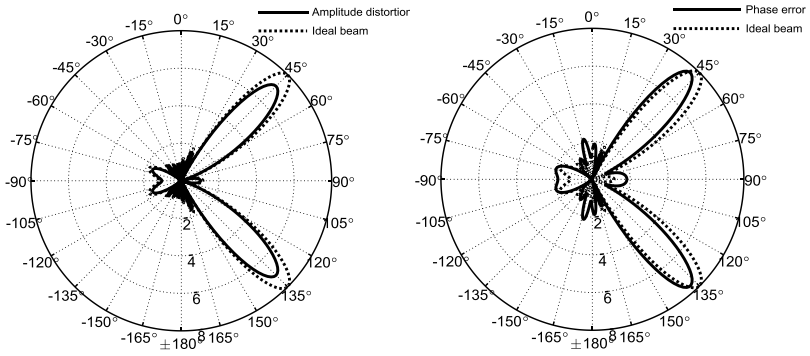

Figure 4. Array factor graphs with amplitude (left) and phase error (right).

2.2 Spectral and power efficient modulation

In general, there are three basic modulation techniques, namely amplitude modulation (AM), frequency modulation (FM), and phase modulation (PM) and each of these has a large number of variants (Oetting 1979). The *M*-ary phase shift keying (MPSK) and quadrature amplitude modulation (MQAM) are popular schemes in modern wireless communication systems. Increasing *M* results in a better spectral efficiency, however, at the cost of an increase in the signal-to-noise ratio per bit E_0/N_0. In theory, the most power efficient modulation scheme would be an orthogonal modulation with *M* approaching infinity (Proakis 2001). This strategy is not popular because E_0/N_0 only decreases incrementally at large *M*, while the occupied bandwidth and system complexity grow steadily. An example of orthogonal modulation is *M*-ary frequency shift keying (FSK) which uses a set of *M* waveforms that all have different frequency. The OFDM (Van Nee & Prasad 2000) is the most known multicarrier technique (Bingham 1990) where the data stream is transmitted over a number of subcarriers which are orthogonal to each other, i.e., the subcarrier spacing is selected such that each subcarrier is located at the zeroes of all other carriers in the spectral domain. The OFDM has high spectral efficiency due to spectral overlap, but due to the central limit theorem (Proakis 2001), addition of many multicarrier components creates a complex Gaussian distributed signal with a Rayleigh amplitude distribution having a high PAPR. All above discussed traditional modulation methods are either spectral or power efficient, and this is the main motivation to consider and present new results for both spectral and power efficient modulation methods in this thesis. A special attention is given to constant amplitude or envelope signals. In addition to the modulation study, the thesis contains new contributions for coding and modulation as an integrated entity (Massey 1974) for power and bandwidth limited systems.

2.2.1 Continuous phase modulation (CPM)

In continuous phase modulation (CPM) the carrier phase is modulated in a continuous manner (Sundberg 1986). The memory in form of phase continuity leads to a small fractional OOB radiation, meaning a good spectral efficiency. When CPM is implemented as a constant envelope waveform, the class of jointly spectral and power efficient modulation schemes is justified, and the signals in this class are very attractive in radio transmitters since they allow to operate a nonlinear transmitter amplifier at the optimum saturation point. The constant envelope modulations are of particular interest for satellite communications, low cost mobile radio, and low capacity digital microwave radio systems (Mengali & D'Andrea 1997). In addition to the commercial applications, the constant envelope modulation is widely used in high power and very low frequency (VLF) long distance military communications as well as in robust public safety emergency vehicles and private mobile radio (PMR) systems. CPM with a small controlled envelope variation is called (Svensson & Svensson 2003) the constrained envelope CPM (ceCPM), and it is suggested for the massive MTC 5G scenarios (Bockelmann et al. 2016).

In CPM, the smoothness and the rate of change of the carrier phase are determined by the frequency pulse function and the modulation index h. In the single-h and multi-h CPM schemes (Sasase & Mori 1991), the modulation index is either fixed or it varies from interval to interval. By adjusting the modulation index value there is a trade-off between detection performance and spectral spreading. Multilevel CPM refers to *M*-ary data symbols, but the minimum shift keying (MSK) (Pasupathy 1979) with a rectangular frequency pulse of length one symbol and the Gaussian filtered MSK (GMSK) (Murota & Hirade 1981) are the most well-known CPM schemes with the binary data modulation. GMSK is the adopted waveform for the Global System for Mobile Communications (GSM).

In this work a special attention is given to constant envelope tamed frequency modulation (TFM) whose spectral OOB radiation is remarkably small (Jager & Dekker 1978) compared with other known CPM techniques. The incoming binary data is processed in a specific premodulation filter which consists of a 3-tap transversal filter and a Nyquist's third criterion low-pass filter (Nyquist 1974). The features of generalized TFM (GTFM) are based on the possibility of selecting different parameter combinations for the premodulation filters (Chung 1984) and the modulation index (Laufer & Kalet 1987). In TFM, the very narrow spectrum is achieved by optimizing the fixed modulation index value to be 0.5. Since a TFM modulator can be simply realized by using a frequency modulator (FM), it makes low cost small size transmitters possible. A basic scheme for the generation of a GTFM signal is presented in Figure 5 where the maximum phase shift during one bit interval is restricted to $\pm\pi h$ rad. As a special case, a TFM signal is achieved with the filter coefficients $b = 0$ and roll-off factor $r = 0$. In general, different implementation ways of CPM modulators are discussed in (Anderson et al. 1986). The analog implementation requires control to achieve accurate phase function while maintaining high sideband suppression. A straight forward way of implementing a CPM transmitter is to use digital quadrature components which are stored in sampled and quantized form

in look-up tables, e.g., in read only memories (ROMs). The sampling rate and quantisation accuracy differ for different applications. Finally, over time the TFM has been studied for point-to-multipoint (PMP) mm-wave systems in the 28 to 31 GHz band where there is high signal attenuation due to the precipitation. In past the TFM was also a candidate for the Worldwide Interoperability for Microwave Access (WiMAX) standard as an optional modulation (Buzid et al. 2007). TFM is an attractive choice for use in high data rate satellites and deep space communications where the limited transmission energy of a space probe and the huge energy loss by the remote transmission present challenges (Bao et al. 2008).

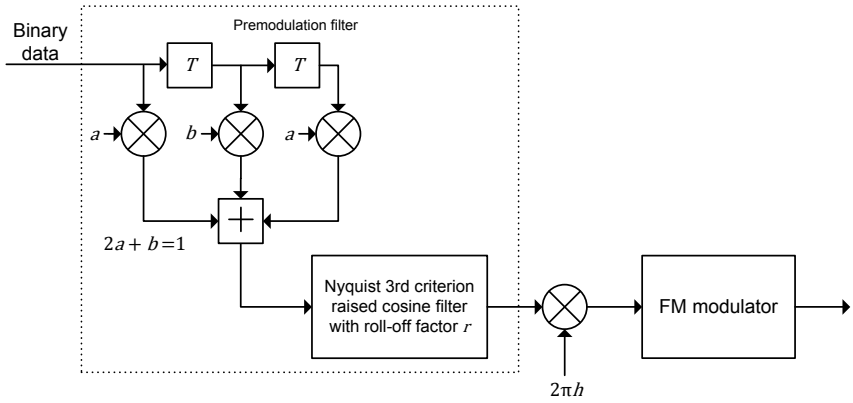

Figure 5. A basic scheme for the generation of a GTFM signal.

For rational modulation indices the cumulative phase of a CPM signal has a trellis description and ML detection can be implemented with a complex Viterbi algorithm (Anderson & Sundberg 1991). The decoder searches the trellis to find the signal path with the minimum squared Euclidean distance, i.e., sum of squared errors from the received sequence. In theory, the detected sequence is given only after processing the whole sequence of symbols meaning a long delay. In practice, looking backwards in time, the surviving paths tend to merge into the same history path at some time with a sufficient decoding delay. Several suboptimal detection algorithms for CPM can be found from the literature, and the detectors which are based on the Viterbi algorithm can be divided (D'Andrea et al. 1993) either into the reduced state sequence detectors (Svensson 1991) or the reduced search sequence detectors (Simmons & Wittke 1983). The first subcategory detectors try to reduce the complexity by deleting some part of the trellis and the Viterbi searches the remainder. The detectors in the second category maintain the entire original trellis but only a small part of it is actually searched. In most cases, both types of suboptimal detectors can reduce remarkably the complexity with limited performance losses com-

pared to the optimal Viterbi detector. The suboptimal detectors such as the differentially coherent and the noncoherent discriminator (Anderson et al. 1986) are not based on the Viterbi algorithm, and these detectors suffer more or less remarkable performance losses. When binary CPM has a modulation index value equal to 0.5, a receiver can use a simple linear receiver with matched filtering. An asymptotically optimum filter (AOF) at high SNR is a design example, where the optimization is based on the maximization of the minimum squared Euclidean distance at the output of the filter (Svensson & Sundberg 1984).

2.2.1.1 Modulation index estimation

A special drawback in the simple analog CPM implementation is the deviation sensitivity of the modulation index during the transmission. For example, in an analog FM implementation of TFM, the index is calibrated to have a rational nominal value, but it can drift due to the temperature variations of analog components. The deviated index generates time varying phase jitter, which may cause substantial performance degradations in a coherent receiver. In the original paper of TFM (Jager & Dekker 1978) the measuring and controlling of the modulation index are made in the transmitter at the cost of complexity. However, by assuming the demand of a simple transmitter we only concentrate on techniques available in the receiver. In general, the standard approach to approximate MLSE in the presence of uncertainty is based on known data-aided (DA) symbols (Proakis 2001). A decision directed (DD) loop uses tentative decisions from the Viterbi algorithm. A larger delay in tentative decisions improves the quality of the decisions but increases excessively the loop time constant. Blind or nondata aided methods are preferred when known data or decisions are not available or reliable. As a drawback, the blind estimators require a large number of samples to calculate complex statistical properties (Bianchi et al. 2004, 2005, Zhong et al. 2011). The uses of theoretical autocorrelation functions and higher order cumulants are proposed (Fonollosa et al. 1993), but according to (Anderson et al. 1986), it seems to be an extremely intractable task to define the autocorrelation function for TFM. Modulation index estimators exist also for the noncoherent receivers (Lampe et al. 2005). Coherent CPM receivers are expected to get a better BER.

2.2.1.2 Per-survivor processing (PSP)

PSP provides a general framework for the approximation of MLSE algorithms whenever the presence of unknown parameters prevents the precise use of the classical Viterbi algorithm (Raheli et al. 1995). Historically, PSP was first applied to the cancellation of residual ISI in reduced state sequence detection (Chevillat & Eleftheriou 1989). In the PSP principle, the symbol sequence associated to each survivor is

used as the DA sequence for the per-survivor estimation of the unknown parameters. The estimation is done for each survivor independently from each other. In multiple survivor technique, aka joint data and channel estimation (JDCE) (Seshadri 1994), each trellis state can have more than one survivor each having its own estimator. In contrast a reduced survivor technique at the cost of decreased performance is proposed in (Safari & Vahlin 2012). The multiple state techniques (Chugg 1998) in turn, convey the idea that for every known channel state, there are several states in an expanded trellis.

A theoretical performance evaluation of a Viterbi algorithm using PSP parameter estimates is extremely difficult. The standard simplifying assumption at high SNR is that the best surviving path at any given time is an estimate of the correct path (Esteves & Sampaio-Neto 1997). One obvious drawback is that the PSP needs extra processing compared to the conventional method. The advantage for one is that the PSP estimator associated with the best survivor is derived from symbol sequence which can perceived as high-quality, zero-delay decisions, thus making PSP very suitable for “difficult” conditions, such as those occurring in the presence of phase jitter. Also since many hypothetical symbol sequences are simultaneously considered in the PSP parameter estimation process, the acquisition of unknown parameters is substantially facilitated with respect to the conventional method. The PSP algorithm is useful to reduce the slip rates and to shorten the reacquisition when the loss of tracking has occurred. Cycle slips must be rare events in a well-designed loop.

2.2.2 Orthogonal frequency division multiplexing (OFDM)

OFDM belongs to the class of multicarrier (Bingham 1990) modulations where several parallel sequential streams of data are transmitted simultaneously. Historically, the multicarrier transmission was first explicitly proposed by Chang (1966), and the modern OFDM system was introduced by Weinstein and Ebel (1971) who proposed the idea on using fast Fourier transform (FFT) (Oppenheim & Schafer 1989) to generate an OFDM signal. The FFT implementation with sinc- shaped spectrum at the subcarriers inherently provides the orthogonality requirement. The OFDM systems were first time proposed for mobile communications by Cimini (1985), and the technique was extended from the single user to the multiuser case and from the terrestrial to the satellite channel by Wei and Schlegel (1995). Since then OFDM has been adopted for the modern wireless standards such the LTE and the digital video broadcasting — terrestrial (DVB-T) (Reimers 1997). The OFDM is also applied in digital subscriber loop (DSL) wireline and optical applications as well as on power line communications (Weinstein 2009).

The application scenarios predicted for the 5G presents challenges for OFDM (Michailow et al. 2014). In addition to a high PAPR, OFDM suffers the OOB radiation. The high spectral sidelobes are caused by the use of rectangular pulse in the time domain which behaves as a slowly decaying sinc function in the frequency

domain (Sahin et al. 2014). Also when a nonconstant envelope signal goes through a nonlinear PA, spectral regrowth appears at the amplifier output (Zhou & Kenney 2002). Therefore, the requirements for the PA linearity are severe (Katz 2001). Unfortunately, when linearity increases, the efficiency of the amplifier decreases. This is not desirable in applications for which the battery life is a key parameter (Qi et al. 2015). In addition to mobile devices, for example, long endurance unmanned aerial vehicles (UAVs) have recently gained attention in the literature (Zeng et al. 2016). An OFDM signal requires also analog/digital conversion with a high resolution. Hence, for upcoming high data rates this represents a power consumption challenge (Fettweis & Alamouti 2014). OOB radiation poses a particular challenge for dynamic spectrum access (Haykin 2005) in the wireless regional area network (WRAN) (Tadayon & Aissa 2013. Phase noise causes a multiplicative disturbance on an OFDM signal and the impact of the phase noise depends on the type of noise and receiver (Piazzo & Mandarini 2002). The coherent receiver requires finite power and low phase noise (Muschallik 1995). With a common phase error correction receiver (Pollet et al. 1995) OFDM is orders of magnitude more sensitive to the infinite power Wiener phase noise than a single carrier system. The higher sensitivity is caused by the longer duration of an OFDM symbol and by the intercarrier interference (ICI) due to loss of the carrier orthogonality (Armada 2001). Sensitivity increases also with the constellation size. A practical rule of thumb for phase noise considerations is that modulation formats up to 64-ary QAM can be supported as long as the 3 dB frequency of the phase noise spectrum is much less than the subcarrier spacing. In OFDM, the CP as a guard interval mitigates ISI and relaxes timing synchronization constraints. The proposed low latency real time 5G applications (Fettweis et al. 2014) demands for short bursts of data, meaning that the OFDM signals with one CP per symbol would present a prohibitive low spectral efficiency. The CP insertion and the long round-trip delay are also particular challenges in the satellite communications (Maral & Bousquet 2010). Concerning the satellite HPA and the PAPR problem of OFDM, signals from geostationary orbit (GEO) satellites becomes increasingly attenuated the further north one goes (Papathanassio et al. 2001). As a stand-alone waveform the OFDM may be overkill for the relatively benign line of sight (LOS) satellite channels (Thompson et al. 2008).

In technical challenge context of the OFDM, alternative modulation candidates are currently being evaluated for the 5G (Wunder et al. 2014). The most known candidate is a single carrier frequency division multiple access (SC-FDMA) that is a low PAPR variant of OFDM (Myung et al. 2006), and it is already adopted waveform for the 4G LTE uplink and the DVB — next generation handheld (NGH) (G´omez-Barquero et al. 2014). The difference between OFDM and SC-FDMA is an additional discrete Fourier transform (DFT) precoding prior to subcarrier mapping which spreads the data symbols over all the subcarriers. Thus, SC-FDMA is also called the DFT spread OFDM (Prasad et al. 2009). In general, SC-FDMA allows zero roll-off signalling to suppress OOB radiation. In CPM SC-FDMA (Wylie-Green et al. 2011, Zaidi et al. 2016) the *M*-ary data symbols are first encoded into the CPM waveform, and then the constant envelope discrete time domain sequence is DFT precoded and subsequently mapped to a set of orthogonal subcarriers for SC-

FDMA transmission. The hybrid CPM-SC-FDMA can potentially retain much of the power efficiency of CPM, and thus result in a lower PAPR than conventional SC-FDMA. In more detail, the modulation index can be used to control the spectral spreading and the PAPR. A similar hybrid approach is proposed for the OFDM transmission in (Tasadduq & Rao 2002). Pulse shaped OFDM (Bölcskei et al. 2003 refers to OFDM-based waveforms with filtering or windowing to suppress the OOB radiation and to relax CP requirements by increasing robustness to the ISI. The windowing techniques such as weighted overlap and add (WOLA) (Qualcomm 2015) smooths the edges of each symbol to increase spectral decay. Filter bank multicarrier (FBMC) (Farhang-Boroujeny 2011), universal filtered multicarrier (UFMC) (Vakilian et al. 2013) or filtered-OFDM (f-OFDM) (Zhang et al. 2015) and generalized frequency division multiplexing (GFDM) (Fettweisr et al. 2009) are examples of other proposed filtered waveforms. In general, filter design (Gardner & Baker 1997, Jeruchim et al. 2000) involves the trade-off between the time- and frequency-domain characteristics, and now the filtering deteriorates or imposes special requirements such as staggered (Gitlin & Ho 1975) or offset QAM (OQAM) for the orthogonality. It is worth noting that filtering induces also a power loss (Lucky et al. 1968). The filtering complexity may not be a problem at the base station, but it does in the terminal. For example, FBMC filters each subcarrier individually, and the subcarrier filters are very narrow and require long filters. The proposed multicarrier signals exhibit large envelope fluctuations, and thus spectral regrowth caused by nonlinear distortions is still a problem (Vihriälä et al. 2015).

2.2.2.1 Constant envelope OFDM

In this thesis a special attention is given to constant envelope (CE) OFDM (Thompson et al. 2008) where frequency modulation (FM) or phase modulation (PM) creates a fully constant envelope. The PA can therefore operate at the optimum (saturation) point, maximizing average transmit power (good for range) and maximizing PA efficiency (good for battery life). CE-OFDM was originally (Casas & Leung 1991, Casas & Leung 1992, Warner & Leung 1993) proposed for mobile radios to retrofit inexpensively and simply existing frequency modulation (FM) systems, and in Japan, CE-OFDM was studied for the digital TV over satellite (Anwar et al. 2007) without affecting the configurations of existing broadcasting systems. Low PAPR allows reducing the hardware cost and power consumption, which is an important point for the future LTE over satellite (Hasan & Sagar 2013), MTC (Kim et al. 2014) and device-to-device (D2D) communication (Lin et al. 2014). The CE-OFDM has also mentioned (Swindlehurst et al. 2014, Magueta et al. 2016) as a candidate for the mm-wave massive multiple-input multiple-output (MIMO). The CE-OFDM is also studied for both optical (Silva et al. 2012, Xie et al. 2016) and power line communications (Rabie et al. 2015) as well as for radar applications (Mohseni 2010).

Simple complex envelope transmitter-receiver models for the CE-OFDM are presented in Figure 6. In CE-OFDM a real signalling is required at the input of the PM,

and thus the frequency-domain OFDM symbols via N-point inverse FFT (IFFT) have to satisfy the Hermitian symmetry (Proakis 2001), and the requirement means that the spectral efficiency is halved. The discrete cosine transform (DCT) (Thompson et al. 2008) and the fast Hartley transform (FHT) (Fabrega et al. 2013) are also used to furnish a real OFDM signal. The DCT and the FHT have no symmetry requirement, but only real constellations (Proakis 2001) such as BPSK can be used. While the subcarrier data modulation in LTE systems is QPSK or MQAM, the wireless local area network (WLAN) (IEEE 802.11 2012) and the WiMAX (IEEE 802.16 2012) are examples of terrestrial standards which support also the BPSK at low SNR. The DVB forward link second generation extension (S2X) (Eroz et al. 2015) proposes also the BPSK for high attenuation satellites. The wireless personal area network (WPAN) (IEEE 802.15.4 2011) uses the robust BPSK (Hanzo et al. 2003) in very low data rate solutions. Therefore, the binary modulated CE-OFDM can be seen as an interesting candidate for the 5G scenarios (Fettweis 2014) when the power efficiency is a more important parameter than the spectral efficiency.

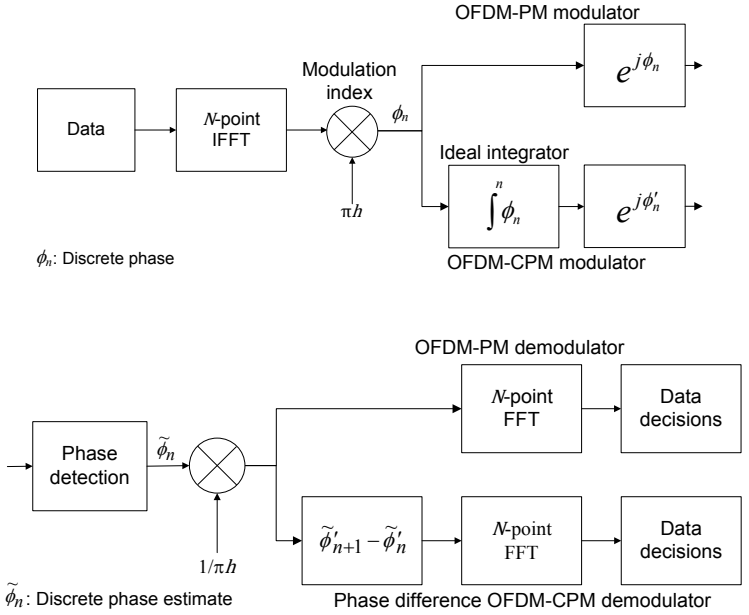

Figure 6. Simple transmitter-receiver structures for the CE-OFDM.

For CE-OFDM, PM can be implemented via FM and vice versa (Lathi 1983). A simple arctangent phase demodulation provides the instantaneous phase which is restricted to the -π to +π range. PM can be also detected without the phase ambiguity by an FM discriminator followed by an integrator. An ideal discriminator is a

differentiator followed by an envelope detector, and since interference and noise perturb the signal amplitude, a limiter is needed (Schwartz et al. 1966). The detection performance and spectral spreading can be controlled using a modulation index (Thompson et al. 2004). The performance gains can be accomplished by increasing the index value. On the other hand, the small and high modulation indices h refer to narrowband and wideband signals, respectively. The modulation index tradeoff is limited by the threshold effect (Ziemer & Tranter 1995) that occurs when the SNR at the detector input decreases below a critical level. Below the threshold, there are occasions when randomly varying noise is large enough to occasionally encircle the origin resulting in a 2π phase shift rotation in the resultant phase. This new type of noise is known as click noise in FM resulting in spikes in the demodulated FM signal or cycle slips in the demodulated PM signal (Ahmed et al. 2007). The multiplicative phase noise disturbance $e^{j\theta}$ causing ICI in the OFDM transforms just into an additive phase term θ in the phase detector of the CE-OFDM. Thus, the CE-OFDM has significant advantage compared to the OFDM.

The spectrum of wideband FM is known to be Gaussian shaped (Schwartz et al. 1966), and the narrowband FM spectrum consist of a carrier term and the original modulating spectrum shifted up symmetrically about the carrier frequency. The spectral peak at the carrier may be used in detection as a carrier phase reference, but otherwise it does not contain information about the data. The FM and PM spectra have a relationship if the phase is band-limited because the frequency is derivative of the phase. In a complex domain, the wideband signal rotates relative to the origin while the unity amplitude narrow band signal rotates close to the point (1, 0) causing the DC offset. A general closed-form expression for the power density spectrum is not available for CE-OFDM. However, the spectrum can be made to meet the OOB mask by decreasing the modulation index. The spectral precoding technique is also proposed for CE-OFDM with an aim to suppress side lobe powers more effectively (Chung 2010). If the spectrum is flat, it may cause less co-channel interference (CCI) than the power is concentrated in one frequency. This kind of phenomenon is considered in the case of unwanted spectral components of intermodulation products in (Spilker 1977). In the PM, the spectral peak vanishes when memory is added via the CPM but at the cost of the need of ML Viterbi receiver (Viterbi 1967). A simple phase difference receiver for CE-OFDM (Tan & Stüber 2002) suffers from degraded performance. The DC offset and spectral peak can be also subtracted (Razavi 1988) and high pass filtered (Wilson et al. 1991) from the transmitted signal, but then the constant envelope property is lost. High pass filtering introducing also ISI (Spilker 1977). In adaptive DC offset compensation (Faulkner et al. 1991), the received complex samples are corrected before the detector.

If the bandwidth of OFDM subcarriers becomes small enough compared to the coherence bandwidth of the channel, the individual subcarriers can be assumed to experience flat fading which allows for simple equalization. In CE-OFDM, the data symbols are spread out over the frequency domain (Thompson et al. 2008), and an equalizer is basically needed prior to nonlinear phase or frequency demodulation (Ahmed et al. 2008). However, depending on the channel condition, such as the 2-

path model with a weak secondary path, equalization might not be required, therefore reducing receiver complexity. For the constant phase error, the FFT generates just a DC value in the receiver to be just ignored (Thompson et al. 2005). Beamforming can also be used to mitigate multipath effects, thus reducing the need for complex equalization (Williamson et al. 1997). Finally, FM, PM and CPM are examples of nonlinear exponential modulation, and for OFDM the nonlinearities cause in- and out-band distortions. CPM and FM have also memory and this unavoidably introduces the ISI.

2.2.3 Trellis-coded modulation (TCM)

Historically, error control coding and modulation have been treated as distinct subjects. However, in a visionary paper Massey (1974) surmised that error control coding and modulation could be treated as an integrated entity. This would allow significant coding gains to be achieved over power and bandwidth limited systems. The first practical coded modulation scheme was proposed by Imai and Hirakawa (1977), followed by Ungerboeck (1982), who introduced first the term trellis-coded modulation (TCM). The simple TCM schemes improve the robustness of digital transmission against additive Gaussian noise by 3 dB, without requiring more power or bandwidth (Biglieri 1986) compared to the conventional uncoded modulations. With more complex TCM schemes, gains of up to 6 dB can be achieved (Ungerboeck 1987). The original trellis-codes were based on one- and two-dimensional signal constellations. From the 1980's to the present numerous publications on TCM have appeared in the literature. Multidimensional trellis-codes, e.g., were first used by Wei (1987) and Calderbank and Sloane (1986), and they are based on the idea that with the given energy the distance between the signal points can be increased. From the application point of view, the TCM schemes have been considered for satellite communications, land- and satellite-mobile services, cellular and personal communications services (PCS), as well as for high frequency (HF) tropospheric long range and optical communications among others (Schlegel & Perez 2015). The standard examples include high speed short range WPAN (IEEE 802.15.3 2003) and European Computer Manufacturers Association (ECMA) (ECMA 387 2010) at 60 GHz (Rappaport et al. 2015). In addition to communications, a recent paper from Ungerboeck's group (Oh et al. 2013) studies the TCM for flash memories.

TCM allows the construction of codes whose minimum Euclidean distance significantly exceeds the minimum spacing of the uncoded modulation signal set at the same power. Assume that k information bits are to be TCM encoded. According to Figure 7, $\hat{k} \leq k$ bits are expanded by a rate $\hat{k}/(\hat{k}+1)$ binary convolutional encoder into $\hat{k}+1$ coded bits. These coded bits select one of $2^{\hat{k}+1}$ subsets of a redundant 2^{k+1} -ary signal set. The remaining rate $k-\hat{k}$ uncoded bits determine which of the $2^{k-\hat{k}}$ signals in this subset is to be transmitted. In this thesis a special attention is given to a rate-2/3 convolutional encoder that has the constraint length $v = 3$ and

the corresponding 8-state (2^{ν}) trellis-code is used in conjunction with two-dimensional 32 point cross (32-CR) constellation. The constraint length represents the number of bits in the encoder memory that affect the generation of the output bits. A smaller code rate and a longer constraint length mean increased complexity. Under the assumption that the channel is known, the optimum ML receiver for the TCM scheme can be implemented using the Viterbi algorithm.

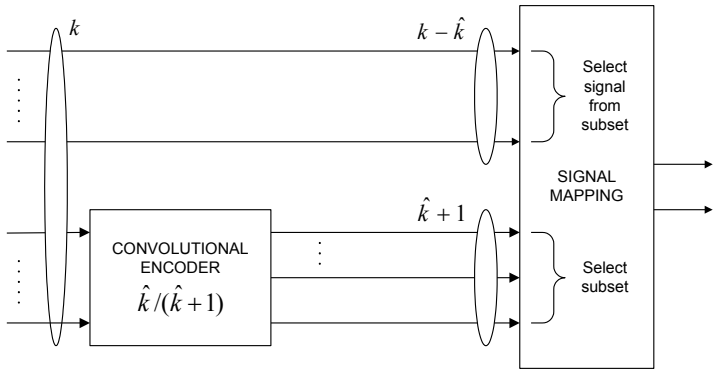

Figure 7. General structure of encoder/modulator for trellis-coded modulation.

The 32 CR TCM scheme achieves an asymptotic coding gain of 4 dB compared to 16QAM, and it is adopted by the ITU Telecommunication Standardization Sector (ITU-T) in the V.32 standard for high speed voiceband modems (Forney 1992). The trellis-code of the V.32 is a variant of Ungerboeck's (1982) original one, so that Ungerboeck's trellis-code is linear while the convolutional encoder in the V.32 modem is nonlinear (Biglieri et al. 1991). With the linear trellis-code, it is only possible to have either no or π rotational invariance. Since many carrier phase synchronization methods exhibit multiples of $\pi/2$ rad phase ambiguity in the recovered carrier phase, it is desirable to have fully rotationally invariant trellis-codes (Wei 1987). The V.32 modem is widely in use and serves as a benchmark for other power and bandwidth efficient modulation schemes. In fact, the recent wired users of TCM are now in digital subscriber line (DSL) technology and its successor called as the fast access to subscriber terminals, in short, the G.fast (Timmers et al. 2013). The letter G stands for the ITU-T G series of recommendations (ITU-T G.9701, 2014). Especially, the latest extension the XG-fast is seen as a cost-effective multi-gigabit backhaul for future 5G wireless networks allowing copper asset reusability in the last meters without being detrimental to performance and speed of fibre (Coomans et al. 2015). In the DSL applications, OFDM subcarriers are coded sequentially by using specially designed TCM. The concept of TCM-OFDM is presented in (Saito et al. 1992).

In general, TCM schemes are sensitive to error bursts caused by the fading and impulse noise. Each incorrectly chosen path in the Viterbi algorithm produces an error burst. Also as a consequence of a phase slip (Esteves & Sampaio-Neto 1997) a burst of errors occurs. In more detail, the TCM scheme may become a catastrophic code (Viterbi & Omura 1979) in the presence of phase noise. There may be no difference in distance between a long segment of received signals and two distinct trellis paths. In this thesis, and as shown in Figure 8, the PSP (see Section 2.2.1.2) is used for carrier phase estimation with multiple trellis-coded modulations (MTCM) (Biglieri et al. 1991). In MTCM different alphabet sizes *M* for the transmitted symbols are used, and the carrier phase estimation is obtained only from the smaller alphabet sizes symbols, which are less sensitive to phase error. Also the Reed-Solomon (RS) (Reed & Solomon 1960) codes are popular linear block codes for applications in burst environment. The concatenation (Forney 1967) of inner TCM with outer RS coding has been extensively studied in the literature. An interleaver is also usually added between the two codes to spread error bursts across a wider range. The non-binary RS code is specified as $\mathrm{RS}(l, \mathrm{s})$ with k-bit symbols. The encoder takes s data symbols and adds parity symbols to make l symbols codeword. A RS decoder can then correct up to $(l - \mathrm{s})/2$ symbols that contain errors in a codeword. RS codes belong to a subclass of cyclic BCH codes where the acronym BCH comprises the initials of the inventors Hocquenghem, Bose and Ray-Chaudhuri and Hocquenghem (Biglieri et al. 1991). Cyclic codes can be easily generated using shift registers. When TCM is not constant envelope, the requirements for the amplifier linearity are more severe (Van Nee & Prasad R. 2000). The combined constant envelope CPM and TCM (Sari et al. 1994) leads to a combined trellis whose number of states is given by the product of the numbers of states of the CPM phase trellis and the code trellis. As discussed in Section 2.2.1, to avoid increase in complexity, reduced complexity receivers are used in practice.

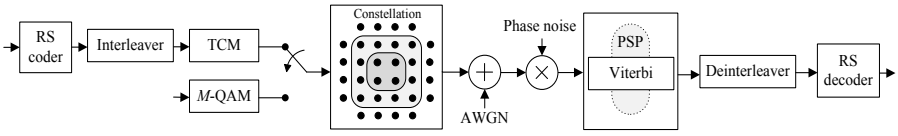

Figure 8. MTCM with concatenation coding.

3. Summary of new results in publications

3.1 A real-time simulation of impairments in the analog parts of the transmitter-receiver

Publication I considers the models for nonlinear analog parts of the transmitter-receiver and proposes that the practical performance simulations of the any communication system take them into account. Realistic models of nonideal parts are needed since the future high data-rate systems are complicated and the impact of the impairments cannot be calculated analytically. It is found that it is usually much simpler to simulate systems without memory than those with memory. A system model for the typical analog impairments at each stage of the transmitter and the receiver with a channel is presented in Figure 1. In order to make a prioritization for the distortions, the following classification is proposed: 1) nonlinear power amplifiers; 2) mixers and oscillators including phase noise, I/Q imbalance and DC offset. The classification includes the expected major problems in future systems where the signals have a nonconstant envelope, such as OFDM where the symbols are also exceptionally long. The high level block diagrams for the selected nonlinearities are presented and their hardware implementations for real time simulation are considered. For example, the AM/AM and AM/PM conversion functions of nonlinear PAs will be known in practice only empirically from the measurements, and in the hardware implementation the measured data can be digitized and then stored into look up tables, as illustrated in Figure 9. Coordinate rotation digital computer (CORDIC) algorithm is for one an iterative and computationally efficient algorithm for computing rectangular to polar translations using combiners and shifters. In general, the real time simulation allows the long simulation times with computing software, such as MATLAB, to be essentially shortened.

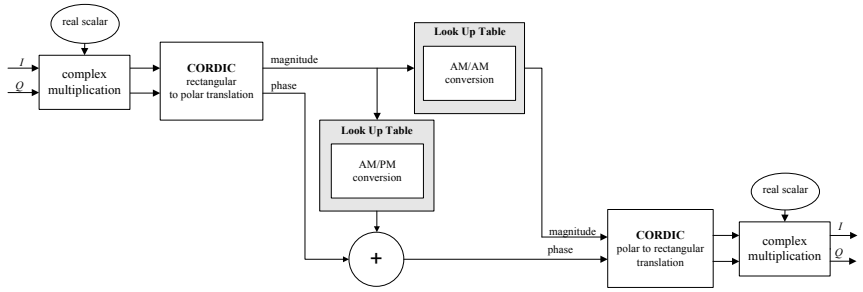

Figure 9. Implementation of PA nonlinearity with look up tables. Redrawn from Publication I. ©[2005] IEEE.

3.2 Constant envelope multicarrier modulation: Performance evaluation in AWGN and fading channel

Publication II considers CE-OFDM which allows PA to operate near saturation levels thus maximizing power efficiency. Transmitter and receiver model for PM signalling is presented in Figure 10; analysis on an AWGN channel determines the performance boundaries. In more detail, the simulation results show that a simple phase difference receiver for the CPM suffers from a 3 dB performance loss. A maximum-ratio combiner (MRC) can be used at the binary data receiver when time domain real signalling for the PM is achieved via the Hermitian symmetry in the frequency domain. The assumption of nearly ideal beamforming reduces the ISI, and CE-OFDM is shown in Figure 11 to perform comparably to MSK and outperform the OFDM in typical 60 GHz fading channel. The CE-OFDM symbols are spread out in the frequency domain while the deep faded subcarriers dominate the performance in the OFDM. In multipath fading channel an equalizer is basically needed prior to phase detector in the CE-OFDM receiver. A frequency domain equalizer requires additional complex *N*-point FFT and IFFT operations, and complexity evaluation in terms of number of real multiplications is carried out. If feedforward filter is required at the time domain decision feedback equalizer of the MSK, the complexity may exceed that of the CE-OFDM receiver. However, depending on the channel condition, such as a weak secondary path, equalization might not be required, therefore reducing receiver complexity.

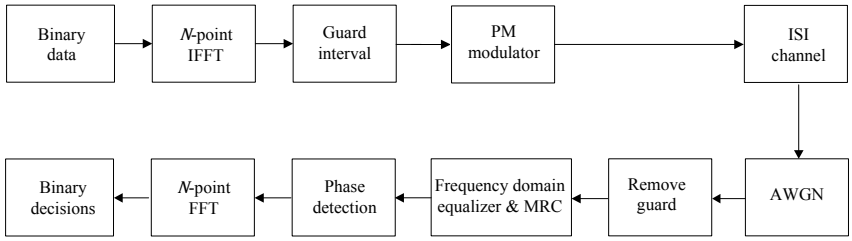

Figure 10. System model for OFDM-PM with ISI. Redrawn from Publication II. ©[2005] IEEE.

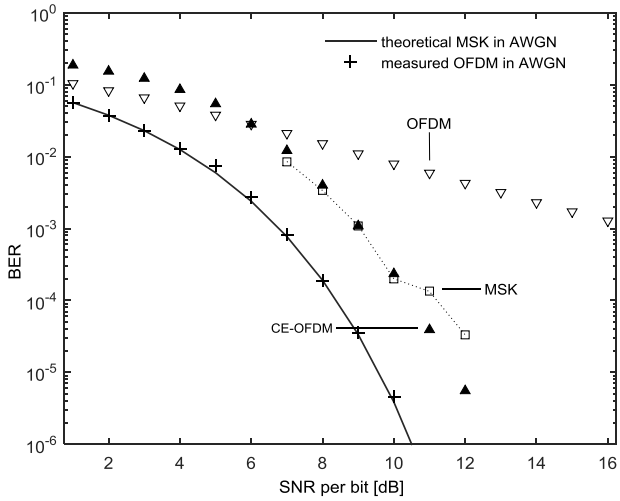

Figure 11. Performance of MSK, OFDM and OFDM-PM in ISI. Redrawn from Publication II. ©[2005] IEEE.

3.3 Digital signal design and nonlinear distortions in antenna array beamforming

Publication III considers the effects of nonlinear analog parts of the transmitter-receiver. The considered impairments are caused by nonlinear amplifiers and oscillators' phase noise. A general system model for the adaptive antenna arrays is presented in Figure 12. At each antenna element the RF phase shifters of Figure 3 provide antenna weights for adaptive beamforming. This work was first to show that there are no impairments in the beamforming if there is oscillator's phase noise at the input of the antenna array. The distortions in beamforming are demonstrated using array factor graphs, as illustrated earlier in Figure 4. Anyhow, the phase noise may dramatically distort the signal constellation. When the separate antenna elements include nonlinear amplifiers with different AM-AM and AM-PM conversions, there are errors in the level of main beam and in the direction of the main beam, respectively. As an example, Figure 13 shows deviation of the AM-AM conversion functions in the 1-dB compression point where the input amplitude results in a 1-dB decrease in gain referenced to the amplifier's linear gain. In practice, a careful device to device design on a single die may lead to deviation of only a very few per cent. It is illustrated in Figure 2 that, due to memory in nonlinear amplifier, each point of the signal constellation becomes a cluster showing ISI. The saturation is also shown to cause warping. Finally, our simulations show that pulse shaping filtering has an impact on the PAPR of linear modulations such as QPSK.

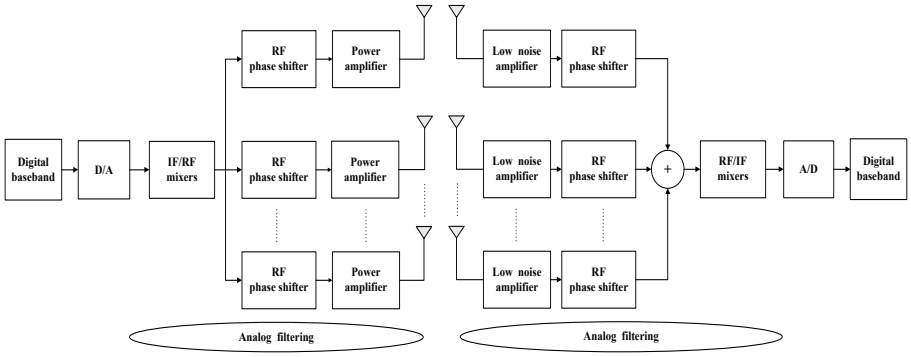

Figure 12. System model for adaptive antenna array. Redrawn from Publication III. ©[2009] IEEE.

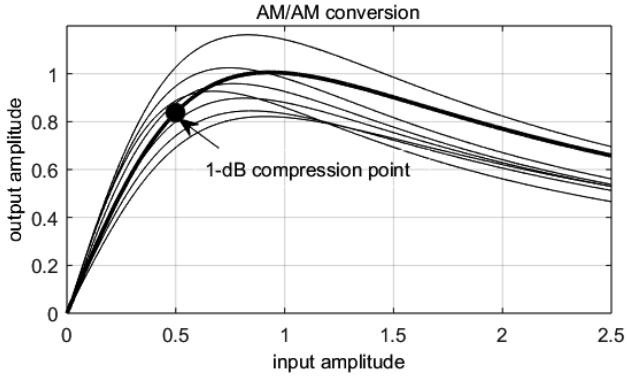

Figure 13. Deviations in AM/AM conversions of nonlinear PA. Redrawn from Publication III. ©[2009] IEEE.

3.4 Receiver structure and estimation of the modulation index for tamed frequency modulated (TFM) signals

Publication IV considers TFM which belongs to the class of jointly spectral and power efficient constant envelope CPM schemes. TFM is a particularly interesting modulation since the spectral OOB radiation is very low. In the FM implementation of Figure 5, the modulation index h is calibrated to have a nominal value of 0.5, but due to temperature variations of analog components it can drift causing time varying phase jitter. A modulation index estimator in the coherent receiver is needed if a simple transmitter is assumed. A digital implementation for the TFM receiver is proposed in Figure 14, and the modulation index estimation is based on the TFM rule and on the symbol decisions made by the joint reduced state sequence detector (RSSD) and PSP carrier phase estimation. The value of the modulation index can be estimated continuously, and the estimator has acquisition and tracking ability as illustrated in Figure 15. The estimation allows making the modulation index in the receiver congruent with the modulation index of the transmitter. The estimated index can be sent to the transmitter, which may correct the modulation index in accordance with the information obtained to be closer to the defined nominal value. Finally, several steps are taken to optimize the performance of the coherent receiver with the modulation index estimator, and it can be observed from Figure 16 that the proposed method has less than 1 dB performance degradation compared to around 4.5 dB exploiting only the PSP estimation on an AWGN channel.

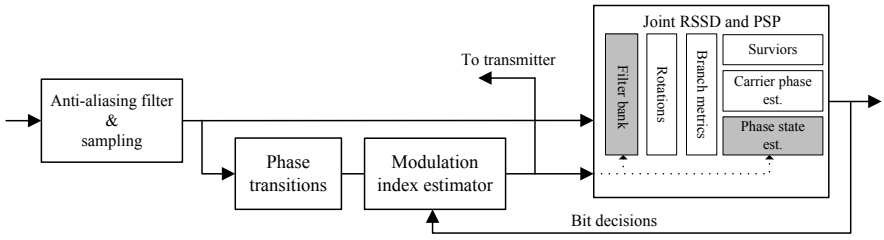

Figure 14. TFM receiver with estimators. Redrawn from Publication IV. ©[2014] Elsevier.

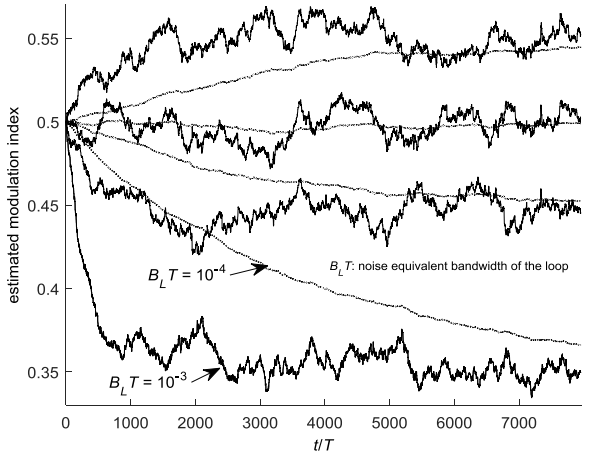

Figure 15. Acquisition and tracking in modulation index estimation. Redrawn from Publication IV. ©[2014] Elsevier.

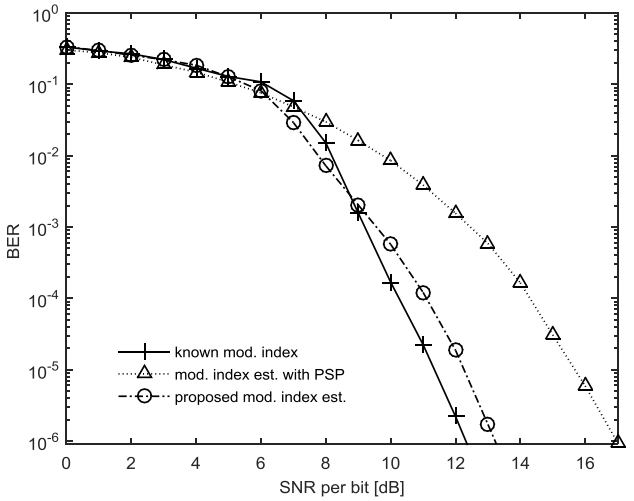

Figure 16. BER performances for modulation index estimation. Redrawn from Publication IV. ©[2014] Elsevier.

3.5 Multiple trellis-coded modulation, per-survivor processing and Reed-Solomon coding in the presence of phase noise

Publication V considers TCM which is a traditional combined coding and modulation technique for power and spectral limited systems. However, due to the phase error a TCM scheme may become a catastrophic code. The starting point for the study is a state-of-the art 8-state 32-CR TCM scheme, and the analysis in an AWGN channel determines the performance boundaries. For comparison results for a 16-state scheme are illustrated, too. The phase noise is modelled as a zero mean, nonstationary, asymptotically infinite power Wiener process. The phase noise has a multiplicative effect on the signal, and it is illustrated in Figure 17 that the spectrum of sinusoid is Lorentzian. A receiver structure for combined MTCM, PSP, and RS is earlier presented in Figure 8. Phase acquisition (transient state) and tracking (steady state) performances are studied. The BER simulations results shown in Figure 18 of the steady state show that a simple combined MTCM, PSP and RS scheme has around 3 dB advantage compared to the pure 32-CR TCM and PSP in the presence of phase noise. For the latter case, the S-curve simulations of Figure 19 in the transient state demonstrate spurious equilibria and extensive dead zones which may cause a long random walk for the estimator before locking. A semianalytical approach is used in the case of RS, and since the measured results meet the semianalytical ones very well, the proposed approach can be used to determine the rate of RS coding in detail.

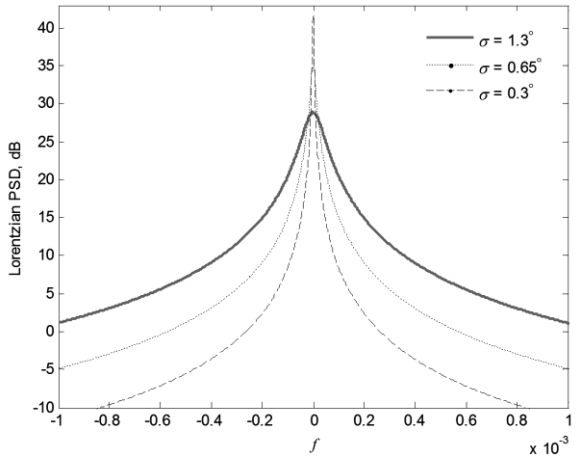

Figure 17. The Lorentzian PSD with different standard deviation σ values. Redrawn from Publication V. ©[2015] Elsevier.

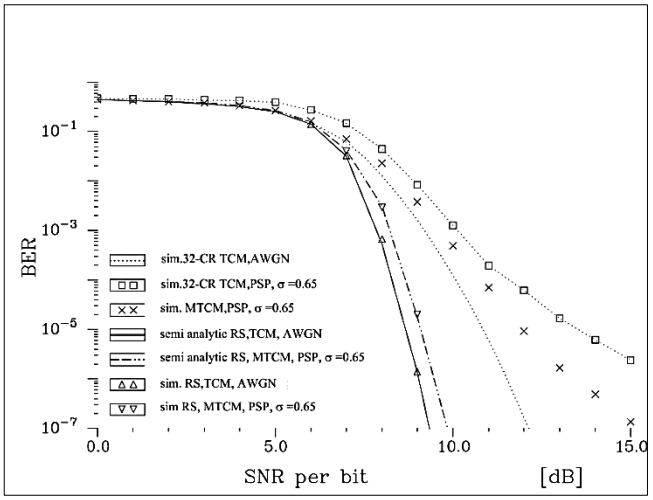

Figure 18. BER for combined MTCM, PSP, and RS in presence of phase noise. Redrawn from Publication V. ©[2015] Elsevier.

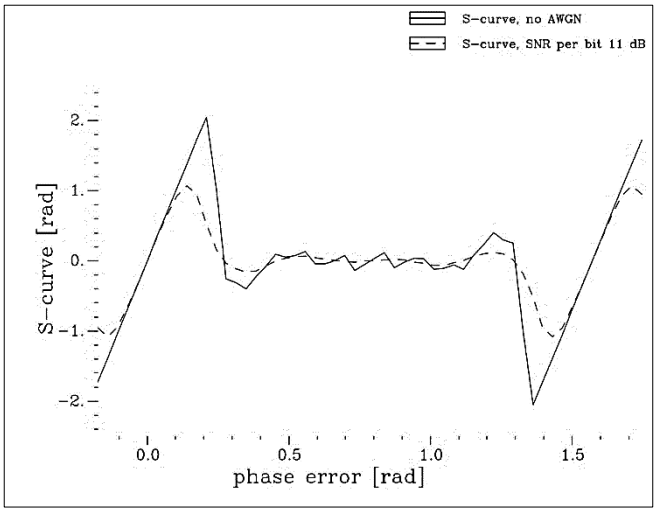

Figure 19. S-curve of the 32-CR TCM. Redrawn from Publication V. ©[2015] Elsevier.

3.6 Power efficiency, phase noise, and DC offset in constant envelope OFDM transceivers

Publication VI considers the CE-OFDM which allows PA to operate near saturation levels. The enhanced PA efficiency enables battery to be smaller or last longer in mobiles devices. We analyse and compare the power consumption in CE-OFDM and OFDM systems with the knowledge of PAs efficiency, distribution of input signal envelope and the amount of backoff. The transceiver power efficiencies are then compared by measuring the BER as a function of average PA input SNR so that the effects of the PA nonlinearities are taken into account in the performance evaluation. The simulation results in Figure 20 show that with a typical satellite PA, the CE-OFDM can have up to 6.0 dB gain compared to the OFDM. This is beneficial especially in a channel having high attenuation. With the terrestrial PA the gain up to 2.5 dB can be achieved.

Simple transmitter and receiver structures for CE-OFDM are considered by keeping in mind that the practical key factor for the rapid uptake of the OFDM enabled 5G systems is the maximization of the technology commonalities. A special attention is given on the binary data modulated CE-OFDM when the SNR is low and when the robustness is a more important design criterion than the high data rate. The block diagram in Figure 21 demonstrates that the structure of the CE-OFDM system fundamentally allows for a significant advantage compared to the very phase noise sensitive OFDM. The phase noise θ has no notable effect to the BER performance of CE-OFDM since the phase noise transforms just into an additive noise term in the phase detector. Finally, a simple method for removing the DC offset in CE-OFDM is presented. As shown in Figure 22, the proposed technique spreads out the peak power over the entire frequency band and preserves the constant envelope nature of the signal. The simulation results show several dB of improvement in channel estimation.

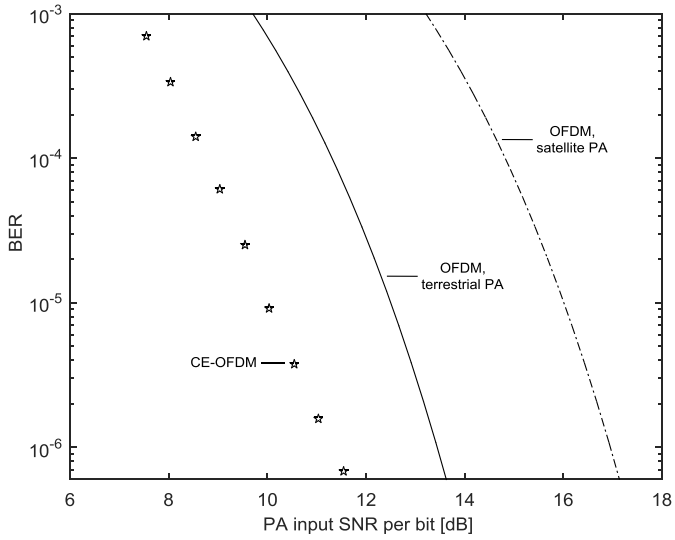

Figure 20. Transceiver efficiencies as BER for OFDM and CE-OFDM. Redrawn from Publication VI. ©[2016] John Wiley & Sons Ltd.

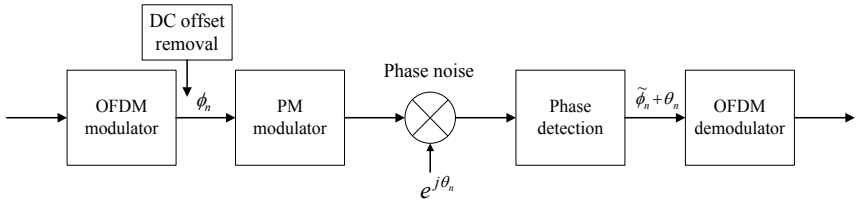

Figure 21. Impact of phase noise in the CE-OFDM. Redrawn from Publication VI. ©[2016] John Wiley & Sons Ltd.

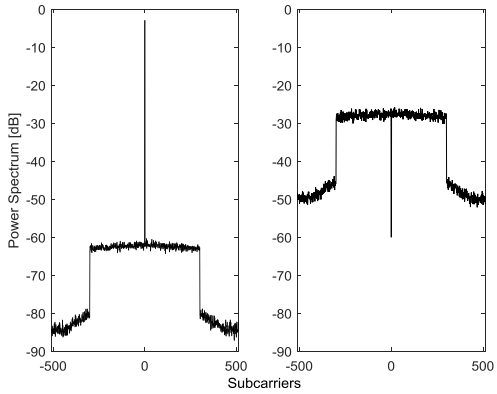

Figure 22. CE-OFDM spectrum with the peak (left) and with the dc offset removal (right). Redrawn from Publication VI. ©[2016] John Wiley & Sons Ltd.

4. Discussion

4.1 Main findings of the thesis

Both the physical channel itself and the nonlinear analog parts of the transmitter-receiver are sources of noise and distortions, and practical performance simulations of the any communication system take both of them into account. This thesis has presented the typical analog impairments at each stage of the transmitter and the receiver. In order to make a prioritization for the distortions, the following classification is proposed: 1) nonlinear power amplifiers; 2) mixers and oscillators including phase noise, I/Q imbalance and DC offset. The classification includes the expected major problems in future systems where the signals have a nonconstant envelope, such as OFDM where the symbols are also exceptionally long.

In general, the nonlinearities cause in-band and OOB distortions to the transmitted signal and effects of distortions can be measured and illustrated using, e.g., BER and power spectra diagrams. In this thesis, the effects of nonlinearities on beamforming are highlighted using array factor graphs. This work was first to show that there are no impairments in the beamforming if there is oscillator's phase noise at the input of the antenna array. Anyhow, the phase noise may dramatically distort the signal constellation. When the separate antenna elements include nonlinear PAs with different AM-AM and AM-PM conversions, there are errors in the level of main beam and in the direction of the main beam, respectively.

This thesis has focused on constant envelope signalling to minimize nonlinear effects of nonlinear PA. In the studies, further development of the OFDM has been selected as the starting point since the one key factor for the rapid uptake of the future 5G systems is the maximization of technology commonalities with existing OFDM based systems. A novel 5G transceiver would include both more spectral efficient OFDM and more power efficient CE-OFDM modes. Adaptive radio might select the more applicable mode. Especially, the CE-OFDM schemes might be useful for outdoor and indoor coverage prioritized low cost massive MTC scenarios. On the other hand, the CE-OFDM might be also useful for mm-wave scenarios with high requirements on transceiver power efficiency and robustness to RF nonlinearities, but with modest requirements on spectral efficiency due to large available bandwidth and ultra-dense network (UDN) enabled by short transmission distances. In this thesis we have shown the advantage of the CE-OFDM with typical satellite and terrestrial PAs by measuring the transceiver power efficiency using the BER as a function of average PA input SNR so that the effect of PA efficiency is taken into account in the performance evaluation. The enhanced PA efficiency is good for range and mobile battery life. In the literature, the CE-OFDM has been studied for both optical and power line technologies which will enable future smart grid applications having direct impact on human life and critical infrastructures. Integration of wired and wireless systems will take advantage of the OFDM based waveform design synergies by exploiting the key findings of both systems. The CE-OFDM is also a way to retrofit existing FM systems for broadcasting, public safety and private

mobile radio communications. This thesis also illustrates with block diagrams that the structure of the CE-OFDM system fundamentally allows for a significant advantage compared to the very phase noise sensitive OFDM. The phase noise transforms just into an additive noise term in the phase detector. Concerning signal waveform, a DC offset causing a spectral peak at the carrier is an inherent property of the phase modulated CE-OFDM. This work was first to present a dedicated DC offset removal technique for the CE-OFDM signals at all, and especially at the transmitter. The proposed technique spreads out the carrier peak power over the entire frequency band and preserves the constant envelope nature of the signal. In the LTE one signal quality parameter is the spectral flatness of the channel estimation is shown to benefit from in this thesis.

In FM and PM, the detection performance and spectral spreading is controlled using a modulation index. In principle, CPM has better spectral containment at the cost of complex ML Viterbi receiver. In a simple analog implementation the modulation index deviates during the transmission and generates time varying phase jitter. In this thesis a modulation index estimator in conjunction with the PSP is presented for the constant envelope TFM who has a very small OOB radiation compared to other known CPM methods. The presented estimator has shown to lead to enhanced detection performance, and it has both acquisition and tracking ability. The estimate might also be sent to the transmitter, which may correct the modulation index in accordance with the information obtained to be closer to the defined nominal value. Recently, the combination of CPM and SC-FDMA has been suggested as an alternative candidate to the LTE uplink modulation which inherits the benefits of both modulations. Regarding the 5G OOB radiation challenges we see that TFM is worth trying. As a stand-alone single carrier technique, the power efficient TFM is appealing for applications where simple transmitter, battery life or long-range communications are the presiding concerns.

Finally, concerning the phase noise and the PSP, this thesis provides also new results and findings on TCM which is a traditional combined coding and modulation method for spectral and power limited systems. TCM scheme may become a catastrophic code. This work was the first to propose a fully integrated MTCM, PSP, and RS system. The performance benefit of the method in the presence of phase noise is shown both semianalytical and measured simulation results. Our results and findings for the TCM are valuable when we are emphasising the maximization of technology commonalities. For example, TCM has recently gained attention in hybrid fiber-copper deployments enabling a cost-effective multi-gigabit backhaul for future 5G wireless networks. When TCM is also added to the wireless transmission, the applications of OFDM can be further expanded.

4.2 Limitations and recommendations for future work

There are some limitations associated with the studies presented here. Many of these could be assumed as topics for future work. Therefore, recommendations for the further work are also discussed.

One requirement of OFDM transmitting and receiving systems is that they must be linear. The FM, PM, and CPM are examples of nonlinear exponential modulations, and therefore the nonlinearity will impair the orthogonality in CE-OFDM. What is an optimal nonlinear description, which provides a constant envelope signal, and which avoids as much as possible the spectral spreading and the ISI? The proposed CE-OFDM is a good approximation to this theoretical objective deserving, however, an own analytical study. In this thesis we have assumed that the nonlinear properties change slowly due to, e.g., temperature changes. On the other hand, the temperature may change rapidly with a transmitter power control. This topic is left for further work. While higher order constellations are usually used in the subcarrier modulation, the binary modulation is selected for CE-OFDM for simplicity. We justify the choice with the scenarios where the robustness and power efficiency are more important than the spectral efficiency. In a multipath fading channel, a frequency domain equalizer is basically needed prior to phase or frequency demodulation. However, depending on the channel condition equalization might not be required, therefore reducing receiver complexity. A simulation campaign, e.g., with a weak secondary path is left for the further study. In this thesis, the focus has been on single antenna transmission. Only the analog impairments in the antenna array beamforming are discussed or nearly ideal beamforming is assumed to mitigate multipath effects. Our results can be seen to serve future MIMO investigations.

We have shown that a two-dimensional MTCM with the PSP and concatenated RS coding performs well in an AWGN channel, in which phase offset or time varying phase noise is introduced. In practice, the concatenated codes require a symbol interleaver between them, and in our study we have assumed an ideal interleaver. Therefore, an interleaver study in the case of channel or nonlinearity with memory is an interesting future research topic. In this work a special attention is given to a two-dimensional TCM scheme but the work can be extended to any multidimensional trellis-codes. In this thesis we present a novel scheme to measure and control the modulation index in a coherent TFM receiver based on the joint RSSD and PSP. The estimate is used to replace the nominal index value in the receiver, but the estimate could be sent to the transmitter, too. Considerations of the feedback and nonideal feedback channel and their effects on the performance could be a topic for future work. The performance of TFM could even be more improved by the use of coding techniques, but this task is left for further work.

5. Summary

The requirements for the 5G vary by applications but will include data rates ranging from very low sensor data to very high video content delivery, stringent low latency requirements, low energy consumption, and high reliability. There is consensus that these goals cannot be met with one single technological solution. However, the maximization of technology commonalities is one key factor for the rapid uptake of new systems and standards. Due to the scarcity of spectrum 5G systems are operating in higher frequencies than the 4G systems. On the other hand, the mm-wave communications suffer from propagation loss, and the analog components are subject to RF impairments. This thesis has made the state-of-the-art review and brought contributions to the waveform design for 5G systems in the presence of analog nonlinearities.

For OFDM evolution we have studied CE-OFDM where phase modulation creates a constant envelope, and the PA can therefore operate at the optimum saturation point to maximize average transmitter power (good for range) and PA efficiency (good for battery life). We have shown the advantage of CE-OFDM compared to OFDM by evaluating the transceiver power efficiency. The effect of the PA efficiency is taken into account by determining the BER as a function of average PA input SNR in the performance simulations. We have demonstrated that since the phase noise transforms just into an additive noise term after the phase detector, CE-OFDM is very resistant to phase noise unlike OFDM. The novel DC offset removal is developed to enhance spectral flatness and performance of channel estimation. Overall, CE-OFDM can be seen as an interesting candidate for the 5G scenarios when the power efficiency is a more important parameter than the spectral efficiency.

With an assumption of nearly ideal beamforming CE-OFDM is shown to outperform OFDM in typical 60 GHz fading channel since the symbols are spread out in the frequency domain. However, an equalizer prior to the nonlinear phase demodulation is needed. A simple way to make beamforming is to use RF phase shifters at each antenna element, and this work was first to show that there are no impairments in the beamforming if there is oscillator's phase noise at the input of the antenna array. Anyhow, the phase noise may dramatically distort the signal constellation. When the separate antenna elements include nonlinear amplifiers with different AM-AM and AM-PM conversions, there are errors in the level of main beam and in the direction of the main beam, respectively.

In phase or frequency modulation spectral spreading and detection performance are controlled using a modulation index. In a simple analog implementation, the modulation index deviates during the transmission and generates time varying phase jitter. In this work a modulation index estimator in conjunction with PSP carrier phase estimation is presented for the inherently constant envelope TFM which has also very small spectral OOB radiation compared to other known CPM methods. The value of the modulation index can be estimated continuously, and the estimator has acquisition and tracking ability. The estimation allows making the modulation index in the receiver congruent with the modulation index of the transmitter. The

estimated index could be sent to the transmitter, too. Concerning the phase noise and the PSP carrier phase estimation, thesis provides also new results and findings on TCM which is a traditional combined coding and modulation technique for spectral and power limited systems. A novel scheme based on the MTCM, PSP and RS is shown to prevent the trellis-code to become a catastrophic code in the presence of phase noise. A semianalytical approach is applied to verify the simulation results. In general, TCM and CPM modulations can complement future adaptive OFDM based 5G systems.

6. References

5G PPP. 2016. A white paper on 5G empowering vertical industries [Online]. Available: http://ec.europa.eu/newsroom/dae/document.cfm?doc_id=14322.

Ahmed U., Thompson S. C., & Zeidler J. R. 2007. Threshold extending receiver structures for CE-OFDM. In Proc. IEEE MILCOM, pp. 1-7.

Ahmed U., Thompson S. C., & Zeidler J. R. 2008. Channel estimation and equalization for CE-OFDM in multipath fading channel. In Proc. IEEE MILCOM, pp. 1-7.

Anderson J. B., Aulin T., & C.-E. Sundberg. 1986. Digital phase modulation. Plenum Press, New York, USA.

Anderson R. R. & Salz J. 1965. Spectra of digital FM. Bell Syst. Tech. J., vol. 44, pp. 1165-1189.

Andrews J. G., Buzzi S., Choi W., Hanly S. V., Lozano A., Soong A. C. K., & Zhang J. C. 2014. What will 5G be? IEEE J. Sel. Areas Commun., vol. 32, pp. 1065-1082.

Anwar K., Hara T., Okada M., & Yamamoto H. 2007. Digital terrestrial television transmission over OFDM/FM using satellite communications system. Electronics and Communications in Japan, Part 2, vol. 90.

Apilo O., Lasanen M., Boumard S., & Mämmelä A. 2013. Energy efficiency of power-adaptive spatial diversity methods. IEEE Trans. Wireless Commun., vol. 12, pp. 4246-4257.

Armada A. G. 2001. Understanding the effects of phase noise in orthogonal frequency division multiplexing (OFDM). IEEE Trans. Broadcast., vol. 47, pp. 153-159.

Bahl I. J. 2009. Fundamentals of RF and microwave transistor amplifiers. Wiley, NJ, USA.

Baldini G., Karanasios S., Allen D., & Vergari F. 2014. Survey of wireless communication technologies for public safety. IEEE Commun. Surveys Tuts., vol. 16, pp. 619-641.

Bao J., Yafeng Z., & Jianhua L. 2008. Concatenated eIRA codes for tamed frequency modulation communications. In Proc. IEEE ICC, pp. 1886-1891.

Baudin P. 2015. Wireless transceiver architecture: Bridging RF and digital communications. Wiley, Chichester, England.

Bello P. 1963. Characterization of randomly time-variant linear channels. IEEE Trans. Commun. Syst., vol. 11, pp. 360-393.

Bello P. A., Goldfein D., Jauniskis K.P., & Lavely A. 1978. Wideband line-of-sight channel simulator. Final technical report, RADC-TR-78-118. CNR, Inc., Needham, MA, USA.

Bianchi P. & Loubaton P. 2005. On the blind estimation of the parameters of continuous phase modulated signals. IEEE J. Sel. Areas Commun., vol. 23, pp. 944-962.

Bianchi P., Loubaton P., & Sirven F. 2004. Non data-aided estimation of the modulation index of continuous phase modulations. IEEE Trans. Signal Processing, vol. 52, pp. 2847-2861.

Biglieri E. 1986. Ungerboeck codes do not shape the signal power spectrum. IEEE Trans. Inf. Theory, vol. 32, pp. 595-596.

Biglieri E., Divsalar D., McLane P. J., & Simon M. K. 1991. Introduction to trellis-coded modulation with applications, Macmillan Publishing, New York, USA.

Bingham J. 1990. Multicarrier modulation for data transmission: An idea whose time has come. IEEE Commun. Mag., vol. 28, pp. 5-14.

Björnson E., Jorswieck E., Debbah M., & B. Ottersten. 2014. Multiobjective signal processing optimization: The way to balance conflicting metrics in 5G systems. IEEE Signal Processing Magazine, vol. 31, pp. 14-23.

Boccardi F., Heath R., Lozano A., Marzetta T. L., & Popovski P. 2014. Five disruptive technology directions for 5G. IEEE Commun. Mag., vol. 52, pp. 74-80.

Bockelmann C., Pratas N., Nikopour H., Au K., Svensson T., Stefanovic C., Popovski P., & Armin Dekorsy. 2016. Massive machine-type communications in 5G: Physical and MAC-layer solutions. IEEE Commun. Mag., vol. 54, pp. 59-65.

Bogale T. E. & Le L. B. 2014. Beamforming for multiuser massive MIMO systems: Digital versus hybrid analog-digital. In Proc. IEEE GLOBECOM, pp. 4066-4071.

Bölcskei H., Duhamel P., & Hleiss R., 2003. Orthogonalization of OFDM-OQAM pulse shaping filters using the discrete Zak transform. Signal Processing, vol. 83, no. 7, 1379-1391.

Buzid T., Huemer M., & Reinhardt S. 2007. SC/FDE combined with MIMO: An improved out of band power and performance via tamed frequency modulation. In Proc. IEEE Sarnoff Symposium, pp. 1-5.

Calderbank A. R. & Sloane N. J. A. 1986. An eight-dimensional trellis code. In Proc. IEEE, pp. 757-759.

Casas E. F. & Leung C. 1991. OFDM for data communication over mobile radio FM channels - Part I: Analysis and experimental results. IEEE Trans. Commun., vol. 39, pp. 783-793.

Casas E. F. & Leung C. 1992. OFDM for data communication over mobile radio FM channels - Part II: Performance improvement. IEEE Trans. Commun., vol. 40, pp. 680-683.

Chang R. W. 1966. Synthesis of band-limited orthogonal signals for multichannel data transmission. Bell Syst. Tech. J., vol. 45, pp. 1775-1797.

Chen Y., Zhang S., Xu S., & Li Y. 2011. Fundamental trade-offs on green wireless networks. IEEE Commun. Mag., vol. 49, pp. 30-37.

Chevillat P. R. & Eleftheriou E. 1989. Decoding of trellis-encoded signals in the presence of intersymbol interference and noise. IEEE Trans. Commun., vol. 37, pp. 669-676.

Chugg K. M. 1988. Blind acquisition characteristics of PSP-based sequence detectors. IEEE J. Sel. Areas Commun., vol. 16, pp. 1518-1529.

Chung C.-D. 2010. Spectral precoding for constant envelope OFDM. IEEE Trans. Commun., vol. 58, pp. 555-567.

Chung K. 1984. Generalized tamed frequency modulation and its application for mobile radio communications. IEEE J. Select. Areas Commun., vol. 2, pp. 484-494.

Cimini L. J. 1985. Analysis and simulation of a digital mobile channel using orthogonal frequency division multiplexing. IEEE Trans. Commun., vol. 33, pp. 665-675.

Coomans W., Moraes R. B., Hooghe K., Duque A., Galaro J., Timmers M., van Wijngaarden A. J., Guenach M., & Maes J. 2015. XG-FAST: The 5th generation broadband. IEEE Commun. Mag., vol. 53, pp. 83-88.

D'Andrea A. N., Mengali U., & Vitetta G.M. 1993. Multiple phase synchronization in continuous phase modulation. Digital Signal Processing, vol. 3, pp. 188-198.

De Coulon F. 1986. Signal theory and processing. Artec House, Dedham, MA, USA.

Demestichas P., Georgakopoulos A., Karvounas D., Tsagkaris K., Stavroulaki V., Lu J., Xiong C, & Jing Yao. 2013. 5G on the horizon: Key challenges for the radio-access network, IEEE Veh. Technol. Mag., vol. 8, pp. 47-53.

Doan C. H., Emami S., Sobel D. A., Niknejad A. M., & Brodersen R. W. 2004. Design considerations for 60 GHz CMOS radios. IEEE Commun. Mag., vol. 42, pp. 132-140.

ECC Report 199. 2013. User requirements and spectrum needs for future European broadband PPDR systems (Wide Area Networks). Electronic Communications Committee.

ECMA 387. 2010. Standard ECMA 387: High Rate 60 GHz PHY, MAC and HDMI PALs. 2nd edition, ECMA International, Geneva, Switzerland.

Eroz M., Lee L.-N., Loghin N., De Bie U., Simoens F., & Delaruelle D. 2016. New DVB-S2X constellations for improved performance on the satellite channel. Int. J. Satell. Commun. Network., vol. 34, pp. 351–360.

Esteves E. S. & Sampaio-Neto R. 1997. A per-survivor phase acquisition and tracking algorithm for detection of TCM signals with phase jitter and frequency error. IEEE Trans. Commun. vol. 45, pp. 1381-1384.

ETSI Report TS 36.101. 2008. User equipment (UE) radio transmission and reception (Release 8). Version 8.3.0.

Fabrega M., Moreolo M. S, Chochol M., & Junyent G. 2013. Impact of modulator driving on constant envelope optical OFDM based on Hartley transform. IEEE Photon. Technol. Lett., vol. 25, pp. 598-601.

Farhang-Boroujeny B. 2011. OFDM versus filter bank multicarrier. IEEE Signal Process. Mag., vol. 28, pp. 92-112.

Farhang-Boroujeny B. & Moradi H. 2016. OFDM inspired waveforms for 5G. IEEE Commun. Surveys Tuts., Web. 7 Sept. 2016.

Faulkner M., Mattson T., & Yates W. 1991. Automatic adjustment of quadrature modulators. Electron. Lett., vol. 27, pp. 214-216.

Fettweis G. 2014. The Tactile Internet: Applications and challenges. IEEE Veh. Technol. Mag., vol. 9, pp. 64-70.

Fettweis G. & Alamouti S. 2014. 5G: Personal mobile internet beyond what cellular did to telephony. IEEE Commun. Mag., vol. 52, pp. 140-145.

Fettweis G., Krondorf M., & Bittner S. 2009. GFDM—Generalized frequency division multiplexing. In Proc. IEEE VTC Spring, pp. 1-4.

Fettweis G., Löhning M., Petrovic D., Windisch M., Zillmann P., & Rave W. 2007. Dirty RF: A new paradigm. International Journal of Wireless Information Networks (IJWIN)., vol. 14, pp. 133-148.

Fonollosa J. R. & Fonollosa J. A. R. 1993. Estimation of the modulation index of CPM signals using higher-order statistics. In Proc. Int. Conf. Acoustics, Speech, and Signal Processing, pp. 268-271.

Fonollosa J. R. & Nikias C. L. 1993. Analysis of CPM signals using higher order statistics. In Proc. IEEE MILCOM, pp. 663-667.

Forney, G. D. 1967. Concatenated codes. MIT Press, Cambridge, MA, USA.

Forney, G. D. 1992. Advances in modem technology since V.32/V.32bis. In Proc. Int. Conf. on Data Transmission - Advances in Modem and ISDN Technology and Applications, pp. 1-6.

Forney G. D. & Ungerboeck G. 1998. Modulation and coding for linear Gaussian channels. IEEE Trans. Inf. Theory, vol. 44, pp. 2384-2415.

Gagliardi R. M. 1984. Satellite communications. Lifetime Learning Publications. Belmont, CA, USA.

Gardner F.M. & Baker J. D. 1997. Simulation Techniques: Models of Communication Signals and Processes. Wiley, New York, USA.

Gitlin R. D. & Ho E. Y. 1975. The performance of staggered quadrature amplitude modulation in the presence of phase jitter. IEEE Trans. Commun., vol. 23, pp. 348-352.

Glaze D. J. 1970. Improvements in atomic cesium beam frequency standards at the national bureau of standards. IEEE Trans. Instrum. Meas., vol. 19, pp. 156-160.

G´omez-Barquero D., Douillard C., Moss P., & Mignone V. 2014. DVB-NGH: The next generation of digital broadcast services to handheld devices. IEEE Trans. Broadcast., vol. 60, pp. 246-257.

Hanzo L., Münster M., Choi B. J., & Keller T. 2003. OFDM and MC-CDMA for broadband multi-user communications, WLANs and broadcasting. Wiley, Chichester, England.

Hasan M. & Sagar S. M. 2013. Wireless communication through long term evolution (LTE) over satellite channel by using MIMO-OFDM model. In Proc. IEEE ICAEE, pp. 170-175.

Haykin S. 2001.Communication Systems. 4th ed., Wiley, New York, USA.

Haykin S. 2005. Cognitive radio: Brain-empowered wireless communications. IEEE J. Sel. Areas Commun., vol. 23, pp. 201-220.

Hekkala A. 2014. Compensation of transmitter nonlinearities using predistortion techniques. Case studies of envelope tracking amplifiers and radio-over-fibre links. Doctoral dissertation. VTT Science 53.

Hubka V. & Eder W. E. 1988. Theory of technical Systems: A total concept theory for engineering Design. Springer-Verlag, New York, USA.

IEEE 802.11. 2012. IEEE standard for information technology - telecommunications and information exchange between systems local and metropolitan area networks - specific requirements - part 11: Wireless LAN medium access control (MAC) and physical layer (PHY) specifications.

IEEE 802.15.3. 2003. IEEE standard for information technology - local and metropolitan area networks - specific requirements - part 15.3: Wireless medium access control (MAC) and physical layer (PHY) specifications for high rate wireless personal area networks (WPAN).

IEEE 802.15.4. 2011. IEEE standard for local and metropolitan area networks - part 15.4: Low-rate wireless personal area networks.

IEEE 802.16. 2012. IEEE Standard for air interface for broadband wireless access systems.

IEEE 1139. 2008. IEEE Standard definitions of physical quantities for fundamental frequency and time metrology - random instabilities.

Imai H. & Hirakawa S. 1977. A new multilevel coding method using error-correcting codes. IEEE Trans. Inf. Theory, vol. IT-23, pp. 371-377.

ITU-R Report M.2047. 2013. Detailed specifications of the satellite radio interfaces of international mobile telecommunications advanced. International Telecommunication Union Radiocommunication Sector.

ITU-R Report M.2083. 2015. IMT vision - framework and overall objectives of the future development of IMT for 2020 and beyond. International Telecommunication Union Radiocommunication Sector.

ITU-T Report G.9701. 2014. Fast access to subscriber terminals (G.fast) - physical layer specification. International Telecommunication Union Telecommunication Standardization Sector.

Jager F. & Dekker C. D. 1978. Tamed frequency modulation: A novel method to achieve spectrum economy in digital transmission. IEEE Trans. Commun., vol. 26, pp. 534-542.

Jeruchim M. C., Balaban P., & Shanmugan K. S. 2000. Simulation of communication systems: Modeling, methodology, and techniques. 2nd ed., Kluwer Academic/Plenum Press, New York, USA.

Karam G. & Sari H. 1991. A data predistortion technique with memory for QAM radio systems. IEEE Trans. Commun., vol. 39, pp. 336-344.

Karttaavi T., Kiviranta M., Lamminen A., Mämmelä A., Säily J., Vimpari A., & Järvensivu P. 2009. Antenna and assembly techniques for cost-effective millimeter-wave radios, in short-range wireless communications: Emerging technologies and applications, R. Kraemer and M. Katz (ed.), pp.239-256 (Chapter 22), Wiley, 2009.

Katz A. 2001. Linearization: Reducing distortion in power amplifiers. IEEE Microwave, vol. 2, pp. 37-49.

Kenington P. B. 2000. High-linearity RF amplifier design. Artech House, Boston, MA, USA.

Ketterling H.-P. A. 2004. Introduction to digital professional mobile radio. Artech House, Norwood, MA, USA.

Kim H. W., Kang K., Ku B.-J, Chang D.-I., & Kim S. 2015. SAT-OFDM: A satellite radio interface for the IMT-advanced system. Int. J. Satell. Commun. Network., vol. 33, pp. 295-314.

Kim J., Lee J., Kim J., & Yun J. 2014. M2M service platforms: Survey, issues, and enabling technologies. IEEE Commun. Surveys Tuts., vol. 16, pp. 61-76.

Kiviranta M. 2000. Trellis-coded modulation and per-survivor processing. University of Oulu, Department of Electrical Engineering. Licentiate thesis, 50 pp.

Kiviranta M. 2003. Method for demodulating signal, US Patent 6597251.

Lampe L., Schober R., & Jain M. 2005. Noncoherent sequence detection receiver for Bluetooth systems. IEEE J. Sel. Areas Commun., vol. 23, pp. 1718-1727.

Lathi B. P. 1983. Modern digital and analog communications systems. CBS Collage Publishing, New York, USA.

Laufer S. & Kaleth I. 1987. Optimization of generalized tamed frequency modulation bit error rate performance subject to a bandwidth constraint. IEEE Trans. on Comm., vol. 35, pp. 560-564.

Li Y. G. & Stuber G. L. 2006. Orthogonal frequency division multiplexing for wireless communications. Springer, New York, USA.

Liebetreu, J. M. 1986. Joint carrier phase estimation and data detection algorithms for multi-h CPM data transmission. IEEE Trans. on Comm., vol. 34, pp. 873-881.

Lin X., Andrews J. G., Ghosh A., & Ratasuk R. 2014. An overview of 3GPP device-to-device proximity services. IEEE Commun. Mag., vol. 52, pp. 40-48.

Litva J. & Lo T. K.-Y. 1996. Digital beamforming in wireless communications. Artech House, Boston, MA, USA.

Liu S., Wu J., Koh C. H., & Lau V. K. N. 2011. A 25 Gb/s(/km2) urban wireless network beyond IMT-advanced. IEEE Commun. Mag., vol. 49, pp. 122-129.

Lucky R. W. 1973. Survey of communication theory literature: 1968-73. IEEE Trans. Inf. Theory, vol. 19, pp. 725-739.

Lucky R. W., Salz J., & Weldon E. J. 1968. Principles of data communication. McGraw-Hill, New York, USA.

Magueta R., Castanheira D., Silva A., Dinis R. & Gameiro A. 2016. Iterative space-frequency equalizer for CE-OFDM mmW based systems. In Proc. IEEE ISCC, pp. 1-6.

Maral G., Bousquet M., & Sun Z. 2010. Satellite communications systems: Systems, techniques and technology 5th ed., Wiley, New York, USA.

Marler R. T. & Arora J. S. 2004. Survey of multi-objective optimization methods for engineering. Struct. Multidisc. Optim., vol. 26, pp. 369-395.

Massey J. L. 1974. Coding and modulation in digital communications. In Proc. Int. Zurich Seminar on Digital Communications, Zurich, Switzerland, pp. 1-4.

Mengali U. & D'Andrea A. N. 1997. Synchronisation techniques for digital receivers. Plenum Press, New York, USA.

Miao G., Himayat. N., & Li. Y.-G. 2009. Cross-Layer optimization for energy-efficient wireless communications: A Survey. Wiley J. Wireless Commun. and Mobile Computing, vol. 9, Apr. pp. 529-542.

Michailow M., Matthé M., Gaspar I. S., Caldevilla A. N., Mendes L. L., Festag A., & Fettweis G. 2014. Generalized frequency division multiplexing for 5th generation cellular networks. IEEE Trans. on Comm., vol. 62, pp. 3045-3061.

Miller M. J. 1993. Detection of CPFSK signals using per survivor processing. In Proc. IEEE MILCOM, pp. 524-528.

Mohseni R., Sheikhi A., & AliMasnadi-Shirazi M.-A. 2010. Multicarrier constant envelope OFDM signal design for radar applications, Int. J. Electron. Commun., vol. 64, pp. 999-1008.

Molisch A. F. & Win M. Z. 2004. MIMO Systems with antenna selection, IEEE Microwave Mag., vol. 5, pp. 46–56.

Murota K. & Hirade K. 1981. GMSK modulation for digital mobile telephony. IEEE Trans. on Comm., vol. 29, pp. 1044-1050.

Muschallik C. 1995. Influence of RF oscillators on an OFDM signal. IEEE Trans. Consumer Electron., vol. 41, pp. 592-603.

Myung H. G., Lim J., & Goodman D. J. 2006. Single carrier FDMA for uplink wireless transmission. IEEE Veh. Tech. Mag., vol. 1, pp. 30-38.

Mämmela A., Kotelba A., Höyhtyä M., & Taylor D.P. 2010. Relationship of average transmitted and received energies in adaptive transmission. IEEE Trans. Veh. Technol., vol. 59, pp. 1257-1268.

Mämmelä A., Kiviranta M., & Paaso H. 2008. Nonlinear phenomena in beamforming. In Proc. XXIX URSI General Assembly.

NetWorld2020. 2015. A white paper for research beyond 5G [Online]. Available: http://networld2020.eu/sria-and-whitepapers.

Neuvo Y. 2004. Cellular phones as embedded systems. In Proc. IEEE ISSCC, pp. 32-37.

NGMN. 2015. A White paper on 5G [Online]. Available: http://www.ngmn.org/5g-white-paper.

Niu Y., Li Y., Jin D., Su L., & Vasilakos A. V. 2015. A Survey of millimeter wave communications for 5G: Opportunities and challenges. Wireless Networks, vol. 21, pp. 2657-2676

Nokia. 2015. Workshop presentation on 5G: Nokia vision & priorities for next generation radio technology. [Online]. Available: http://www.3gpp.org/news-events/3gpp-news/1734-ran_5g.

Nordman R. & Mämmelä A. 1998. A semi-analytical approach for assessing the performance of a concatenated code. In Proc. IEEE GLOBECOM Communications Theory Mini-Conference, pp. 179–184.

Ochiai H. 2013. An analysis of band-limited communication systems from amplifier efficiency and distortion perspective. IEEE Trans. Commun., vol. 61, pp. 1460-1472.

Oetting J. D. 1979. A Comparison of modulation techniques for digital radio. IEEE Trans. on Comm., vol. 27, pp. 1752-1762.

Oh J., Ha J., Moon J., & Ungerboeck G. 2013. RS-enhanced TCM for multilevel flash memories. IEEE Trans. Commun., vol. 61, pp. 1674-1683.

Oppenheim A. V. & Schafer R. W. 1989. Discrete-time signal processing. 1st ed. Prentice-Hall, Englewood Cliffs, NJ, USA.

Osseiran A., Boccardi F., Braun V., Kusume K., Marsch P., Maternia M., Queseth O., Schellmann M., Schotten H., Taoka H., Tullberg H, Uusitalo M.-A., Timus B., & Fallgren M. 2014. Scenarios for 5G mobile and wireless communications: The vision of the METIS project. IEEE Commun. Mag., vol. 52, pp. 26-35.

Papathanassiou A., Salkintzis A. K., & Mathiopoulos, P. T. 2001. A comparison study of the uplink performance of W-CDMA and OFDM for mobile multimedia communications via LEO satellites. IEEE Pers. Commun., vol. 8, pp. 35-43.

Pasupathy S. 1974. Nyquist's third criterion, IEEE Proc., vol. 62, pp. 860-861.

Pasupathy S. 1979. Minimum shift keying: A spectrally efficient modulation. IEEE Commun. Mag., vol. 17, pp. 14-22.

Piazzo L. & Mandarini P. 2002. Analysis of phase noise effects in OFDM modems. IEEE Trans. Commun., vol. 50, pp. 1696-1705.

Pollet T., Van Bladel M., & Moeneclaey M. 1995. BER sensitivity of OFDM systems to carrier frequency offset and Wiener phase noise. IEEE Trans. Commun., vol. 43. pp. 191-193.

Prasad N., Wang S., & Wang X. 2009. Efficient receiver algorithms for DFT-spread OFDM systems. IEEE Trans. Wireless Commun., vol. 8, pp. 3216-3225.

Proakis J. G. 2001. Digital communications. 4th ed. McGraw-Hill, New York, USA.

Proakis J. G. & Manolakis D. G. 1996. Digital signal processing - principles, algorithms and applications. Prentice-Hall, New Jersey, USA.

Qi Y. Ul Quddus A., Imran M. A., & Tafazolli, R. 2015. Semi-persistent RRC protocol for machine type communication devices in LTE networks. IEEE Access, vol. 3, pp. 864-874.

Qiao J., Shen X., Mark J. W., Shen Q., He Y., & L. Lei. 2015. Enabling device-to-device communications in millimeter-wave 5G cellular networks. IEEE Commun. Mag., vol. 53, pp. 209-215.

Qualcomm. 2015. 5G Waveform & Multiple Access Techniques. [Online]. Available: https://www.qualcomm.com/media/documents/files/5g-research-on-waveform-and-multiple-access-techniques.pdf.

Raab F. H., Asbeck P., Cripps S., Kenington P. B., Popovic Z. B., Pothecary N., Sevic J. F., & Sokal N. O. 2002. Power amplifiers and transmitters for RF and microwave. IEEE Trans. Microwave Theory Tech., vol. 50, pp. 814-826.

Rabie K. M., Alsusa E., Familua, A. D., Cheng, L. 2015. Constant envelope OFDM transmission over impulsive noise power-line communication channels. In Proc. IEEE ISPLC, pp. 13-18.

Raheli R., Polydoros A., & Tzou C.-K. 1995. Per survivor processing: a general approach to MLSE in uncertain environments. IEEE Trans. Commun. vol. 43, pp. 354-364.

Rappaport T. S, Heath R. W., Daniels R. C., Murdock J. N. 2015. Millimeter wave wireless communications. Prentice Hall, Upper Saddle River, NJ, USA.

Razavi B. 1997. Design considerations for direct-conversion receivers. IEEE Trans. Circuits Syst. II, vol. 44, pp. 428-435.

Razavi B., Bateman A., Haines D. M., & Wilkinson R. J. 1988. Linear transceiver architectures. In Proc. IEEE VTC, pp. 478-484.

Reed I. S. & Solomon G. 1960. Polynomial codes over certain finite fields. SIAM Journal of Applied Mathematics, vol. 8, pp. 300-304.

Reimers U. 1997. DVB-T: The COFDM-based system for terrestrial television. IEE Electron. Commun. Eng. J., vol. 9, pp. 28-32.

Safari S. & Vahlin A. 2012. Low complexity implementation of per-survivor processing for carrier-phase tracking in uncertain environments. In Proc. IEEE RWS, pp. 195-198.

Sahin A., Guvenc I., & Arslan H. 2014. A Survey on multicarrier communications: Prototype filters, lattice structures, and implementation aspects. IEEE Commun. Surveys Tuts., vol. 16, pp. 1312-1337.

Saito M., Moriyama S., Yamada O. 1992. A digital modulation method for terrestrial digital TV broadcasting using trellis coded OFDM and its performance. In Proc. IEEE GLOBECOM, pp. 1694-1698.

Saleh A. A. M. 1981. Frequency-independent and frequency-dependent nonlinear models of TWT amplifiers. IEEE Trans. Commun., vol. 29, pp. 1715-1720.

Sari H., Karam G., & Maalej K. 1994. Multilevel CPM with 4-D trellis coding and linear receivers. In Proc. IEEE GLOBECOM, pp. 1274-1278.

Sasase I. & Mori, S. 1991. Multi-h phase-coded modulation. IEEE Commun. Mag., vol. 29, pp. 46-56.

Schetzen M. 2006. The Volterra and Wiener theories of nonlinear systems. 2nd ed., Krieger, Malabar, USA.

Schlegel C. B. & Perez L. C. 2015. Trellis and turbo coding: Iterative and graph-based error control coding. 2nd ed., Wiley, Hoboken, NJ, USA.

Schwartz M., Bennett W. R., & Stein S. 1966. Communication systems and techniques. McGraw-Hill, New York, USA.

Seshadri N. 1994. Joint data and channel estimation using blind trellis search techniques. IEEE Trans. Commun., vol. 42, pp. 1000-1011.

Shannon, C.E. 1948. A mathematical theory of communication. Bell Syst. Tech. J. 1948, 27, pp. 379-423, 623-656.

Silva J. A. L., Cartaxo A. V. T., & Segatto M. E. V. 2012. A PAPR reduction technique based on a constant envelope OFDM approach for fiber nonlinearity mitigation in optical direct-detection systems. J. Opt. Commun. Netw., vol. 4, 296-303.

Simsek M., Aijaz A., & Dohler M. 2016. 5G-enabled Tactile Internet. IEEE J. Sel. Areas Commun., vol. 34, pp. 460-473.

Simmons S.J. & Wittke P.H. 1983. Low complexity decoders for constant envelope digital modulations. IEEE Trans. Commun. vol. 31, pp. 1273-1280.

Spilker J. J. 1977. Digital Communications by Satellite. Prentice-Hall, Englewood Cliffs, NJ, USA.

Sundberg C.-E., 1986. Continuous phase modulation. IEEE Commun. Mag., vol. 24, pp. 25-38.

Stuber G. L, Barry J. R., McLaughlin S. W., Li Y., Ingram M. A., & Pratt T. G. 2004. Broadband MIMO-OFDM wireless communications. IEEE Proc., vol. 92, pp. 271-294.

Svensson A. 1991. Reduced state sequence detection of partial response continuous phase modulation. IEE Proceedings, vol. 138, pp. 256-268.

Svensson A. & Sundberg C.-E., 1984. Optimum MSK-type receivers for CPM on Gaussian and Rayleigh fading channels. IEE Proc., vol. 131, pp. 480-490.

Svensson T. & Svensson A. 2003. Constrained envelope continuous phase modulation. In Proc. IEEE VTC, pp 2623-2627.

Swindlehurst A. L., Ayanoglu E., Heydari P., & Capolino F. 2014. Millimeter-wave massive MIMO: The next wireless revolution? IEEE Commun. Mag., vol. 52, pp. 56-62.

Tadayon N. & Aissa S. 2013. Modeling and analysis of cognitive radio based IEEE 802.22 wireless regional area networks. IEEE Trans. Wireless Commun., vol. 12, pp. 4363-4375.

Tasadduq I. A. & Rao R. K. 2002. OFDM-CPM signals for wireless communications, Electron. Lett., vol. 38, pp. 80-81.

Tan J. & Stüber G. L. 2002. Constant envelope multicarrier modulation. In Proc. IEEE MILCOM, pp. 607-611.

Timmers M., Guenach M., Nuzman C., & Maes, J. 2013. G.fast: evolving the copper access network. IEEE Commun. Mag., vol. 51, pp. 74-79.

Thompson S. C., Ahmed A. U., Proakis J. G., & Zeidler J. R. 2004. Constant envelope OFDM phase modulation: Spectral containment, signal space properties and performance. In Proc. IEEE MILCOM, pp. 1129-1135.

Thompson S. C., Ahsen A. U, Proakis J. G., Zeidler J. R., & Geile M. J. 2008. Constant envelope OFDM. IEEE Trans. Commun., vol. 56, pp. 1300-1312.

Thompson S. C., Proakis J. G., & Zeidler J. R. 2005. Noncoherent reception of constant envelope OFDM in flat fading channels. In Proc. IEEE PIMRC, pp. 517-521.

Ucci D. R. & Petroit R. G. 1989. The effects of ADC nonlinearities on digital beamformers. In Proc. IEEE MILCOM, pp. 279-283.

Ungerboeck G. 1982. Channel coding with multilevel/phase signals. IEEE Trans. Inf. Theory, vol. 28, pp. 55-67.

Ungerboeck G. 1987. Trellis-coded modulation with redundant signal sets. Part I: Introduction. IEEE Commun. Mag., vol. 25, pp. 5-11.

Ungerboeck G. 1987. Trellis-coded modulation with redundant signal sets. Part II: State of the art. IEEE Commun. Mag., vol. 25, pp. 12-21.

Vakilian V., Wild T., Schaich F., ten Brink S., & Frigon J.-F. 2013. Universalfiltered multi-carrier technique for wireless systems beyond LTE. In Proc. IEEE GLOBECOM, pp. 223-228.

Van Nee R. & R. Prasad R. 2000. OFDM for wireless multimedia communications. Artech House, Boston, MA, USA.

Vihriala J., Ermolova N. Lahetkangas E., Tirkkonen O., & Pajukoski K. 2015. On the waveforms for 5G mobile broadband communications. In Proc. IEEE VTC Spring, pp. 1-5.

Viterbi A. J. 1967. Error bounds for convolutional codes and an asymptotically optimum decoding algorithm. IEEE Trans. Inf. Theory, vol. 13, pp. 260-269.

Viterbi A. J. & Omura J. K. 1979. Principles of digital communications and coding. McGraw-Hill, Inc., New York, USA.

Walden R. H. 1999. Analog-to-digital converter survey and analysis. IEEE J. Sel. Areas Commun., vol. 7, pp. 539-550

Warner W. D. & Leung C. 1993. OFDM/FM frame synchronization for mobile radio data communications. IEEE Trans. Veh. Technol., vol. 42, pp. 302-313.

Wei L.-F. 1987. Trellis-coded modulation with multidimensional constellations. IEEE Trans. Inf. Theory, vol. 3, pp. 483-501.

Wei L. & Schlegel C. 1995. Synchronization requirements for multi-user OFDM on satellite mobile and two-path Rayleigh fading channels. IEEE Trans. Commun., vol. 43, pp. 887-895.

Weinstein, S. B. 2009. The history of orthogonal frequency-division multiplexing [History of Communications]. IEEE Commun. Mag., vol. 47, pp. 26-35.

Weinstein S. B. & Ebert P. M. 1971. Data transmission by frequency-division multiplexing using the discrete Fourier transform. IEEE Trans. Commun., vol. 19, pp. 628-634.

Williamson M. R., Athanasiadou G. E., & Nix A. R. 1997. Investigating the effects of antenna directivity on wireless indoor communication at 6O GHz. In Proc. IEEE PIMRC, pp. 635-639.

Wilson J. F., Youell R., Richards T. H., Luff G., & Pilaski R. 1991. A single-chip VHF and UHF receiver for radio paging. IEEE J. Solid-State Circuits, vol. 26, pp. 1944-1950.

WRC. 2015. World Radiocommunication Conference. [Online]. Available: http://www.itu.int/en/ITU-R/conferences/wrc/2015.

Wu Y. S. 1987. Constant capacity, DSP architecture – an historical prospective. in digital signal processing. V. Cappellini and A. G. Constantinides (Eds.), Elsevier Science Publishers B.V., pp. 3-14.

Wunder G., Jung P., Kasparick M., Wild T., Schaich F., Chen Y., ten Brink S., Gaspar I., Michailow N., Festag A., Mendes L., Cassiau N., Kténas D., Dryjanski M., Pietrzyk S., Eged B., Vago P., & Wiedmann F. 2014. 5GNOW: Non-ortogonal, asynchronous waveforms for future mobile applications. IEEE Commun. Mag., vol. 52, pp. 97-105.

Wylie-Green M. P., Perrins E., & Svensson T. 2011. Introduction to CPM-SC-FDMA: A novel multiple-access power-efficient transmission scheme. IEEE Trans. Commun., vol. 59, pp. 1904-1915.

Xie G.-T., Yu H.-Y, Zhu Y.-J., & Ji X.-S. 2016. A linear receiver for visible light communication systems with phase modulated OFDM. Optics Communications, vol. 371, pp. 112–116.

Xue H., Beach M. & McGeehan J. 1994. Non-linearity effects on adaptive antennas. In Proc. Int. Symp. Antennas and Propagation, pp. 352-355.

Zaidi A. A., Luo J., Gerzaguet R., Wolfgang A., Weiler R. J., Vihriälä J., Svensson T., Qi T., Halbauer H., Zhao Z., Zetterberg P., & Miao H. 2016. A preliminary study on waveform candidates for 5G mobile radio communications above 6 GHz. In Proc. IEEE VTC, pp. 1-6.

Zeng Y., Zhang R., & Lim T. J. 2016. Wireless communications with unmanned aerial vehicles: Opportunities and challenges. IEEE Commun. Mag., vol. 54, pp. 36-42.

Zhang X., Jiay M., Chen L., May J., & Qiu J. 2015. Filtered-OFDM — enabler for flexible waveform in the 5th generation cellular networks. In Proc. IEEE GLOBECOM, pp. 1-6.

Zhong Z., Zhang L., Wu H., & Xia S. 2011. Non prior knowledge estimation of modulation index for angle modulation signals, Procedia Eng., vol. 23, pp. 642–646.

Zhou G. T. & Kenney J. S. 2002. Predicting spectral regrowth of nonlinear power amplifiers. IEEE Trans. Commun., vol. 50, pp. 718-722.

Ziemer R. E. & Peterson R. L. 1985. Digital communications and spread spectrum systems. Macmillan Publishing, New York, USA.

Ziemer R. E. & Tranter W. H. 1995. Principles of communications. 4th ed., Wiley, New York, USA.

Publications

I

Real-Time Simulation of Impairments in the Analog Parts of the Transmitter-Receiver

Markku Kiviranta, Aarne Mämmelä, Yan Zhang,
Ilkka Moilanen, Sandrine Boumard
VTT Electronics
Oulu, Finland
{Markku.Kiviranta, Aarne.Mammela, Yan.Zhang,
Ilkka.Moilanen, Sandrine.Boumard}@vtt.fi

Timo Sarkkinen, Tommi Jämsä
Elektrobit Ltd
Oulu, Finland
{Timo.Sarkkinen, Tommi.Jamsa}@elektrobit.com

Abstract—We propose a method to simulate impairments caused by the nonideal analog parts of the transmitter-receiver. They include for example a high-power amplifier (HPA), mixers, and oscillators. The major advantage in our approach is that the model parameters are adjustable and the system works in real time in the digital domain. Conventional methods have either not been real time, or they have been implemented with analog circuits. The HPA model is implemented with the coordinate rotation digital computer (CORDIC) algorithm for rectangular to polar translations. A look-up table (LUT) is used for AM/AM and AM/PM distortion. To minimize the size of the LUT we have used cubic spline interpolation. For phase noise of the oscillators we propose a simple rotation mode CORDIC implementation that does not need any complex multiplication. Only one field-programmable gate array (FPGA) circuit is needed to implement the power amplifier and phase noise models.

Keywords - real-time simulation; nonideal analog parts; power amplifier; phase noise

I. INTRODUCTION

In fast data transmission the modulation method is often single-carrier quadrature amplitude modulation (QAM) or orthogonal frequency division multiplexing (OFDM) with QAM sub-carriers. In these systems the analog parts will play a significant role for the performance since the modulation method is very sensitive. For example M up to 64 is used in M-ary QAM. The modulation methods are not constant envelope, which imply that the requirements for the amplifier linearity are severe [1]. Therefore it is crucial to take the impairments into account when comparing different air interface technologies and when developing new high data-rate products. Since the future high data-rate systems are complicated and the impact of the impairments cannot be calculated analytically, it is very important to simulate it with realistic models of nonideal parts.

It is well known how to simulate the multipath propagation in physical radio channels [2, 3]. Modern simulation tools (for example MATLAB/Simulink) include also models for the nonideal analog parts of the transmitter-receiver. The problem is that this kind of simulation is very time-consuming. We have found only one reference [4] where real-time simulation is done, but this system was implemented with analog components.

In this paper, we propose an efficient method to simulate impairments caused by the nonideal analog parts of the transmitter-receiver. They include for example high-power amplifier (HPA), mixers, and oscillators. The low noise amplifier (LNA) in the receiver can be assumed to operate in a linear region. The major advantage in our approach is that the model parameters are adjustable and the system works in real time in the digital domain. Conventional methods have either not been real time, or they have been implemented with analog circuits.

Our approach is to simulate the impairments in real time using digital FPGA circuits. Two case examples were selected, including models for high-power amplifier and oscillator phase noise.

The paper is organized as follows. First the system model is presented, after which the expected major analog impairments are discussed. The next two sections describe the high level implementation and the floating point simulation results for the proposed nonlinear models. Finally, the FPGA implementation is presented and some conclusions are drawn.

II. SYSTEM MODEL

The basic block diagram for a transmitter-receiver with a channel is presented in Figure 1. We have considered modeling of the analog parts of the transmitter and the receiver, excluding antennas and analog-to-digital (A/D) and digital-to-analog (D/A) converters. The order of the blocks can be changed depending on the current application, and, of course, the number of the required filters depends on the performance requirements. In a direct conversion receiver, only one radio frequency (RF) mixer is needed since the band of interest is directly translated to zero frequency. In general, the receivers' mixers can be adjustable, and the control signal for the intermediate frequency (IF) mixer is provided by automatic frequency control (AFC). The automatic gain control circuit (AGC) operates in the receiver where the power control command for the transmitter is also generated. An alternative for the AGC circuit in the receiver is a limiter.

The typical analog impairments at each stage of the transmitter and the receiver are also illustrated in Figure 1. In order to make a prioritization for the distortions, the following classification is proposed: (1) nonlinear power amplifiers; (2) mixers and oscillators including phase noise, I/Q imbalance

0-7803-8887-9/05/$20.00 (c)2005 IEEE

and DC offset. The classification includes the expected major problems in future systems where the signals have complicated modulation with a nonconstant envelope, such as QAM, and in OFDM where the symbols are also exceptionally long. Finally, we found that it is usually much simpler to simulate systems without memory than those with memory. For example an AGC block would in general need to implement all the parts in the actual hardware.

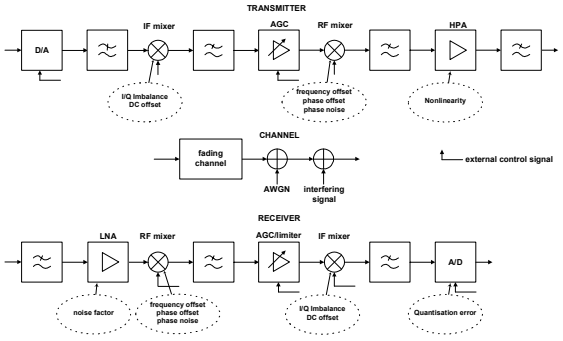

Figure 1. System model for transmitter-receiver with channel.

III. EXPECTED MAJOR ANALOG IMPAIRMENTS

A. Nonlinear Power Amplifier

All amplifiers are nonlinear if driven hard enough; they all exhibit saturation effects, whereby the output is not linearly proportional to the input at the high input signal levels. In the transmitter HPA is typically operated close to saturation, or even saturated, so as to maximize power efficiency. In the receiver low noise amplifier (LNA) can be usually assumed to operate in a linear region. In general, the effects of nonlinearities include intersymbol interference (ISI), constellation warping [5] and widening of the transmitted signal spectrum, or spectral regrowth, causing adjacent channel interference (ACI).

Models for amplifiers can be divided into (1) memoryless or instantaneous nonlinear systems, represented by amplitude modulation to amplitude modulation (AM/AM) conversion, (2) quasi-memoryless systems, represented by input AM/AM and amplitude modulation to phase modulation (AM/PM) conversions, or (3) nonlinear systems with memory [2, 3]. In memoryless systems, the output at any time instant depends at most on the input at the same time, but not on past or future time instants of the input. A memoryless system cannot generate AM/PM distortion. In quasi-memoryless amplifiers, the memory time constants are in the order of the period of the RF carrier. In amplifiers with memory, the time constants are in the order of the period of the envelope signal. The AM/AM and AM/PM functions depend on frequency. A precise characterization and simulations require more complex describing techniques such as Volterra series.

B. Distortions in Mixers and Oscillators

The ideal mixer can be modeled by a multiplier (see Figure 1) and is a linear operation [6]. However, practical mixers are nonlinear devices. Practical imperfections include local oscillator (LO) leakage, resulting in direct current (DC) offset in the output of the mixer. In the case of the quadrature frequency translations, shifting either the input signal or the LO output by 90˚ is required. In binary modulation a phase shift of 180˚ must be performed. Differences in the gain factors and the errors in the phase shift cause a mismatch between the in-phase and quadrature-phase branches, which is called an I/Q imbalance [7]. Finally, phase noise is introduced in a practical oscillator.

Phase noise has a very large impact especially when M is large in M-ary modulation. For a given energy, the signal points are close together as the alphabet size M for the signal set gets larger, which for a given phase perturbation is more likely to cause errors in data detection.

Phase noise is of two different types: finite power or asymptotically infinite power [8]. When the system is phase locked, the resulting phase noise is small and it can be modeled as a zero mean, stationary, finite power autoregressive moving average (ARMA) process. The time discrete model for ARMA process is achieved by filtering white noise samples Δ_n as

$$\varphi_n = \sum_{i=1}^{p} a_i \varphi_{n-i} + \sum_{i=0}^{q} b_i \Delta_{n-i} \qquad (1)$$

where a_i and b_i are the filter coefficients. The order of the ARMA process is denoted by (p, q). The second type of phase noise is obtained by assuming that the system is only frequency locked, as it is the case if the oscillator is tuned to carrier frequency but is free running. The resulting phase noise is slowly varying but not limited, and it is modeled as a zero mean, nonstationary, asymptotically infinite power Wiener process. Wiener model is a special (1, 0) order ARMA process with $a_1 = 1$.

IV. HIGH LEVEL IMPLEMENTATION

We are proposing a real-time method to simulate the impairments of the analog parts of the transmitter-receiver. The important challenge for the simulation tool itself and its FPGA implementation is that the selected nonlinear models are as generic as possible and all the parameters are adjustable. The complex baseband structures in Figures 2, 3 and 4 show the proposed high level structures for the expected major analog impairments.

For nonlinear power amplifier we focus memoryless or quasi-memoryless models, which can be expressed as AM/AM or AM/PM conversions. The models with a memory are more demanding and they are the aim of the further study. Usually the AM/AM or AM/PM conversion functions will be known only empirically from the measurements. In the hardware implementation of the nonlinearities, the measured data can be digitized and then stored into look up tables (LUT) as illustrated in Figure 2. In order to minimize the size of LUT or to produce values not appearing on the table, two methods, namely, curve fitting and interpolation are used [3].

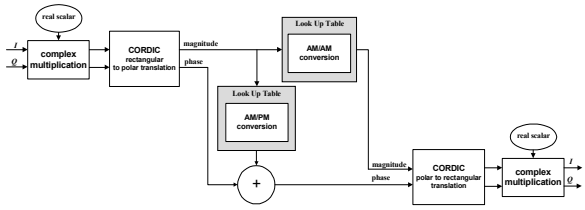

Figure 2. A model for power amplifier nonlinearity.

The least-square fit of a rational function to the measured data includes the use of predefined models for the nonlinear power amplifiers, such as Rapp's [9] and Saleh's [10] models available in MATLAB/Simulink. The drawback is, however, that the user can only adjust the parameters of the selected model. The prederived functions for AM/AM and AM/PM conversions are also relatively complex to implement.

The simplest form of the interpolation is a zero order hold circuit. However, polynomials have classically been used in interpolation [3]. A polynomial interpolator contributes small noise to the output signal because the interpolation slopes are not continuous from one table interval to the next. Noise contributions tend to be invisible in the time domain but appear in the frequency domain as elevated noise floors. Cubic spline interpolation technique can reduce some of the slope-discontinuity noise. A cubic spline matches the first and second derivatives of adjacent tabular intervals so that slope noise arises only from discontinuities in higher derivatives. The spline interpolation algorithm gives the coefficients of the interpolation function

$$y = A_i + B_i(x - x_i) + C_i(x - x_i)^2 + D_i(x - x_i)^3 \qquad (2)$$

for x in the interval $[x_i, x_{i+1}]$, where the x_i are the abscissa of known values y_i. In order to easy the hardware implementation the coefficients A_i, B_i, C_i, D_i can be initialized by software.

Coordinate rotation digital computer (CORDIC) algorithm [11] is an iterative and computationally efficient algorithm for computing rectangular to polar translations (see Figure 2) using combiners and shifters. The CORDIC is very suitable for FPGA implementation. The vectoring mode of the CORDIC algorithm aims at aligning the result vector with the *I*-axis. It consists of minimizing the *Q* component of the residual vector at each rotation. In this configuration, the CORDIC equations are

$$\begin{aligned} I_{i+1} &= I_i - Q_i \cdot d_i \cdot 2^{-i} \\ Q_{i+1} &= Q_i + I_i \cdot d_i \cdot 2^{-i} \qquad i = 0, 1, 2, ..., n \\ z_{i+1} &= z_i - d_i \cdot \alpha_i \end{aligned} \qquad (3)$$

where $d_i = +1$ if $Q_i < 0$ and -1 otherwise. The step angles α_i are chosen such that $\alpha_i = \arctan 2^{-i}$. After n iterations we obtain

$$\begin{aligned} I_n &= K_n \sqrt{I_0^2 + Q_0^2} \\ Q_n &= 0 \\ z_n &= z_0 + \arctan(Q_0 / I_0) \\ K_n &= \prod_n \sqrt{1 + 2^{-2i}} \end{aligned} \qquad (4)$$

and the magnitude and phase of the rectangular to polar translation are provided simultaneously. The scaling factor K_n is a rotator gain, and in general, the CORDIC algorithm produces one additional bit of accuracy for each iteration.

By selecting $d_i = -1$ if $z_i < 0$ and $+1$ otherwise, the CORDIC algorithm (3) operates in a rotation mode. The rotation mode is initialized so that $I_0 \triangleq$ "polar magnitude", $z_0 \triangleq$ "polar phase", and $Q_0 = 0$. Finally, after n iterations the polar to rectangular translation is as

$$\begin{aligned} I_n &= K_n [I_0 \cos z_0 - Q_0 \sin z_0] \\ Q_n &= K_n [Q_0 \cos z_0 + I_0 \sin z_0] \\ z_n &= 0 \\ K_n &= \prod_n \sqrt{1 + 2^{-2i}} \end{aligned} \qquad (5)$$

The CORDIC algorithm is also an essential part when modeling distortions in mixers and oscillators. Figure 3 illustrates a general block diagram for the I/Q imbalance and DC offset. In the figure, the amplitude and phase imbalances are first applied separately for both I and Q components of the complex input signal, after which the DC offset is added to the resulting complex sum signal.

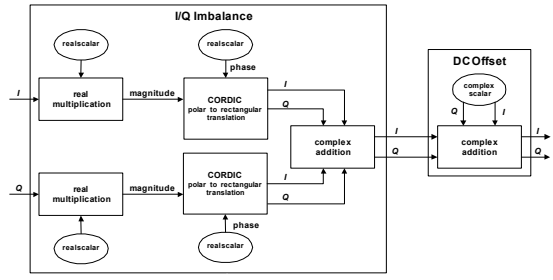

Figure 3. A model for I/Q imbalance and DC offset.

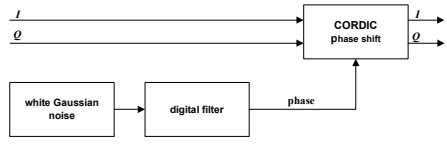

Figure 4. A model for phase noise.

Figure 4 shows a general block diagram for the phase noise. In the figure, white Gaussian noise samples are first digitally filtered so that the resulting phase noise is finite power ARMA process (1) of order (*p*, *q*). As discussed earlier, asymptotically infinite power Wiener process is obtained by selecting (1, 0) order ARMA process with $a_1 = 1$. Finally, the resulting phase noise is added to the complex input signal by using the CORDIC algorithm (5) in the rotation mode. By using the CORDIC principle we can avoid the complex multiplication needed otherwise. In general, phase noise φ_n causes a disturbance $e^{j\varphi_n}$ on the input signal [8]. The spectrum of $e^{j\varphi_n}$ is: (1) Lorentzian when the phase noise is nonstationary Wiener

process; (2) spectrum of phase noise itself plus the impulse in origin when the phase noise is stationary ARMA process.

V. SIMULATION RESULTS

Floating-point simulations were done to ensure the performance of the proposed structures for the expected major analog impairments. LUT is used for AM/AM and AM/PM distortions when modeling nonlinear HPA. One reason is flexibility: LUT can contain data based on any theoretical models or measurement results. To minimize the size of LUT cubic spline interpolation (2) is proposed for implementation. The performance of the interpolation was evaluated by using an absolute error metric

$$e_{AM/AM} = \left| F_{AM/AM}(u) - \widetilde{F}_{AM/AM}(u) \right| \tag{6}$$

where $F_{AM/AM}(u)$ and $\widetilde{F}_{AM/AM}(u)$ are ideal and interpolated AM/AM curves, and u is input amplitude. The similar metric is also derived for AM/PM conversions.

Figure 5 compares the measured results for cubic spline and linear interpolations when the AM/AM function of Rapp model [9] with LUT of 256 equally spaced points is used. As the figure shows, the cubic spline interpolation is more accurate compared to linear interpolation, especially when the AM/AM graph has a sharp curvature. As discussed earlier, this phenomenon can be explained by matching the first and second order derivates in cubic spline interpolation.

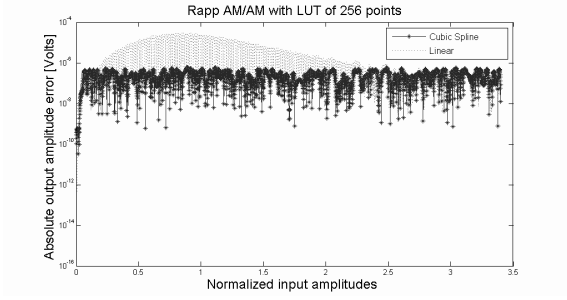

Figure 5. Interpolation comparison when LUT contains 256 points.

For modeling phase noise (1, 0) order ARMA process (1) is proposed for implementation. The transfer function of the ARMA process can then be given as

$$H(z) = \frac{b}{1 - az^{-1}} . \tag{7}$$

The power spectral density of ARMA process, i.e., the phase φ_n, can be adjusted using the constants a and b. By setting $a = 1$ Wiener process is achieved. As discussed earlier, and now demonstrated in Figure 6, the ARMA process has a finite power spectral density when the frequency approaches zero. If we increase the order of the ARMA process, we have freedom to generate different and smoother spectral shapes at the cost of more complex filter.

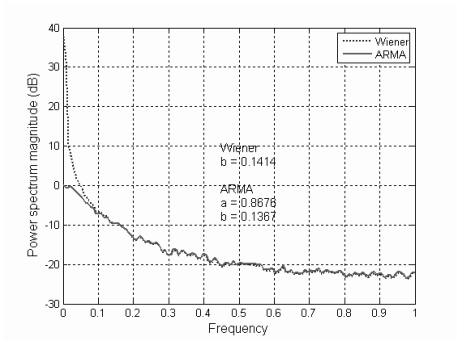

Figure 6. Power spectral density comparison for ARMA and Wiener process.

VI. FPGA IMPLEMENTATION

Separate very high speed integrated circuit hardware description language (VHDL) models were developed for the expected major analog impairments including nonlinear HPA and phase noise. The VHDL models were mostly based on the bit-true simulations. Xilinx Virtex-II Pro FPGA was used for the implementations. There were two basic implementation assumptions at the system level: (1) both the incoming and outgoing sampling rates were 80 MHz; (2) the data path for both I and Q component was 16-bit including the sign bit. The input signal was scaled between the values [-3.2767, 3.2767].

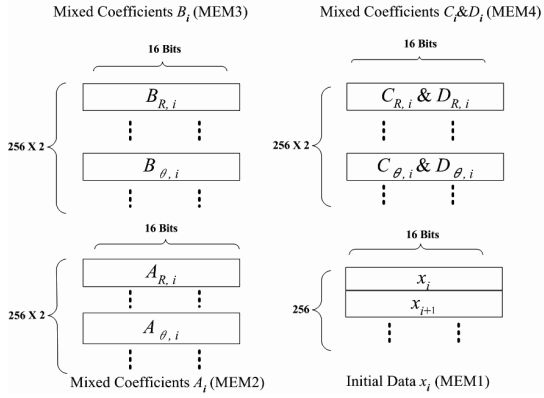

Figure 7. Memory structure of the HPA model.

In all VHDL models the CORDIC cores were generated from the Xilinx CoreGenerator™ with different options. User-controllable registers were used in all of our designs. These registers can be accessed by a separate 16-bit control bus. Through these registers the model parameters become adjustable; this gives one of the major advantages in our proposed real-time simulation approach.

The nonlinear HPA model was implemented using the LUT method presented in the previous sections. Xilinx provides a dual-port embedded memory called block random access memory (RAM), which is very suitable for such kind of approach. Based on the cubic spline interpolation algorithm (2)

a proper memory structure for the HPA model was developed and it is presented in Figure 7. A LUT of 256 equally spaced points was used so that adequate absolute error metrics for AM/AM and AM/PM conversions (6) could be achieved. The subscripts R and θ refer to the AM/AM and AM/PM curves, respectively. Altogether 3.5K bytes on-chip memory was needed to store the LUT values. The memory banks MEM1, MEM2, MEM3 and MEM4 can be updated in real-time and various nonlinear models, including the user-defined models can be realized through these memory banks.

Using Xilinx ISE 6.3i design tool shows that the maximum system speed for the nonlinear HPA model is 102 MHz with -6 speed grade. The model occupies about 12% all resources of a Virtex-II Pro40 chip. Table 1 summarizes resource utilization in different categories. For example, the HPA occupies 11% of the total number of MUL18X18 multipliers.

Table 1. Resource utilization of nonlinear HPA model.[1]

RESOURCE TYPE	NUMBER	PERCENTAGE
MULT18X18s	22	11%
RAMB16s	4	2%
SLICEs	2501	12%

The post-place & route hardware simulation results were compared with those of the floating point models. Figure 8 shows the measured difference for the complex baseband output signals when Saleh's nonlinear HPA model [10] is used. The figure shows that the maximum absolute errors for both I and Q data are about $4 \cdot 10^{-4}$.

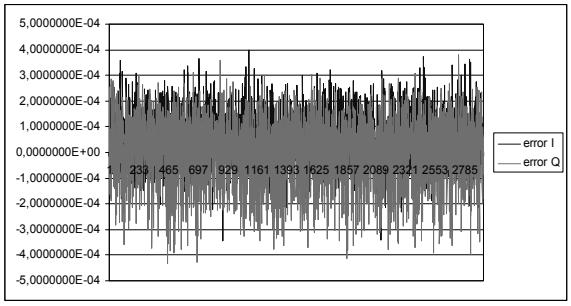

Figure 8. Measred difference between floating point and hardware implementations.

The implementation for the phase noise model was quite straightforward. We used the approach presented in Figure 4. The Wiener process with (1, 0) order ARMA option was implemented with an infinite impulse response (IIR) filter. The phase noise model occupies about 6% resources of a Virtex-II Pro40 chip and the maximum system speed is 90 MHz with -6 speed grade. Table 2 shows resource utilization.

Table 2. Resource utilization of phase noise model.[2]

RESOURCE TYPE	NUMBER	PERCENTAGE
MULT18X18s	12	6%
SLICEs	1199	6%

VII. CONCLUSION

We proposed a real-time method to simulate the impairments of the analog parts of the transmitter-receiver. The method is very versatile since all parameters are adjustable. Models with a memory are more demanding and they will need a more detailed study. The simulation approach can be used for real-time performance measurements of fast modems without implementing the analog parts whose parameters are difficult to change.

It is rather straightforward to simulate the I/Q imbalance. The CORDIC algorithm is used for polar to rectangular translations. In the phase noise model we found that an efficient approach is to use the CORDIC algorithm in the rotation mode. In this case no complex multiplication is needed. LUT is used for AM/AM and AM/PM distortions when modeling the nonlinear HPA. One reason is flexibility: LUT can contain data based on any theoretical models or measurement results. To minimize the size of LUT we used cubic spline interpolation.

Floating-point and bit true simulations were done to define the required word lengths of each parameter. The cubic spline interpolation was evaluated by using an absolute error metrics. VHDL architecture models were developed based on the bit-true simulations. Only one Virtex-II Pro40 FPGA chip is needed to implement the HPA and phase noise model.

REFERENCES

[1] R. van Nee and R. Prasad, *OFDM for Wireless Multimedia Communications*. Boston, MA: Artech House, 2000.

[2] M. C. Jeruchim, P. Balaban, and K. S. Shanmugan, *Simulation of Communication Systems*, 2nd ed. New York: Plenum Press, 2000.

[3] F. M. Gardner and J. D. Baker, *Simulation Techniques*. New York: Wiley, 1997.

[4] P. A. Bello, "Wideband line-of-sight channel simulation system," in *AGARD Conf. Proc.*, Cambridge, MA, Oct. 3-7, 1977, pp. 12.1 - 12.13.

[5] G. Karam and H. Sari, "A data predistortion technique with memory for QAM radio systems," *IEEE Trans. Commun.*, vol. 39, Feb. 1991, pp. 336 - 344.

[6] S. Haykin, *Communication Systems*, 4th ed. New York: Wiley, 2001.

[7] B. Razavi, "Design considerations for direct-conversion receivers," *IEEE Trans. Circuits Syst. II*, vol. 44, June 1997, pp. 428 - 435.

[8] L. Piazzo and P. Mandarini, "Analysis of phase noise effects in OFDM modems," *IEEE Trans. Commun.*, vol. 50, Oct. 2002, pp. 1696 - 1705.

[9] C. Rapp, "Effects of HPA-nonlinearity on a 4-DPSK/OFDM-signal for a digital sound broadcasting system," in *Proc. European Conference on Satellite Commun.*, Oct. 22-24, 2002, pp. 179 - 184.

[10] A. A. M Saleh, "Frequency-independent and frequency-dependent non-linear models of TWT amplifiers," *IEEE Trans. Commun.*, vol. COM-29, no. 11, Nov. 1981, pp. 1715 - 1720.

[11] R. Andraka, "A survey of CORDIC algorithms for FPGA based computers," in *Proc. ACM/SIGDA International Symposium on Field Programmable Gate Arrays*, Monterey, CA, Feb. 22-24, 1998, pp. 191 - 200.

[1] The area also includes the wrappers for Xilinx CORDIC cores.

[2] This does not include the white noise source component.

II

CONSTANT ENVELOPE MULTICARRIER MODULATION: PERFORMANCE EVALUATION IN AWGN AND FADING CHANNELS

Markku Kiviranta, Aarne Mämmelä
VTT Electronics
Oulu, Finland

and

Danijela Cabric, David A. Sobel, Robert W. Brodersen
Berkeley Wireless Research Center,
University of California, Berkeley, CA

ABSTRACT

In this paper we study the suitability of constant envelope multi-carrier modulation technique for the implementation of 1Gbps wireless link at 60 GHz. This technique combines orthogonal frequency division multiplexing (OFDM) and phase modulation (PM) where: (1) PM creates a constant envelope signal which allows high power amplifier to operate near saturation levels thus maximizing power efficiency, (2) OFDM increases robustness to multipath fading. Since OFDM-PM symbols satisfy symmetry property, maximum-ratio combiner (MRC) can be used at the receiver. Our simulations show that in an AWGN channel at bit error level 10^{-3}, the OFDM-PM with MRC has about 0.8 dB performance loss compared to OFDM or single carrier minimum shift keying (MSK). For Rician fading channels, we find that OFDM-PM performs comparably to MSK and outperforms uncoded OFDM. Furthermore, we show that both OFDM and OFDM-PM have similar bit error distribution characteristics, and thus the performance of OFDM-PM can be improved by the use of water-filling or coding techniques.

INTRODUCTION

With the availability of 7 GHz of unlicensed spectrum around 60 GHz, there is growing interest in using this resource for new consumer applications requiring very high-data-rate wireless transmission [1]. At 60 GHz a critical component is efficient power amplification because of the range limitations due to the oxygen absorption, which is further emphasized by the voltage reduction of advanced complementary metal oxide semiconductor (CMOS) circuitry and the high linearity requirements of sophisticated transmission schemes, such as nonconstant envelope modulation and adaptive beamforming. Multicarrier signaling, antenna array systems and adaptive equalization are regarded as the most suitable means of combating multipath effects in high-speed indoor applications [2].

In this paper we investigate the suitability of constant envelope multicarrier modulation technique for the implementation of 1Gbps wireless link at 60 GHz. This technique combines OFDM and phase modulation where: (1) phase modulation creates a constant envelope signal which allows high power amplifier to operate near saturation levels thus maximizing power efficiency, (2) OFDM increases robustness to multipath fading. We consider OFDM-PM and compare it with OFDM-CPM (continuous phase modulation) and single carrier MSK, both of which are also constant envelope modulation schemes. Since CPM signal can be viewed as both phase and frequency modulations, the term OFDM-FM (frequency modulation) is also known in the literature [3, 4, 5]. The idea is that OFDM-FM can be implemented simply and inexpensively by retrofitting existing FM communication systems.

For OFDM-CPM signaling, the ML receiver is based on the Viterbi algorithm, and this work shows that the earlier proposed low complexity phase difference receiver [6] suffers from a 3dB performance loss compared to coherent OFDM-PM receiver. In OFDM phase modulated systems, detection performance and spectral spreading can be controlled using the modulation index. Spectral containment [7] can be improved when using small modulation indices. On the other hand, performance gains can be accomplished by increasing the modulation index [8]. With 7 GHz of available bandwidth, it is possible to use less spectrally contained schemes that are more tolerant of the limited performance of e.g. CMOS circuits. Thus, several steps are taken in this work to optimize the performance of the coherent OFDM-PM receiver.

OFDM-PM is not as spectrally efficient as OFDM or MSK since real signaling is required at the input of the phase modulator. In [9] a complex OFDM signal is divided into real and imaginary parts before the phase modulator, while discrete cosine transform (DCT), instead of discrete Fourier transform (DFT), is used in [6]. In our paper, a real time-domain OFDM signal is achieved by satisfying the complex conjugate symmetry property in the frequency-domain. The resulting OFDM-PM signal is also symmetrical when we assume binary data modulation. This work is the first to propose a technique to exploit the redundancy of this symmetric waveform; through the use of MRC at the receiver, error rates in AWGN and fading channels can be greatly reduced. Furthermore, we show that both OFDM and OFDM-PM have similar bit error distribution characteristics, and thus the performance of OFDM-PM can be improved by the use of water-filling or coding techniques.

The paper is organized as follows. First the transmitter and receiver structures are presented, after which the parameter optimization is discussed. The MRC is then studied and performance results are compared with OFDM and MSK under same channel conditions. Before the conclusion, complexity of OFDM-PM and MSK receivers are evaluated.

PERFORMANCE IN AWGN CHANNEL

A. Transmitter structure

During an OFDM symbol period $0 \le t \le T$, the discrete time multicarrier signal can be given using the N-point inverse fast Fourier transform (IFFT) as

$$x_n = \frac{1}{N} \sum_{k=0}^{N-1} X_k e^{j2\pi kn/N}, \quad n = 0, ..., N-1 \tag{1}$$

where N is the number of subcarriers and X_k are uncorrelated frequency-domain M-ary data symbols with rate $1/T_b$. From the central limit theorem [10] it follows that for large values N, the OFDM signal becomes Gaussian distributed. The amplitude of the signal has therefore Rayleigh distribution with variance

$$E\left[|x_n|^2\right] = \frac{1}{N^2} \sum_{k=0}^{N-1} \left[|X_k|^2\right]. \tag{2}$$

The peak-to-average power ratio (PAPR) can be defined as

$$\text{PAPR} = 10\log_{10} \frac{\max\left(|x_n|^2\right)}{E\left[|x_n|^2\right]} \text{ [dB]}. \tag{3}$$

We next concentrate binary data modulation $M = 2$ and by choosing $X_k = \pm\sqrt{N}$, the variance (2) and PAPR (3) are equal to 1 and $10\log_{10}(N)$ dB, respectively. Since real OFDM signalling is required at the input of the phase modulator, the frequency-domain OFDM symbols have to satisfy a symmetry property by assuming N is an even number, and

$$\begin{aligned} X_{N/2} &= 0 \\ X_{N-k} &= X_k, \; k = 1, \ldots, N/2-1. \end{aligned} \tag{4}$$

The general continuous phase modulated (CPM) signal can be expressed as [10]

$$s(t) = e^{j\phi(t,x)}, \quad 0 \le t \le T_b. \tag{5}$$

where the phase $\phi(t, x)$ has the form

$$\phi(t,x) = 2\pi h \sum_{i=n-L+1}^{n} x_i q(t - iT_b) + \left[\pi h \sum_{i=-\infty}^{n-L} x_i\right] \bmod 2\pi \tag{6}$$

In (6) x_i are discrete time OFDM samples (1) and h is the modulation index. The phase pulse $q(t)$ is normalized in such a way that

$$q(t) = \begin{cases} 0 & t \le 0 \\ 1/2 & t \ge LT_b \end{cases}. \tag{7}$$

Its derivative $dq(t)/dt \triangleq g(t)$ is the frequency pulse of the modulator. The frequency pulse is limited to the interval $0 < t < LT_b$, and by selecting different pulses, a large number of different CPM methods can be obtained. Memory is introduced into the CPM signal by means of its continuous phase. Further memory can be achieved by choosing a pulse with $L > 1$. Smoother phase transitions can result in better spectral containment. However, we next concentrate on schemes with $L = 1$; if the integrating term in (6) is ignored, PM signal without memory is achieved.

The complex envelope model for both OFDM-CPM and OFDM-PM transmitters are shown in Figure 1. By selecting a rectangular frequency pulse $g(t)$ and $L = 1$, the discrete time filtering becomes a constant multiplication so that $g(n) = ½\,\delta(n)$ where $g(n) \triangleq g(nT_b)$ and $\delta(n)$ is the discrete time unit impulse.

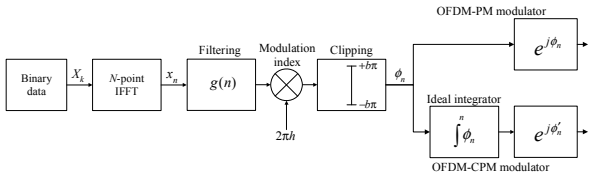

Figure 1. Complex envelope model for OFDM-CPM and OFDM-PM transmitters.

The clipping is required to ensure that the phase modulator input signal is in the range $[-b\pi, b\pi]$ where $0 < b < 1$. By combining equations (3) and (6), we can find that there is no clipping if

$$h < b/\sqrt{N}. \tag{8}$$

If we would ignore OFDM signaling in Figure 1, and assume binary data modulation so that $X_k = \pm 1$, discrete time MSK type CPM signal is achieved by selecting $h = ½$.

B. Receiver structure and measured results

In general, the maximum likelihood (ML) bit error probability for CPM signal can be upper bounded as

$$P_b = Q\left(\sqrt{\frac{d_{\min}^2 E_b}{N_0}}\right) \tag{9}$$

where the ratio E_b/N_0 is signal-to-noise ratio (SNR) per bit and $d_{\min}^2$ is the minimum Euclidean distance between all the possible pairs of signals in the Viterbi algorithm. For MSK signal $d_{\min}^2 = 2$ [10]. When using binary data modulation,

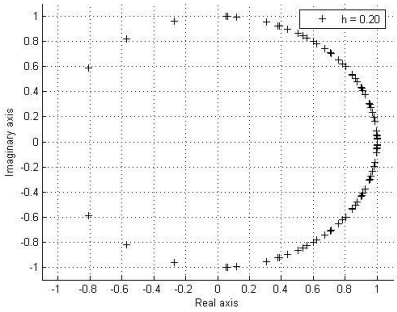

Figure 2. Phase modulator input signal in a unit circle, $N = 16$.

single carrier MSK and multicarrier OFDM have an equivalent performance in a known AWGN channel. In OFDM-CPM system the error probability is, however, more difficult to derive. In Figure 2, the phase modulator input signal is mapped into a unit circle. As figure shows, the constellation is not evenly spaced. On the other hand, the points in constellation are not all equally likely since the large values corresponds OFDM signal peak values with low probability and vice versa.

Besides the difficulty of deriving the performance of the optimum receiver for OFDM-CPM, the ML receiver is complex to implement. By taking into account the symmetry property in (4), the optimum OFDM-CPM receiver with binary data would require $2^{N/2}$ matched filters. We therefore consider the simple heuristic receiver [6] by determining the phase difference at the receiver as

$$\Delta\phi_n = \tilde{\phi}_{n+1} - \tilde{\phi}_n, \qquad (10)$$

where $\tilde{\phi}_n$ is the phase estimate of ϕ_n. By selecting $g(n) = \frac{1}{2}\delta(n)$ in Figure 1 and with the calculation of

$$\tilde{x}_n = \frac{1}{\pi h}\Delta\phi_n \qquad (11)$$

the estimate of the transmitted symbol X_k can be obtained by taking the N-point fast Fourier transform (FFT) as

$$\tilde{X}_k = \sum_{n=0}^{N-1} \tilde{x}_n e^{-j2\pi kn/N}, \quad k = 0, ..., N-1. \qquad (12)$$

In the OFDM-PM transmitter (see Fig. 1) the phase integrating term is ignored, and therefore the angle demodulator makes just symbol-by-symbol decisions, i.e., $\Delta\phi_n = \tilde{\phi}_n$. Finally, the complex envelope model for the OFDM-CPM and OFDM-PM receivers are shown in Figure 3.

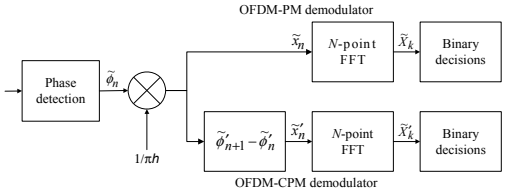

Figure 3. Complex envelop model for OFDM-CPM and OFDM-PM receivers.

The performances of the proposed OFDM-CPM and OFDM-PM systems are compared in Figure 4 when modulation index h = 0.2, N = 16 and clipping factor b is approximately one (see Eq. 8). As the simulation results show, OFDM-CPM suffers from a 3dB performance loss due to the differential phase demodulation. We next concentrate on OFDM-PM system since it shows significant performance gain with respect to OFDM-CPM.

Figure 4 shows that the bit error rate (BER) of an OFDM-PM system depends greatly on system parameters. In our study the target bit error rate is 10^{-3}, and Figure 5 indicates that the BER varies in a convex manner with respect to OFDM signal clipping factor b and modulation index h of PM signal [9]. This ensures the existence of optimum admissible b and h. For fixed value of h, smaller b induces more clipping noise, while larger b increases phase ambiguity problem in the noisy channel. On the other hand, for fixed value of b, smaller h makes signal points close to each other in constellation, while larger h induces more clipping noise. Figure 4 illustrates that it is also beneficial to use a large number of subcarriers N in OFDM symbol. With larger number of subcarriers, the PAPR increases, but the peak values occur with very low probability.

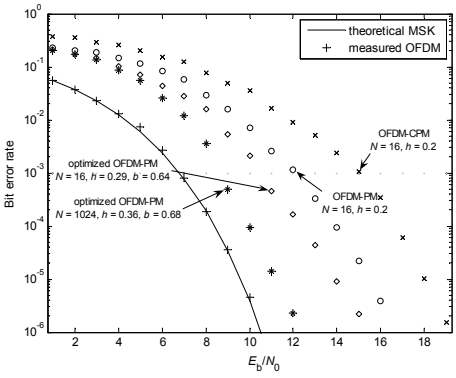

Figure 4. OFDM-CPM versus OFDM-PM in AWGN.

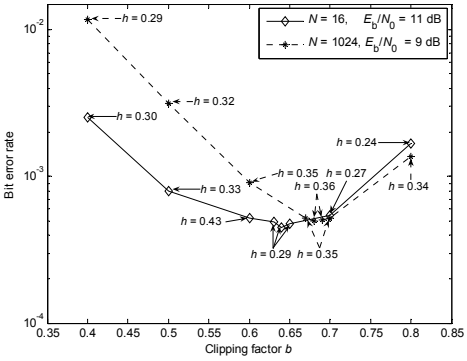

Figure 5. Optimization of OFDM-PM in AWGN.

C. Maximum-ratio combiner (MRC)

In general, OFDM-PM is not as spectrally efficient as OFDM or MSK since real signaling is required at the input of the phase modulator. This requirement forces frequency-domain OFDM symbols to satisfy a symmetry property (4) resulting in halved spectrum efficiency. Due to the nature of the IFFT transform, the real OFDM signal, and thus the complex OFDM-PM signal are also symmetrical when we assume binary data modulation. The OFDM-PM signal properties are demonstrated in Figure 6.

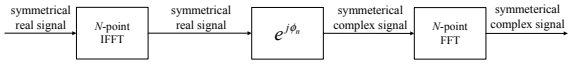

Figure 6. OFDM-PM signal properties.

We now propose a technique to exploit the redundancy of this symmetric waveform through the use of MRC at the receiver. We assume frequency domain signaling since we present later in this paper a combined MRC and frequency domain channel equalizer for fading channel. The MRC principle is shown in Figure 7. In the figure, $X'_1, X'_2, \ldots, X'_{N-1}$ are frequency domain data samples at the output of OFDM-PM transmitter and $V_1, V_2, \ldots, V_{N-1}$ are frequency domain AWGN samples with variance σ^2. In an AWGN channel, the symmetry of the transmitted symbols can be viewed as a form of interleaved repetition coding. Therefore, averaging two symbols with identical signal content and uncorrelated noise should result in an improvement to SNR of ideally 3dB. Actual improvement to SNR is, however, limited due to nonlinearity in the phase demodulation following the MRC operation. BER simulation results in Figure 8 shows that at bit error level 10^{-3}, the optimized binary OFDM-PM with $N = 1024$ and MRC has 0.8 dB performance loss compared to OFDM or single carrier MSK. This performance difference decreases at high SNR values.

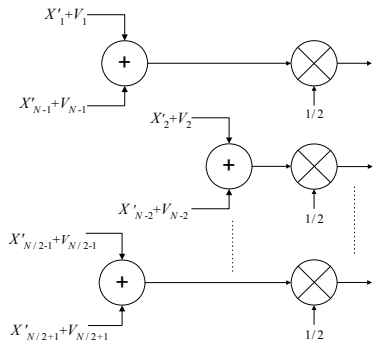

Figure 7. The principle of MRC[1].

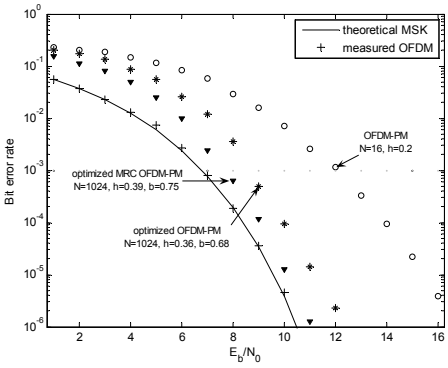

Figure 8. Optimized OFDM-PM with MRC in AWGN.

D. Nonlinear power amplifier

Simulation results show that both OFDM-CPM and OFDM-PM systems have performance loss compared to multicarrier OFDM system. However, if the maximum allowable transmit power is limited by the saturation level of the power amplifier, an OFDM system must have a back-off to accommodate the PAPR of the transmitted waveform. In comparison, constant envelope systems such as MSK do not require any backoff. Theoretical PAPR (3) for binary data modulated OFDM signal with $N = 16$ and $N = 1024$ are 12 dB and 30 dB, respectively. However, the actual amount of backoff required depends on the amount of clipping allowed to OFDM, i.e. $\text{PAPR}_{\text{clip}} < \text{PAPR}$. Thus, the constant envelope systems have the capability to transmit roughly $\text{PAPR}_{\text{clip}}$ dB more energy into the channel for a given power amplifier than an OFDM system utilizing an identical power amplifier. For example, the FCC[2] regulations allow for up to 500 mW transmit power in the 60 GHz band, which is significantly higher than what is available for the other WLAN/WPAN standards. On the other hand, getting power

[1] Subcarrier at zero frequency is ignored.
[2] FCC: Federal Communications Commission

out of the power amplifier at 60GHz will be very difficult [1]. Therefore, for a fixed power amplifier saturation level, the constant envelope modulation performance curves in Figures 4 and 8 could be shifted by $PAPR_{clip}$ dB to the left when compared to the OFDM curves. This benefit is referred to as a power gain in [8].

PERFORMANCE IN FADING CHANNEL

A. System model and measured results

The performance of the constant envelope multicarrier modulation is next considered in 60 GHz indoor multipath Rician fading channel. The measurements at 60 GHz indoor environment [2] show that signals are heavily attenuated by standard building materials, thus the transmission is likely to be restricted to locations where there is either a line-of-sight (LOS) between the transmitter and the receiver or reflections which does not undergo wall transmission. As antenna dimensions are inversely proportional to carrier frequency, more antennas can be used in a fixed area. The adaptive antenna array can increase the gain and help track the LOS or significant components and eliminate many unwanted multipath components.

In a single carrier receiver a time domain decision feedback equalizer (DFE) can be used to combat the multipath effects. A typical DFE consists of both feedforward (FF) and feedback (FB) filters, of which latter one is driven by a decision unit [10]. Practical filters are FIR filters, and their length depends on two factors: the delay spread of the channel and the specified BER. With the assumption of nearly ideal beamforming, FF filter could be ignored. However, nonlinear analog parts of a modem including e.g. nonlinear amplifier, phase noise and I/Q imbalance [11] can cause degradation in the antenna amplitude and phase weightings causing impairments in beamwidth, sidelobe level, null depth and null direction. On the other hand, acquisition of LOS path in a spatial domain is a critical issue. In a multicarrier system, a single wideband multipath channel is divided into multiple parallel narrowband flat fading channels, and a cyclic guard interval is inserted to avoid the ISI. Finally, frequency-domain equalization is used to compensate for channel complex gain at each subcarrier.

When we combine OFDM and phase modulation, the main aim is that the phase modulation creates a constant envelope signal which relaxes power amplifier linearization requirements and OFDM increases robustness to multipath fading. We next study the performance of OFDM-PM with ISI using a simplified single antenna model of Figure 9.

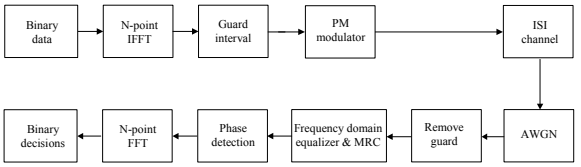

Figure 9. System model for OFDM-PM with ISI.

The proposed frequency-domain equalizer is shown in Figure 10. We denote H_k as N-point FFT of the discrete channel impulse response. The equalizer combines the MRC principle presented earlier in Figure 7 and minimum mean square estimation (MMSE). The MMSE equalizer minimizes the combined effect of ISI and the additive noise. If the noise variance term σ^2 is ignored, zero forcing equalizer (ZFE) is achieved. The ZFE type equalizer is simply the inverse of channel response. Inversion of the channel response leads, however, to infinite noise enhancement at frequencies corresponding spectral nulls. Therefore, in this paper, we focus on MMSE.

BER results for single carrier MSK, multicarrier OFDM and OFDM-PM systems were compared in typical 60 GHz indoor multipath Rician fading channel [2]. The assumption of nearly ideal beamforming reduces the ISI problem, and when bit rate is 1Gbps, the rms delay spread and K-factor were chosen to be 15 ns and 5 dB, respectively. The K-factor is taken as the ratio of the power in the LOS to sum of that in the random multipath components. The simulated channel had 71 complex taps with 1 ns spacing between taps. Each channel tap was an independent complex Gaussian random value; therefore each channel tap amplitude had a Rayleigh distribution. The number of trial channels was 20.

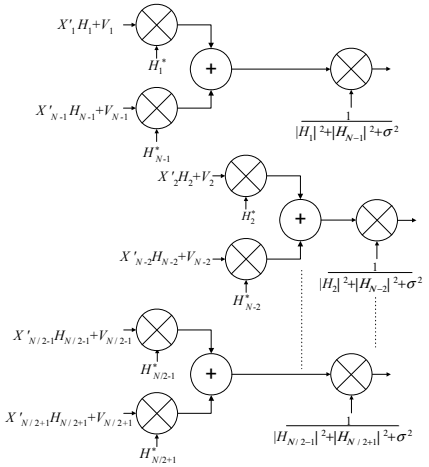

Figure 10. Combined MRC and MMSE[3].

[3] Subcarrier at zero frequency is ignored.

A DFE of 15 FB taps was used for MSK, where the placement of the taps was adaptively selected based on the MMSE criterion. The lengths of the OFDM symbol and the guard interval were 1024 ns (N = 1024) and 128 ns, respectively. The equalizer for the OFDM system was placed after the FFT (see Fig. 9) but prior to the data demodulator. In all study cases, ideal knowledge of the channel coefficients was assumed. Finally, the BER results are shown in Figure 11. Our simulations show that in Rician fading channels, OFDM-PM performs comparably to MSK and outperforms OFDM. In the case of OFDM, a null in channel frequency response results in one or more subcarriers having a very low SNR, and these subcarriers will dominate the overall error rate.

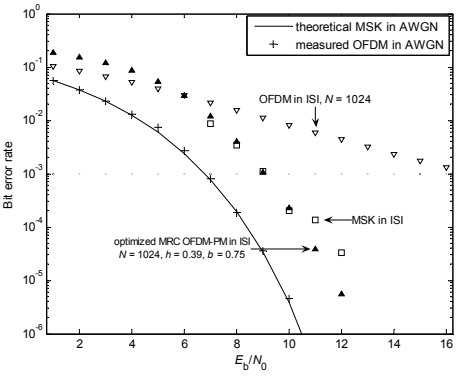

Figure 11. MSK, OFDM and OFDM-PM in ISI.

Figure 12 presents how the measured bit errors are distributed across the subcarriers in the case of OFDM. As we can see, deeper channel fades directly correspond to higher error rates at that frequency. However, coding or water filling techniques frequently used in other multicarrier systems can be employed to reduce the deleterious effect of these channel fades.

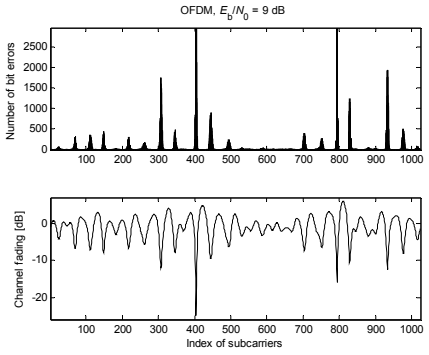

Figure 12. Bit error distribution in OFDM.

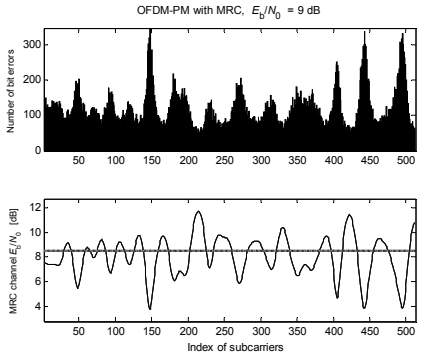

Figure 13. Bit error distribution in OFDM-PM with MRC.

The upper subfigure in Figure 13 illustrates measured bit errors distribution across the subcarriers in the OFDM-PM system with MRC. The lower subfigure shows the effective channel fading after taking the MRC operation into account. The same channel fading before MRC is presented in Figure 12. The MRC can be considered a form of diversity in that it smoothes deep amplitude depressions in the channel response, thus reducing the number of bit errors at those frequencies. The error distributions have similar characteristics in both OFDM and OFDM-PM systems. Thus, coding and water-filling could offer additional gain in OFDM-PM.

B. Complexity evaluation

One key complexity issue between OFDM-PM and MSK is FFT versus equalizer. In an OFDM-PM receiver, the channel equalization requires both complex FFT and IFFT operations, and the OFDM demodulator requires one real FFT block. The total number of real multiplications is shown in Table 1 when the split-radix FFT [12] and MRC (Fig. 10) are used. The average multiplications per second are achieved by multiplying the results by the length of OFDM symbol $1/NT_b$. In our comparison the target data rate $1/T_b$ is 1Gbps.

Table 1. Number of real multiplications.

	per OFDM symbol			per sec
N	split-radix FFT	MRC	total	total
16	50	70	120	$7.5 \cdot 10^9$
1024	17930	5110	23040	$22.5 \cdot 10^9$

If we assume a DFE of L_D complex taps, the number of real multiplications per symbol and sec are $4L_D$ and $4L_D/T_b$, respectively. Referring to Table 1, OFDM-PM receiver is less complex than DFE if

$$N = 16 \text{ and } L_D > 1 \ (4 \cdot L_D \cdot 10^9 > 7.5 \cdot 10^9)$$
$$N = 1024 \text{ and } L_D > 5 \ (4 \cdot L_D \cdot 10^9 > 22.5 \cdot 10^9).$$

Although the modulation method will have a bearing on the DFE length, binary decisions would also mean that no multiplications are needed in FB filter. The complexity even decreases if FF filter with complex taps can be ignored e.g. with the assumption of nearly ideal beamforming. If the DFE is adaptive, the coefficients can be calculated using the relatively simple least mean square (LMS) algorithm [10]. Since the LMS principle can also be used in OFDM-PM receiver, the complexity for the two schemes is similar.

CONCLUSIONS

In this paper we investigated the suitability of constant envelope multi-carrier modulation technique for the implementation of 1Gbps wireless link at 60 GHz. This technique combines OFDM and phase modulation where: (1) phase modulation creates a constant envelope signal which allows high power amplifier to operate near saturation levels thus maximizing power efficiency, (2) OFDM increases robustness to multipath fading. We studied OFDM-PM and compared it with OFDM-CPM and single carrier MSK, both of which are also constant envelope modulation schemes. It was found that OFDM-CPM receiver suffers a 3dB performance loss due to the differential demodulation.

Several steps were taken in this work to optimize the performance of the OFDM-PM receiver. It was found that the optimal values for OFDM signal clipping factor and modulation index of PM signal are determined by the trade-offs between clipping noise, minimum Euclidean distance, and phase ambiguity in the PM demodulator. We found also that it is beneficial to use a large number of subcarriers in OFDM. With larger number of subcarriers, the PAPR increases, but the peak values occur at very low probability.

OFDM-PM is not as spectrally efficient as OFDM or MSK since real signaling is required at the input of the phase modulator. This requirement forces OFDM symbols to satisfy a symmetry property resulting in halved spectrum efficiency. The OFDM-PM signal is also symmetrical when we assume binary data modulation. This work was the first to propose a technique to exploit the redundancy of this symmetric waveform; through the use of MRC at the receiver, error rates in AWGN and fading channels can be greatly reduced. Our simulations showed that in an AWGN channel at bit error level 10^{-3}, the optimized binary OFDM-PM with MRC has about 0.8 dB performance loss compared to OFDM or MSK. The performance difference decreases at high SNR values. For Rician fading channels, we compared BER performance of uncoded MSK, OFDM, and OFDM-PM with adequate channel equalizations, and we found that OFDM-PM performs comparably to MSK and outperforms uncoded OFDM. Furthermore, simulations showed that both OFDM and OFDM-PM have similar bit error distribution characteristics, and thus the performance of OFDM-PM can be improved by the use of water-filling or coding techniques. One key complexity issue between OFDM-PM and MSK is FFT versus equalizer. With the assumption of nearly ideal beamforming FF filter could be ignored and no multiplications are needed in DFE. If FF filter is required, the complexity of the OFDM-PM receiver containing FFT, MMSE and MRC blocks is easily below the MSK receiver with DFE.

REFERENCES

[1] C. H. Doan, S. Emami, D. A. Sobel, A. M. Niknejad & R. W. Brodersen, "Design considerations for 60 GHz CMOS radios," *IEEE Commun. Mag*., vol. 42, no. 12, pp. 132-140, Dec., 2004.

[2] M. R. Williamson, G. E. Athanasiadou, & A. R. Nix, "Investigating the Effects of Antenna Directivity on Wireless Indoor Communication at 6O GHz," *in Proc. PIMRC'97*, 1997, pp. 635-639.

[3] Casas E. F. & Leung C., "OFDM for data communication over mobile radio FM channels-Part I: Analysis and experimental results," *IEEE Trans. Commun*., vol. 39, no. 5, pp. 783-793, May, 1991.

[4] Casas E. F. & Leung C., "OFDM for data communication over mobile radio FM channels-Part II: Performance improvement," *IEEE Trans. Commun*., vol. 40, no. 4, pp. 680-683, Apr., 1992.

[5] Warner W. D. & Leung C., "OFDM/FM frame synchronization for mobile radio data communications," *IEEE Trans. Veh. Technol*., vol. 42, no. 3, pp. 302-313, Aug., 1993.

[6] Jun Tan & G.L. Stüber, "Constant envelope multicarrier modulation," *in Proc. MILCOM'02*, 2002, pp. 607-611.

[7] S. C. Thompson, A. U. Ahmed, J. G. Proakis, & J. R. Zeidler, "Constant Envelope OFDM Phase Modulation: Spectral Containment, Signal Space Properties and Performance," *in Proc. MILCOM'04*, 2004.

[8] S. C. Thompson, J. G. Proakis & J. R. Zeidler, "Constant Envelope Binary OFDM Phase Modulation," *in Proc. MILCOM'03*, 2003, pp. 621-626.

[9] C.-D. Chun and S.-M. Cho, "Constant-Envelope Orthogonal Frequency Division Multiplexing Modulation," *in Proc. APCC/OECC'99*, 1999, pp. 629-632.

[10] J. G. Proakis, "Digital Communications," 3rd ed., New York: McGraw-Hill, 1995.

[11] M. Kiviranta, A. Mämmelä, Y. Zhang, I. Moilanen, S. Boumard, T. Sarkkinen and T. Jämsä, "A. Real-Time Simulation of Impairments in the Analog Parts of the Transmitter-Receiver," *in Proc. VTC-Spring'05*, 2005.

[12] J. G. Proakis & D. G. Manolakis, "Digital Signal Processing," 3rd ed., New Jersey: Prentice Hall, 1996.

III

This full text paper was peer reviewed at the direction of IEEE Communications Society subject matter experts for publication in the WCNC 2009 proceedings.

Digital Signal Design and Nonlinear Distortions in Antenna Array Beamforming

Markku Kiviranta, Aarne Mämmelä, Henna Paaso, Marko Höyhtyä, Ilkka Moilanen
VTT Technical Research Centre of Finland, Oulu, Finland
markku.kiviranta@vtt.fi

***Abstract*—Antenna array beamforming reduces multipath fading components, and decreases the complexity of equalizer in a single carrier receiver. Nonlinear analog parts cause, however, impairments in the beamforming. In this paper we show that when the separate antenna elements include nonlinear amplifiers with different amplitude modulation to amplitude modulation (AM-AM) and amplitude modulation to phase modulation (AM-PM) conversions, there are errors in the level of main beam and in the direction of the main beam, respectively. There are no impairments in the beamforming if there is phase noise at the input of the antenna array. Anyhow, the phase noise may dramatically distort the signal constellation. A common method to avoid nonlinear distortions is to use modulation which has constant envelope. This is not enough if the nonlinear amplifier has memory.**

Keywords-signaling; modulation; beamforming; nonlinearities

I. INTRODUCTION

In general, adaptive antenna array beamforming, multicarrier signalling, and adaptive equalization can be used to combat the effects of multipath fading. The beamforming increases the gain and help to track the line-of-sight (LOS) component. Beamforming reduces also multiple access interference (MAI) and eliminates many unwanted multipath components thus decreasing intersymbol interference (ISI).

In a multicarrier orthogonal frequency division multiplexing (OFDM) system, a single wideband multipath channel is divided into multiple parallel narrowband flat fading channels, and a cyclic guard interval is inserted to avoid the ISI and interchannel interference (ICI). Finally, frequency-domain equalization is used to compensate for channel complex gain at each subcarrier. In OFDM systems the nonlinear analog parts play, however, a significant role for the performance since the modulation method is very sensitive [1, 2]. Phase noise has very large impact [3], and since the modulation method is not constant envelope, the requirements for amplifier linearity are severe.

When the system is frequency locked, the resulting phase noise is slowly varying but not limited, and it is modeled as a zero mean, nonstationary, asymptotically infinite power Wiener process. If the system is phase locked, the phase noise is small and it can be modeled as a zero mean, stationary, finite power autoregressive moving average (ARMA) process [4]. Models for nonlinear amplifiers can be divided into (1) memoryless or instantaneous nonlinear systems, represented by AM-AM conversion, (2) quasi-memoryless systems, represented by input AM-AM and AM-PM conversions, or (3) nonlinear systems with memory. If the nonlinear amplifier has memory, the system response depends not only on the input amplitude but also on its frequency [5]. Nonlinear systems typically create spectral components (harmonic and intermodulation distortions) that are totally absent from the input spectrum. The same phenomenon is also possible in linear time variant systems. Spectral spreading causes adjacent channel interference (ACI). Other usual distortions on the signal constellation are warping, clustering, attenuation, rotation, and origin offset.

A constant envelope minimum shift keying (MSK) modulation is a common method to avoid distortions caused by the nonlinear analog parts. The pulse shape filtering destroys the constant envelope property in linear *M*-ary quadrature amplitude modulation (QAM). In general, a time domain decision feedback equalizer (DFE) can be used to combat the residual multipath effects in a single carrier receiver. A typical DFE consists of both feedforward (FF) and feedback (FB) filters, of which latter one is driven by a decision unit. Practical filters are finite impulse response (FIR) filters, and their length depends on two factors: the delay spread of the channel and the specified bit error rate (BER). With the assumption of nearly ideal beamforming, FF filter could be removed, and as a consequence of that, implementation complexity decreases [6]. However, the nonlinear analog parts cause impairments in beamwidth, directivity, sidelobe level, null depth, and null direction [7, 8, 9, 10]. In beamforming, the acquisition of LOS path in a spatial domain is also a critical issue as well as blockage or shadowing due to human bodies.

In [6] we proposed a constant envelope multicarrier signaling technique which combines OFDM and phase modulation where 1) phase modulation creates a constant envelope signal, and 2) OFDM increases robustness to multipath fading. For Rician fading channels, we found that OFDM-PM performs comparably to MSK and outperforms uncoded OFDM. We also showed that if the FF filter is required in the MSK receiver, the complexity of the OFDM-PM receiver becomes easily below the MSK receiver with DFE.

If a PM signal with a rectangular pulse shape and sudden instantaneous phase shifts is first filtered, its envelope is no longer constant [11] and the following nonlinearity will distort the signal. The topic is important since separable nonlinear systems are preferred due to complexity reasons [12]. For example, the Wiener model [5] is cascade of the linear filter with memory and nonlinear memoryless system. In general, the continuous phase modulation (CPM) signals, such as MSK, are better in this respect since the amplitude changes will be small after filtering because there are no sudden changes in the phase.

978-1-4244-2948-6/09/$25.00 ©2009 IEEE

In this paper we explain in more detail how the nonlinearities cause impairments in beamforming. A simple way to make beamforming is to use RF phase shifters at each antenna element. We present a complex envelope model for a linear antenna array. The nonideal analog parts include nonlinear amplifiers and oscillators' phase noise.

The effects of nonlinearities in antenna array systems are demonstrated using array factor graphs. This work is first to show that there are no impairments in the beamforming if there is oscillator's phase noise at the input of the antenna array. Anyhow, the phase noise may dramatically distort the signal constellation. We also explain in more detail why the level and direction of the main beam changes, if there are nonlinear amplifiers at the antenna array.

Since many modern modulation methods are not constant envelope signals, we first summarize the peak-to-average power ratio (PAPR) values of *M*-ary QAM and OFDM. The simulation results confirm that the PAPR of QAM depends on the pulse shaping filtering, and for OFDM the high peak values occur with very low probability.

The paper is organized as follows. First the system model for the linear antenna array is presented, after which we discuss the signal design in the presence of nonlinear amplifier. The distortions in beamforming and signal constellation are then studied. Finally, conclusions are drawn.

II. SYSTEM MODEL

The general system model for the adaptive antenna arrays is presented in Fig. 1. In the transmitter, the digital-to-analog (DA) converter reconstructs the analog signal from a digital signal and the analog-to-digital (AD) converter in turn is used in the receiver. In the superheterodyne transmission scheme, mixers perform frequency translations from baseband to radio frequency (RF) and vice versa via intermediate frequency (IF). In a direct conversion scheme, a zero IF is assumed. At RF frequency N_A antenna elements are assumed. At each antenna element RF phase shifters provide antenna weights for adaptive beamforming.

In the implementation point of view, RF phase shifter architecture is simple since only one DA or AD converter and RF mixer is needed in the transmitter and the receiver. A high power amplifier (HPA) and a low noise amplifier (LNA) are assumed in each antenna element in the transmitter and the receiver, respectively. Before the AD converter and after the DA converter continuous time filters are needed in the signal chain. For example, low pass analog smoothing filtering is needed after DA. In superheterodyne receiver, bandpass IF and RF filters are needed to avoid ACI and image frequencies, respectively. Finally, the digital baseband produces either a single carrier or a multicarrier complex signal.

III. SIGNAL DESIGN

The constant envelope MSK signal may allow power amplifier to operate near saturation levels thus maximizing power efficiency. However, and since *M*-ary QAM and OFDM are used in many modern systems, we next investigate their PAPR values. In the literature (see, e.g., [2]), the PAPR is usually presented as

$$\mathrm{PAPR}' = 10\log_{10}\frac{\max\left(|x_n|^2\right)}{E\left[|x_n|^2\right]} \quad [\mathrm{dB}] \tag{1}$$

where x_n are uncorrelated and independent *M*-ary complex symbols, and max(·) and $E[\cdot]$ refer to the maximum and mean values of the argument. Since in practice the amplifiers operate with real signals, we next define the PAPR for them. Assuming the lowpass-to-bandpass transformations, a complex valued baseband signal

$$x_n = I_n + jQ_n \tag{2}$$

where I_n is the in-phase component and Q_n is the quadrature component, can be transmitted in real valued channel as

$$s_n = I_n \cos(\omega n + \varphi) - Q_n \sin(\omega n + \varphi) \tag{3}$$

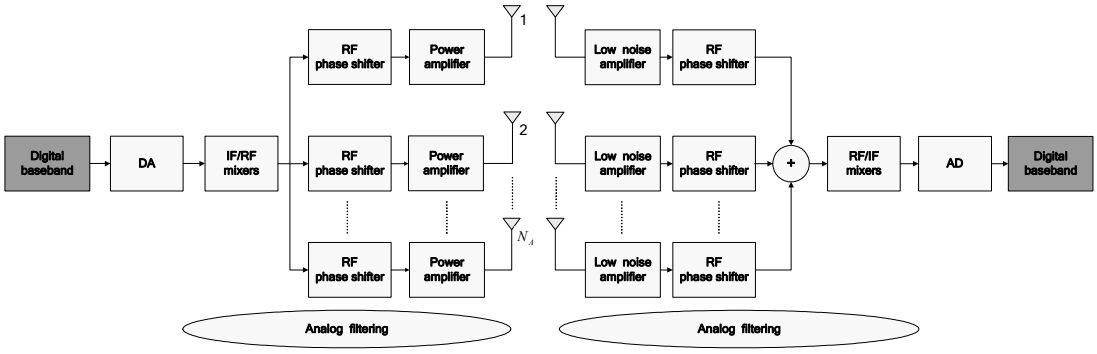

Figure 1. General system model for adaptive antenna array.

where ω denotes the angular frequency and φ is a random phase. Finally, the PAPR for the real signaling is

$$\mathrm{PAPR} = 10\log_{10}\frac{\max\left(s_n^2\right)}{E\left[s_n^2\right]} \quad [\mathrm{dB}] \tag{4}$$

where

$$E\left[s_n^2\right] = \frac{1}{2}E\left[\left|x_n\right|^2\right] \tag{5}$$

and

$$\max\left(s_n^2\right) = \max\left(\left|x_n\right|^2\right). \tag{6}$$

If the variance $E[|x_n|^2] = 1$, the theoretical PAPR (1) for the complex OFDM signal is equal to $10\log_{10}(N)$ dB where N is the number of subcarriers [2]. The PAPR is, however, 3 dB more if the definition (4) for the real OFDM signal is used. In any case, with the large values of N the PAPR increases for OFDM, but on the other hand, the peak values occur with very low probability. This phenomenon is simulated in Fig. 2.

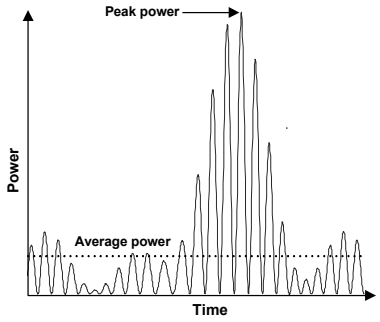

Figure 2. Instantaneous power of OFDM signal.

As known, the complex MSK symbols x_n have a constant envelope, but the real bandpass signal s_n has the PAPR of 3 dB due to sinusoid. Fig. 3 shows the complex envelope model for a linear M-ary modulator. In the case of binary phase shift keying (BPSK, M = 1) or quadrature phase shift keying (QPSK, M = 2), the complex symbols x_n have also constant envelope, but the PAPR of the real bandpass signal s_n depends on the pulse shaping filtering, too. A common filter is a square root raised cosine (SRRC) filter [13]

$$f(t) = \frac{4\beta}{\pi\sqrt{T}}\frac{\cos[(1+\beta)\pi t/T] + T\sin[(1-\beta)\pi t/T]/(4\beta t)}{1-(4\beta t/T)^2} \tag{7}$$

where β is called the roll-off factor and T is the symbol interval.

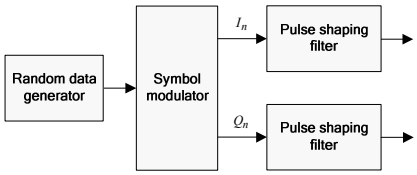

Figure 3. Complex envelope model of linear M-ary modulator.

Theoretical results without SRRC and simulated results with SRRC are shown in the PAPR Table 1. Interestingly, 32-QAM has slightly smaller theoretical PAPR than 16-QAM. This can be explained by the observation that there are no corner points in the 32-QAM constellation in Fig. 4.

TABLE I. PAPR [dB] FOR LINEAR M-ARY MODULATOR.

Modulation	PAPR with no SRRC	PAPR with SRRC[1]
BPSK, QPSK	3.0	8.0
16-QAM	5.6	9.7
32-QAM	5.3	9.6
64-QAM	6.7	9.9

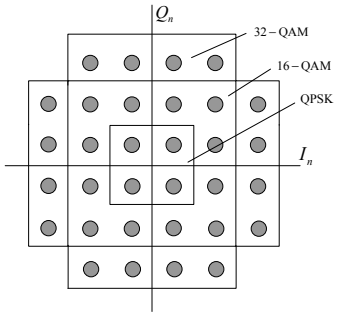

Figure 4. Linear M-ary constellations.

IV. NONLINEAR DISTORTIONS

A. *Impairments in beamforming*

By creating beams and nulls in the antenna array system, we can increase the gain in the direction of wanted signals and decrease the gain in the direction of interference and noise. Nonlinear distortions cause, however, impairments in beamforming. A simple way to make beamforming is to use RF phase shifters at each antenna element. Fig. 5 presents a complex envelope model for a linear antenna array. As the figure shows, the linear array consists of N_A radiators which are equally spaced by a distance d [10]. When λ is wavelength, the beam can be steered to the wanted direction θ_o by changing progressive phase shift

[1] In the simulations, β was 0.25.

$$\alpha_z = \frac{2\pi}{\lambda} d \sin\theta_o . \quad (8)$$

The progressive phase shift can be digitally controlled by multipliers $v_I(n)$ and $v_Q(n)$, so that

$$\alpha_z = \arg[v_I(n) + jv_Q(n)] \quad (9)$$

and the amplitude weighting

$$A_i = \sqrt{v_I^2(n) + v_Q^2(n)} , \quad (10)$$

where $i = 0, 1, \ldots, N_A-1$.

As in the I/Q modulator (3) of IF/RF mixer, dc offset, phase and amplitude imbalances are introduced in practical phase shifters. The imbalances are also called as I/Q imbalance or I/Q mismatch [14].

The array factor represents the far-field radiation pattern of an array of isotropically radiating elements. The ideal three dimensional (3D) array factor of a phased array is given by

$$F_a(\theta,\phi) = \sum_{i=1}^{N_A} A_{i-1} e^{j(i-1)(kd\sin\theta\sin\phi - \alpha_z)} \quad (11)$$

where $k = 2\pi/\lambda$ and θ is the elevation angle which defines zy and zx planes [15]. The angle ϕ describes xy plane. Two dimensional (2D) array factor is a special case of 3D, so that ϕ is 90°. Fig. 6 shows that for a linear array $F_a(\theta,\phi)$ is rotationally symmetric about the axis it is placed.

In general, the isotropic antenna element antenna is a mathematical fiction, and it can radiate or receive energy uniformly in all directions. All practical antenna elements have nonuniform radiation patterns. On the other hand, practical antenna elements include, for example, conductor loss, dielectric loss, surface wave excitation as well as losses due to feed lines and associated feed circuitry [10]. In this paper, we assume the ideal isotropic antenna elements.

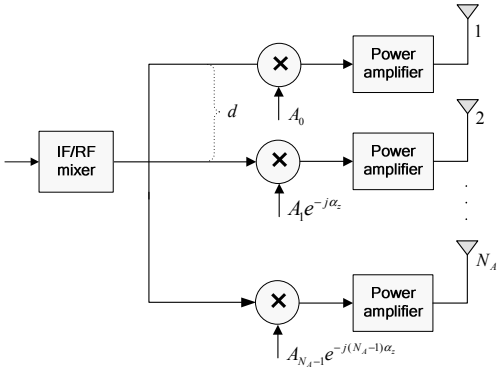

Figure 5. Complex envelope model of a linear antenna array.

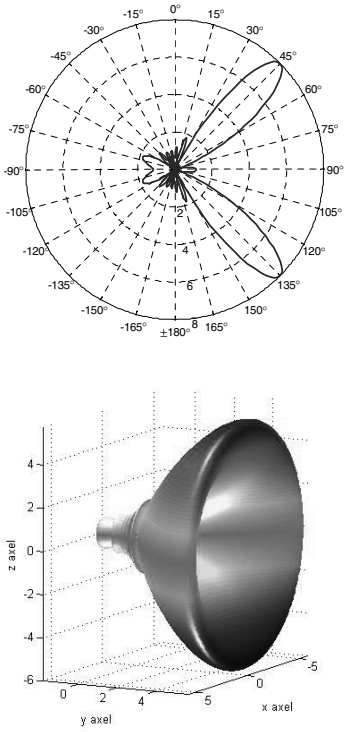

Figure 6. 2D (upper) and 3D (lower) array factors.

The main beam of an antenna radiation pattern is the lobe containing the direction of maximum radiation power. If the antenna element spacing d is too large compared to the wavelength λ, a second main lobe can appear in the antenna array factor. The extra main lobes are referred to as grating lobes (see Fig. 7), and to prevent them, we have to select

$$\frac{d}{\lambda} < \frac{1}{1+|\sin\theta_o|} . \quad (12)$$

In this paper, we assume ideal antenna element spacing, but in practice the antenna element spacing has to be precise, especially at high frequencies. For example, the wavelength λ in (12) is only 5 mm at 60 GHz.

When there are amplitude distortions in the antenna elements, we can rewrite the amplitude weighting as

$$A_i' = A_i \varepsilon_i \quad (13)$$

where ε_i is an amplitude error factor. If there are errors in the progressive phase shift α_z between the antenna elements, we can rewrite the progressive phase shift as

$$\alpha_z' = \alpha_z + \upsilon_i \quad (14)$$

where υ_i is a phase error between the antenna elements as shown in Fig. 8.

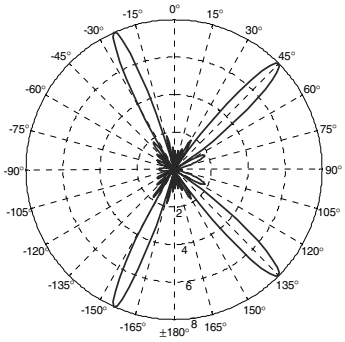

Figure 7. Grating lobes with element spacing $d = 0.9\lambda$.

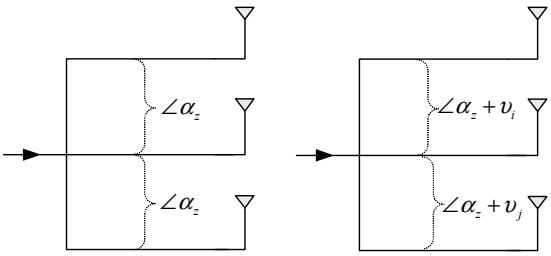

Figure 8. Ideal progressive phase shift (left) and errors υ_i and υ_j, $i \neq j$, in progressive phase shift (right).

The amplitude distortion in the input of an antenna array, or equivalently $\varepsilon_i = \varepsilon_j$, generates error in the level of the main beam. There are also changes in the shape of sidelobes if each antenna element has own and big enough amplitude distortion, i.e., $\varepsilon_i \neq \varepsilon_j$. The direction of the main beam changes if there are different phase errors $\upsilon_i \neq \upsilon_j$ between the antenna elements. The above statements are illustrated in Fig. 9 and Fig. 10.

In practice, there are always some differences between the antenna elements even if they are designed to be similar. Thus, the nonlinear amplifiers with different AM-AM and AM-PM conversions generate errors in the level of main beam and in the direction of the main beam, respectively. For the simulations, the AM/AM and AM/PM conversions of Saleh's nonlinear amplifier model [16] are set to deviate maximally 20 per cent. As shown in Fig. 11 and Fig. 12, the deviations are assumed in the 1-dB compression point where the input amplitude results in a 1-dB decrease in gain referenced to the amplifier's linear gain. However, the variation of antenna elements highly depends, among others, whether or no the elements are integrated into the same die in silicon. A careful device to device design on a single die may lead to deviation of only a very few per cent.

When there is a common phase error between the antenna elements, i.e. $\upsilon_i = \upsilon_j$, the progressive phase shift remains, and thus there is no error in the array factor. This is also true when the oscillator exhibits phase noise in the RF mixer at the input of the antenna array (see Fig. 1).

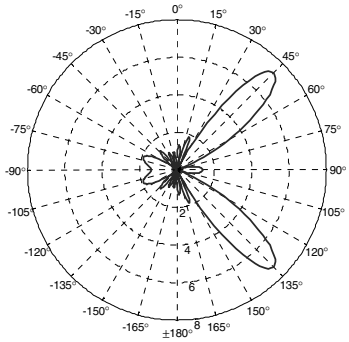

Figure 9. Impairments due to amplitude distortions in the antenna elements.

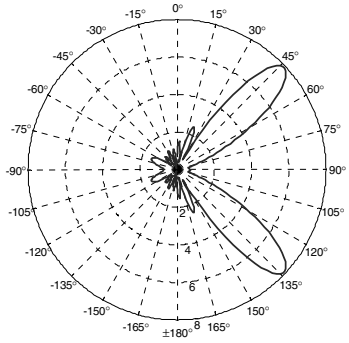

Figure 10. Impairments due to phase errors between the antenna elements.

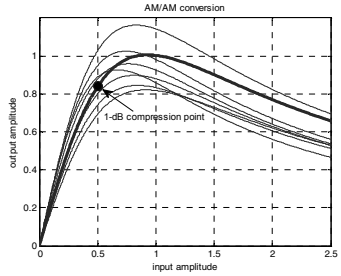

Figure 11. AM/AM conversions based on Saleh's nonlinear amplifier.

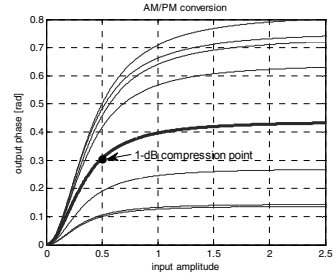

Figure 12. AM/PM conversions based on Saleh's nonlinear amplifier.

B. *Impairments in signal design*

Even though the array factor seems to be undistorted or only slightly distorted, the signal constellation can be dramatically distorted. The oscillator's phase noise at the input of the antenna array has a very large impact especially when the alphabet size M is large in QAM and OFDM subcarrier constellations. The effects of infinite power Wiener and finite power ARMA phase noises [4] on the signal constellation are illustrated in Fig. 13.

The effects of nonlinear amplifier with memory on the signal constellation are shown in Fig. 14. Due to memory each point of the signal constellation becomes a cluster showing ISI. The saturation may mean that the constellation points are not on a rectangular grid as in the original constellation. This phenomenon is called as warping.

Finally, when the constellation is distorted, the bit error rate may be significantly degraded. Also, if the signal is distorted, this may have indirect effects also on synchronization and estimation in the receiver.

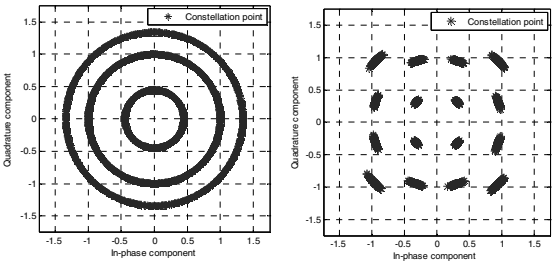

Figure 13. 16-ary QAM constellation distortion due to Wiener (left) and ARMA (right) phase noises.

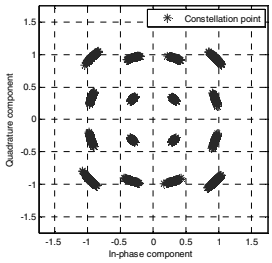

Figure 14. 16-ary QAM constellation warping with clusters.

V. CONCLUSIONS

In this paper we studied the effects of nonlinear analog parts in beamforming. The system model for the linear antenna array was first presented, after which the signal design in the presence of nonlinearities were discussed. Finally, the distortions in the beamforming and signal constellation were demonstrated using array factor graphs and constellation diagrams.

A common method to avoid distortions of nonlinear amplifiers is to use MSK modulation whose complex symbols have constant envelope and the real bandpass signal has PAPR of 3 dB due to sinusoid. Linear M-ary modulations require additional pulse shaping, and our simulation results showed that PAPR is about 8 dB and 10 dB for QPSK and 64-QAM, respectively. With the large values of subcarriers the PAPR increases for OFDM, but on the other hand, the peak values occur with very low probability.

The array factor represents the far-field radiation pattern of an array of isotropically radiating elements. We illustrated that when the separate antenna elements include nonlinear amplifiers with different AM-AM and AM-PM conversions, there are errors in the level of main beam and in the direction of the main beam, respectively. If the antenna element spacing is too large compared to the wavelength, a second main lobe can appear in the antenna array factor. Finally, we concluded that even though the array factor seems to be only slightly distorted, the signal constellation can be dramatically distorted. For example, the oscillator's phase noise at the input of the antenna array does not cause any distortions on beamforming, but the phase noise has very large impact on the signal constellations.

The focus of this paper was to study the effects of nonlinear analog parts in beamforming. On the other hand, radiation from antenna elements in an array differs from isolated because of mutual coupling between elements [10]. For example, the amount of coupling that is tolerable between power amplifiers is an interesting research topic in the future.

VI. ACKNOWLEDGEMENTS

The work was done in the WIPLA project funded by VTT.

VII. REFERENCES

[1] M. Kiviranta, A. Mämmelä, Y. Zhang, I. Moilanen, S. Boumard, T. Sarkkinen and T. Jämsä, "A real-time simulation of impairments in the analog parts of the transmitter-receiver," in Proc. VTC-Spring'05, 2005.

[2] R. van Nee and R. Prasad, OFDM for wireless multimedia communications. Boston, MA: Artech House, 2000.

[3] K. Feher, Telecommunications measurements, analysis, and instrumentation. New Jersey: Prentice-Hall, 1987.

[4] L. Piazzo and P. Mandarini, "Analysis of phase noise effects in OFDM modems," IEEE Trans. Commun., vol. 50, Oct. 2002, pp. 1696 - 1705.

[5] M. C. Jeruchim, P. Balaban, and K. S. Shanmugan, Simulation of communication systems: Modeling, methodology, and techniques, 2nd ed. New York: Kluwer Academic/Plenum Press, 2000.

[6] M. Kiviranta, A. Mämmelä, D. Cabric, D. Sobel, and R. W. Brodersen, "Constant envelope multicarrier modulation: Performance evaluation in AWGN and fading channel," in Proc. MILCOM'05, 2005.

[7] D. R. Ucci and R. G. Petroit, "The effects of ADC nonlinearities on digital beamformers," in Proc. MILCOM'89, 1989.

[8] H. Xue, M. Beach, and J. McGeehan, "Non-linearity effects on adaptive antennas," in Proc. Int. Symp. Antennas and Propagation, 1994.

[9] P. B. Kenington, High-linearity RF amplifier design. Boston, MA: Artech House, 2000.

[10] J. Litva and T. K.-Y. Lo, Digital beamforming in wireless communications. Boston, MA: Artech House, 1996.

[11] R. Ziemer and R. Peterson, Digital communications and spread spectrum systems. New York: Macmillan, 1985.

[12] A. Mämmelä, M. Kiviranta, and H. Paaso, "Nonlinear phenomena in beamforming," in Proc. XXIX URSI General Assembly, 2008.

[13] Lee E. A. and D. G. Messerschmitt, Digital communication., 2nd ed. Boston, MA: Kluwer, 1994.

[14] B. Razavi, "Design considerations for direct-conversion receivers," IEEE Trans. Circuits Syst. II, vol. 44, pp. 428–435, June 1997.

[15] D. Parker and D. C. Zimmermann, "Phased arrays–part I: Theory and architectures," IEEE Trans. Microwave Theory and Tech., vol. 50, pp. 678–687, Mar. 2002.

[16] A. A. M. Saleh, "Frequency-independent and frequency dependent non-linear models of TWT amplifiers," IEEE Trans. Commun., vol. 29, pp. 1715–1720, Nov. 1981.

IV

Physical Communication 10 (2014) 61–71

Contents lists available at ScienceDirect

Physical Communication

journal homepage: www.elsevier.com/locate/phycom

Full length article

Receiver structure and estimation of the modulation index for tamed frequency modulated (TFM) signals

Markku Kiviranta *, Aarne Mämmelä

VTT Technical Research Centre of Finland, P.O. Box 1100, FI-90571 VTT, Finland

ARTICLE INFO

Article history:
Received 11 December 2012
Received in revised form 4 October 2013
Accepted 29 November 2013
Available online 7 December 2013

Keywords:
Frequency modulation
Continuous phase modulation
Viterbi algorithm
Parameter estimation
Demodulation

ABSTRACT

Tamed frequency modulation (TFM) is a spectrally efficient constant amplitude continuous phase modulation (CPM) scheme which can be simply realized by using a frequency modulator (FM). In the implementation the modulation index of TFM is calibrated to have a nominal value of 0.5, but due to temperature variations it can drift causing time varying phase jitter. In this paper we present novel algorithms and performance results to measure and control the modulation index in a coherent receiver based on the joint reduced state sequence detector (RSSD) and per-survivor processing (PSP) carrier phase estimation. The modulation index estimator measures phase transitions in the receiver and derives estimates by comparing the result to the coding rule of the TFM signal. The estimator has acquisition and tracking ability, and the current estimate can be used to replace the nominal index value. Our simulation results show that the proposed coherent receiver with the novel modulation index estimator has less than 1 dB performance degradation compared to around 4.5 dB exploiting only the PSP carrier phase estimation.

1. Introduction

In telecommunications the performance is normally measured in terms of spectral efficiency and energy or power efficiency since frequency and energy are seen as the most important resources. Energy or power is a good measure of the complexity [1] but it must be traded off against the spectral efficiency. When the spectral efficiency is increased, the energy or power efficiency is decreased and vice versa. Tamed frequency modulation (TFM) [2] is a known spectrally efficient constant amplitude continuous phase modulation (CPM) scheme [3]. Spectral out of band radiation in the TFM is very small compared with other known CPM techniques such as the minimum shift keying (MSK), Gaussian minimum shift keying (GMSK), continuous phase frequency shift keying (CPFSK), and Gaussian frequency shift keying (GFSK). An extension [4] of TFM, called generalized tamed frequency modulation (GTFM), provides flexibility to trade off an increased spectrum leakage into neighboring bands for a lower bit error rate (BER), and vice versa.

Due to the constant amplitude, TFM allows the power amplifier to operate at or near the saturation level thus maximizing power efficiency. Due to high spectral and power efficiency, TFM is an attractive choice for use in high data rate satellite, cellular, point-to-point or point-to-multipoint links all requiring linear performance from their RF transmitters. Deep space communications present also special challenges including the very low signal-to-noise ratio (SNR) caused by the limited transmission energy of space probe and the huge energy loss by the remote transmission [5]. Since a TFM modulator can be simply realized by using a frequency modulator (FM), it makes low cost small size transmitters possible, especially for satellite downlink and terrestrial uplink from terminals to a base station.

Single carrier frequency division multiple access (SC-FDMA) is the uplink multiple access scheme in 3GPP Long Term Evolution (LTE). Compared to multicarrier

* Corresponding author. Tel.: +358 40 5890642; fax: +358 20 7222320.
E-mail addresses: markku.kiviranta@vtt.fi (M. Kiviranta), aarne.mammela@vtt.fi (A. Mämmelä).

1874-4907/$ – see front matter © 2013 Elsevier B.V. All rights reserved.
http://dx.doi.org/10.1016/j.phycom.2013.11.012

orthogonal frequency division multiple access (OFDMA) in downlink, the SC-FDMA has the lower peak-to-average power ratio (PAPR) due to its single carrier structure. In the literature, suitability of CPM OFDMA [6] and CPM SC-FDMA modulation techniques for achieving constant envelope is studied, and the TFM is an interesting candidate [7].

The drawback of the TFM implementation via the FM modulator is the deviation sensitivity of the modulation index during the transmission. For TFM the index is calibrated to have a nominal value 0.5, but it can drift due to the temperature variations of analog components. The deviated index generates time varying phase jitter, which may cause substantial performance degradations in a coherent receiver. The other type of transmitter for TFM is based on a quadrature modulator, and in digital implementation the in-phase and quadrature components are read from look-up tables. The two parts of the quadrature modulator should have the same amplitude and phase characteristic in order to avoid the amplitude and phase imbalances [2].

In this paper we assume simple FM implementation, and in the original paper of TFM [2] it has been proposed that the measuring and controlling of the modulation index should be made in the transmitter itself. In that way the nonidealities of the channel could be avoided at the cost of the complex transmitter. By assuming the demand of a simple transmitter we only concentrate on techniques available in the receiver. In general, the estimators can be categorized in blind or non-data aided (NDA), data aided (DA), and decision directed (DD) methods. While DA and DD techniques offer better acquisition and tracking capability, NDA methods are preferred when the data or preamble and the decisions are not available or reliable.

In the literature, blind estimators of the modulation index are proposed, e.g., for passive listening in the military applications [8–10]. The estimators require the prior knowledge either of the symbol period, the time of the arrival, the carrier frequency, or the frequency offset. The blind techniques need usually a large number of received samples to calculate complex statistical properties. For example, the uses of theoretical autocorrelation functions and higher order cumulants are proposed in [11,12], and the methods are originally aimed for the CPFSK format of CPM. According to [13], it seems to be extremely intractable task to define the autocorrelation function for the TFM.

In this paper we concentrate on coherent DA and DD CPM receivers due to the expected better bit error rate of detection. The estimation of the modulation index in a noncoherent receiver is discussed in [14], and the idea is to perform detection for a small number of different index hypotheses and after some estimation period choose the hypotheses yielding the maximum metric. Especially, in a coherent CPFSK receiver [15], per-survivor processing (PSP) carrier phase estimation [16] is used to compensate the phase jitter caused by the deviated modulation index. However, we show with simulations that if the modulation index deviation of TFM is high enough, the mere carrier phase estimation is not enough. Iterative decoding for coded and interleaved CPFSK signals is considered in [17], and the PSP is integrated into a Soft-Input Soft-Output (SISO) demodulator in [18]. The fundamentally drawbacks are the complexity of the iterative process and the problem that the PSP SISO algorithm needs the knowledge of the transmit modulation index value.

This work is the first to present algorithms and performance results to measure and control the modulation index of TFM especially in the coherent receiver. Since the optimal maximum likelihood (ML) demodulation of a TFM signal involves a complex Viterbi algorithm, a reduced state sequence detector (RSSD) [19] is first applied and a receiver structure for the carrier phase estimator is introduced. We then show that the measured performance results meet well the theoretical bit error probability of TFM. The principle of the modulation index estimator is originally described in our patent [20]. The idea is to measure the phase transitions in the receiver and derive the estimate by comparing the result to the coding rule of the TFM signal. The index estimate has acquisition and tracking ability, and it can be used to replace the nominal modulation index value. In this work several steps are taken to optimize the performance of the joint RSSD and PSP receiver with the modulation index estimator, and we show that the proposed method has less than 1 dB performance degradation compared to around 4.5 dB exploiting only the PSP.

The paper is organized as follows. First the system model is presented, after which the performance degradations due to the deviated modulation index are discussed in a known additive white Gaussian noise (AWGN) channel. Then the novel method to estimate the modulation index in the receiver is presented, and the performance is verified through floating point simulations. Finally, conclusions are drawn.

2. Signaling with joint detection and carrier phase estimation

2.1. Transmitter structure

The complex envelope of general CPM signal [3] is given by

$$s(t) = e^{j\phi(t)}. \tag{1}$$

The information-bearing phase $\phi(t)$ during the symbol interval $kT < t < (k+1)T$ has the form

$$\phi(t) = \eta(t, C_k) + \Phi_k \tag{2}$$

where

$$\eta(t,\ C_k) = 2\pi h \sum_{i=k-L+1}^{k} \alpha_i q(t - iT) \tag{3}$$

$$\Phi_k = \left[\pi h \sum_{i=-\infty}^{k-L} \alpha_i\right] \bmod 2\pi. \tag{4}$$

In the above equations α_i are M-ary data symbols and $C_k = (\alpha_{k-L+1}, \ldots, \alpha_{k-2},\ \alpha_{k-1})$ and Φ_k denote the correlative and phase states of the modulator, respectively. The modulation index is denoted by h, and the phase pulse of the modulator is normalized so that

$$q(t) = \begin{cases} 0 & t \le 0 \\ 1/2 & t \ge LT. \end{cases} \tag{5}$$

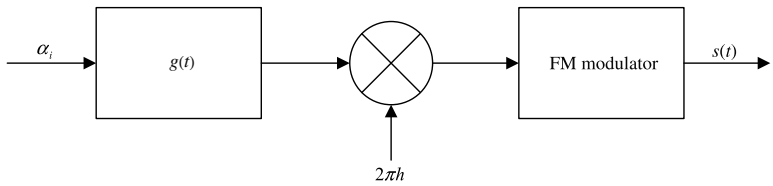

Fig. 1. FM modulator implementation.

The derivative $dq(t)/dt = g(t)$ is the frequency pulse of the modulator. The frequency pulse has the length of L symbol intervals. If $L = 1$, the scheme is called full response CPM. In other cases ($L > 1$), the scheme is called partial response CPM. By choosing different frequency pulses $g(t)$ and varying the parameters h and M, a great variety of CPM schemes such as MSK, GMSK, CPFSK, GFSK, and TFM can be obtained. The TFM is a particularly interesting modulation since the spectral out of band deviation is very low [2].

TFM is a binary ($M = 2$) scheme with the nominal modulation index h value of 0.5. The specific coding rule for the TFM signal at $t = kT$ can be written as

$$\begin{aligned}&\phi(kT+T) - \phi(kT)\\ &\quad = 2\pi h \sum_{i=-\infty}^{\infty} \alpha_{k-i}\left[q(iT+T) - q(iT)\right],\\ &\quad k = 1,\ 2, \ldots\end{aligned} \tag{6}$$

in which

$$\begin{aligned}q(iT+T) - q(iT) &= \int_{iT}^{(i+1)T} g(t)dt\\ &= \begin{cases} 1/8 & \text{for } |i| = 1,\\ 1/4 & \text{for } |i| = 0,\\ 0 & \text{otherwise.}\end{cases}\end{aligned} \tag{7}$$

The frequency pulse $g(t)$ is defined in [3] as

$$g(t) = \frac{1}{8}g_0(t-T) + \frac{1}{4}g_0(t) + \frac{1}{8}g_0(t+T) \tag{8}$$

where

$$g_0(t) \approx \sin\left(\frac{\pi t}{T}\right)\left[\frac{1}{\pi t} - \frac{2 - \frac{2\pi t}{T}\cot\left(\frac{\pi t}{T}\right) - \frac{\pi^2 t^2}{T^2}}{\frac{24\pi t^3}{T^2}}\right]. \tag{9}$$

The different implementation ways of general CPM modulators are discussed in [13]. Fig. 1 shows the FM modulator implementation, which has low implementation expenses, and it is very suitable for high data rates. The disadvantage is the deviation sensitivity of the nominal modulation index h during the transmission.

2.2. Receiver structure

In a known AWGN channel the optimal ML detector of the general CPM signal can be implemented with a bank of matched filters and the Viterbi algorithm [21]. If the carrier phase θ is the only channel parameter, the input signal to the receiver is

$$r(t) = e^{j\phi(t)}e^{j\theta} + w(t) \tag{10}$$

where $w(t)$ is a complex additive white Gaussian noise. The filter bank over one symbol interval consists of $l = 1,\ 2, \ldots, M^L$ filters with impulse responses

$$h^l(t) = \begin{cases} e^{-j\eta^l(T-t,\ C_0^l)} & 0 \le t \le T\\ 0 & \text{elsewhere.}\end{cases} \tag{11}$$

When k is 0, $C_0^l = (\alpha_{-L+1}, \ldots, \alpha_{-2}, \alpha_{-1})$ and $\eta^l(t,\ C_0^l)$ is a realization of (3). The filter outputs are sampled at $(k+1)T$ and are used to produce the statistics

$$Z_k^l = \int_{kT}^{(k+1)T} r(t)\, h^l(T-t)dt \tag{12}$$

for branch metric computation. When the numbers of correlative C_k and phase Φ_k states are denoted as M^{L-1} and P, the Viterbi algorithm operates totally on a trellis of PM^{L-1} states, of which the overall state is denoted as $S_k = (C_k, \Phi_k)$. There are M branches stemming from each state, one for each possible transmitted symbol α_k. The general metric

$$\lambda_k(S_k, \tilde{\alpha}_k) = \mathrm{Re}\left\{Z_k(\tilde{\alpha}_k)e^{-j(\theta+\Phi_k)}\right\} \tag{13}$$

is assigned to the branch associated with bit decisions $\tilde{\alpha}_k$, and the algorithm searches for the best path in the trellis. In general, the bit decisions are delivered with a delay d.

In [19] an RSSD is proposed for partial response CPM schemes. The idea is to construct a trellis with a reduced number of states compared with the ML trellis, and to use this reduced trellis in the Viterbi decoder. In more detail, the Viterbi algorithm searches the data only from the correlative state C_k diagram and is thus simpler than the full-state Viterbi algorithm. Although the phase state Φ_k is not included in the trellis diagram, the phase state must be estimated from the survivors in the Viterbi algorithm.

Let us assume next that the only unknown parameter in the receiver is carrier phase θ. When data symbols α_k are known in the receiver, the so-called data aided (DA) method is used and the associated likelihood function becomes

$$\Lambda(r|\tilde{\theta}) = \exp\left\{\frac{1}{N_0}\sqrt{\frac{2E_s}{T}}\sum_{k=0}^{L_0-1}\mathrm{Re}\left\{Z_k(\alpha_k)e^{-j(\tilde{\theta}+\Phi_k)}\right\}\right\} \tag{14}$$

where L_0 is the observation length and $\tilde{\theta}$ is the carrier phase estimate. Clearly, the maximum of $\Lambda(r|\tilde{\theta})$ corresponds to the maximum of the sum in (14). Thus, setting the partial derivative of the sum to zero yields

$$\sum_{k=0}^{L_0-1}\mathrm{Im}\left\{Z_k(\alpha_k)e^{-j(\tilde{\theta}+\Phi_k)}\right\} = 0. \tag{15}$$

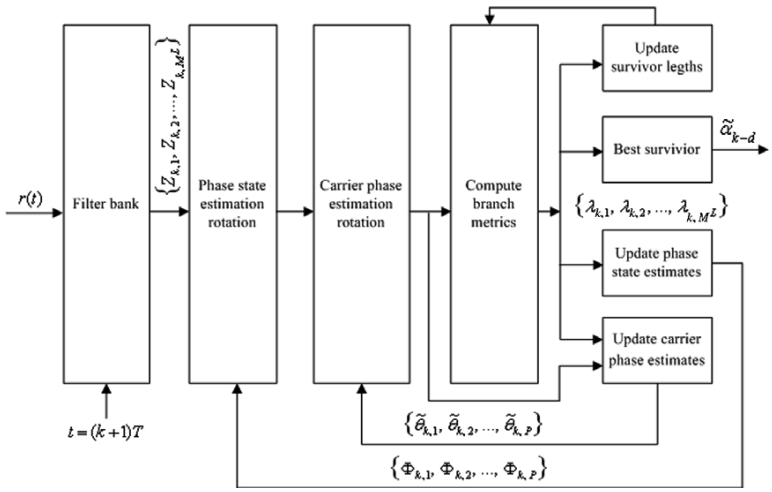

Fig. 2. Joint RSSD and PSP carrier phase estimation receiver.

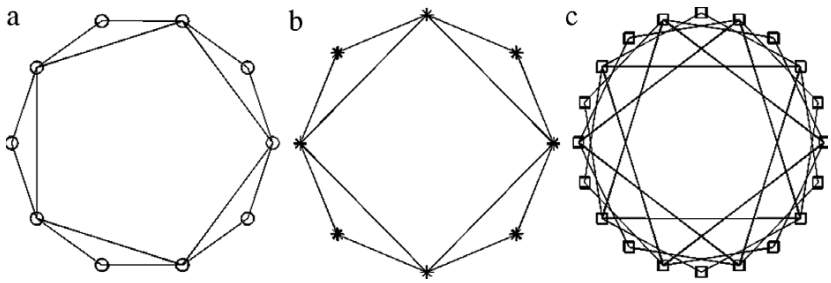

Fig. 3. Constellation points and phase transitions when $h = 0.4$ (a), $h = 0.5$ (b) and $h = 0.6$ (c).

To solve (15) the k-th term in each sum is used as an error signal to update the current estimate of θ. If the known data symbols α_k are replaced with the decisions from the best survivors $\tilde{\alpha}_{k-d}$, the so-called decision directed (DD) method is used. Finally, the next first order loop equation

$$\tilde{\theta}_{k+1} = \tilde{\theta}_k + \gamma_\theta e_\theta(k-d) \tag{16}$$

can be achieved where γ_θ is the updating constant with

$$e_\theta(k-d) = \mathrm{Im}\left\{Z_{k-d}(\tilde{\alpha}_{k-d})e^{-j(\tilde{\theta}_{k-d}+\Phi_{k-d})}\right\}. \tag{17}$$

A large d entails more reliable decisions but also large delays in the loops [21].

In [16] a PSP carrier phase estimation technique has been proposed to be very suitable in the presence of time varying phase jitter. In the PSP principle, the idea is to use the Viterbi algorithm with as many carrier phase estimates (16) as there are phase states P, and the estimation is done for each survivor independently from each other. Finally, Fig. 2 shows the block diagram of the proposed joint RSSD and PSP carrier phase estimation receiver. In order to emphasize the subject that there are independent phase state and carrier phase estimators in the receiver, the corresponding phase rotators are also presented separately, but they can be combined in the real implementation.

2.3. Measured results in a known AWGN channel

In the original paper of TFM [2] the length of the transmitter's frequency pulse L_{TX} is truncated to be 5 symbol intervals. The solid lines with stars in Fig. 3 show eight constellation points and phase transitions $\{0, \pm\pi/4, \pm\pi/2\}$ for the TFM signal with the nominal modulation index value 0.5. The separate lines with circles and squares illustrate the modulation index values 0.4 and 0.6, respectively. In general, the modulation index values 0.4 and 0.6 mean the generalized TFM (GTFM) signals [4]. Since the number of constellation points depends on the modulation index value, it actuates the implementation of A/D and D/A converters, too.

Theoretically, increasing the modulation index value h leads to a better BER performance since the minimum Euclidean distance increases, but at the cost of signal bandwidth expansion [3]. For ideal coherent transmission over the AWGN channel, the bit error probability for the binary CPM signal at high signal-to-noise ratios can be approximated as

$$P_b \approx Q\sqrt{d^2_{\min} E_b/N_0} \tag{18}$$

where $Q(\cdot)$ is the Gaussian Q-function, $d^2_{\min}$ is the squared minimum Euclidean distance and E_b/N_0 is the signal-to-

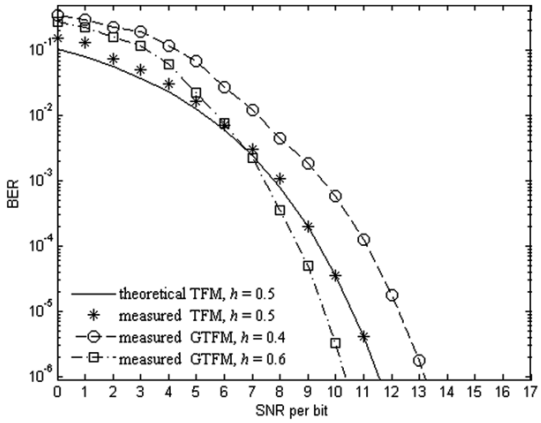

Fig. 4. Theoretical versus measured BER with different modulation index values.

noise ratio (SNR) per bit. For the TFM $d^2_{\min}$ is observed to be 1.58 in [22]. Fig. 4 shows that at the high SNR the measured BER results meet the theoretical bit error probability (18) very well even though the length of the receiver's frequency pulse L_{RX} is truncated to be 3 symbol intervals. The shorter frequency pulse corresponds to a filter bank of 8 filters (11). In the simulations the bit decisions delay d was 9 and the carrier phase estimation was deactivated. In general, the exact error probability is difficult to analyze because the RSSD receiver [19] requires inherently phase state estimation with a decision feedback (see Fig. 2). The error propagation is causing additional bit errors at the low SNR, and especially, when the modulation index is high.

2.4. Measured results in the presence of phase jitter

Ideally, the modulation index of the TFM signal is calibrated to have a nominal value 0.5, but it can drift due to the temperature variations. The alteration in the nominal index value causes the change in the bandwidth of the transmitted TFM signal. On the other hand, when there is a mismatch between the modulation indexes of the transmitter and the receiver, the deviation errors have a time varying phase jitter type characteristic. In the coherent receiver the phase jitter may cause substantial performance degradations as discussed next.

Apart from noise and some intersymbol interference (ISI) due to the receiving filter, the phase jitter of the TFM received signal at symbol time $t = kT$ can be written as

$$e_\theta(kT) = \pi(h' - h)\left\{\alpha_{k-2} + \frac{3}{4}\alpha_{k-1} + \frac{1}{4}\alpha_k\right\} + \pi(h' - h)\sum_{i=-3}^{k-3}\alpha_i \tag{19}$$

where h' is the deviated modulation index and α_k is the binary data with the values of ± 1. Due to the central limit theorem, the phase jitter is approximately Gaussian and its mean is zero. The variance can be expressed as

$$\sigma^2_h(k) = \pi^2(h' - h)^2 \sum_i |c_i|^2 \tag{20}$$

where c_i are the coefficients of the binary data symbols in (19) as

$$\begin{aligned} c_{k-2} &= \pm 1 \\ c_{k-1} &= \pm 3/4 \\ c_k &= \pm 1/4 \\ c_i &= \pm 1 \end{aligned} \tag{21}$$

Finally, by combining (20) and (21) we obtain

$$\sigma^2_h(k) = \pi^2(h' - h)^2 \left\{\frac{13}{8} + k\right\}. \tag{22}$$

Since there is no modulo operation, the phase jitter itself can be approximated asymptotically as a Wiener process [21] since the variance is increasing linearly all the time when $k \to \infty$.

In [15], the PSP technique is used to compensate the phase jitter due to the deviated modulation index of the CPFSK format of CPM. Fig. 5 shows the phase jitter caused by the deviated modulation index $h' = 0.45$ in TFM. The same figure illustrates also the PSP carrier phase estimates. Known data (DA) is assumed to be used in the receiver during the preamble of 31 bits. The preamble is assumed to be a pseudo-random m-sequence. Otherwise, the bit decisions (DD) are used with the delay $d = 9$. The updating constant $\gamma_\theta = 0.49$ in (16) is experimentally optimized at the SNR per bit value 11.5 dB that corresponds the theoretical TFM BER at 10^{-6}. The figure shows that the PSP can follow the shape of the phase jitter curve. On the other hand Fig. 6 shows that the BER performance is, however, decreased around 5.5 dB compared to the nominal index value 0.5 and 4.5 dB if the index value 0.45 is known in the receiver, i.e., GTFM signaling with the modulation index 0.45. A curiosity BER is approximately 0.5 if the PSP estimation is not used at all for the deviated modulation index.

3. Method to estimate the modulation index in the receiver

3.1. Principle of the novel algorithm

Next we present a novel method to measure and control the modulation index of the TFM signal at the receiver.

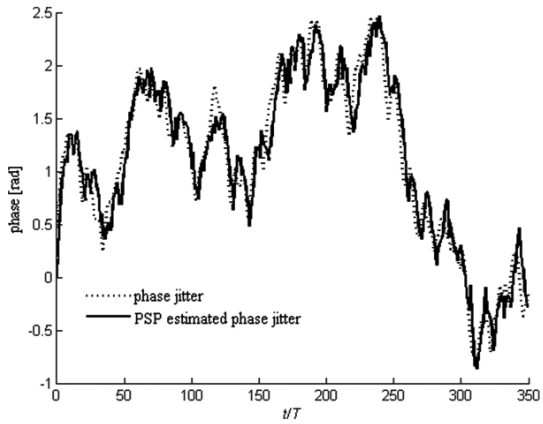

Fig. 5. Phase jitter and PSP estimate when $h' = 0.45$.

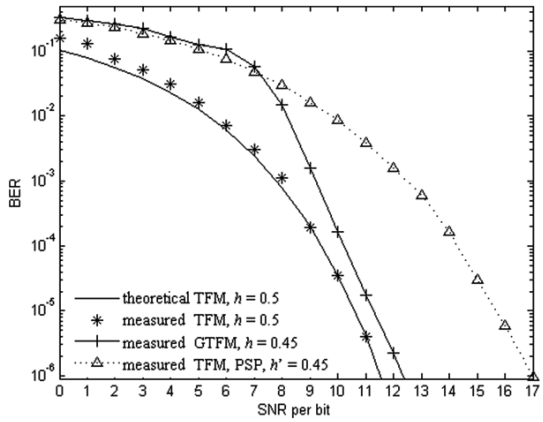

Fig. 6. BER in the presence of phase jitter and PSP estimate when $h' = 0.45$.

The method is based on the coding rule (6) so that, combining it with (7), we can determine the ideal phase transitions ψ_{k+1} for TFM as

$$\begin{aligned}\psi_{k+1} &= \phi(kT+T) - \phi(kT) \\ &= \pi h\left(\frac{1}{4}\alpha_{k-1} + \frac{1}{2}\alpha_k + \frac{1}{4}\alpha_{k+1}\right), \\ &\quad k = 1,\ 2,\ \ldots. \end{aligned} \tag{23}$$

Accordingly, the phase transition Table 1 can then be created since TFM is a binary modulation. In the receiver, the phase transition estimates $\tilde{\psi}_{k+1}$ are for one measured as

$$\tilde{\psi}_{k+1} = \tilde{\phi}(kT+T) - \tilde{\phi}(kT) \tag{24}$$

where $\tilde{\phi}(kT)$ is the phase of the received signal at $t = kT$. By comparing the estimated phase transitions with ideal ones in Table 1, an estimate $\hat{h}$ for the modulation index can be calculated. Heuristically, the next first-order loop can also be determined

$$\hat{h}_{k+1} = \hat{h}_k + \eta e_k \tag{25}$$

Table 1
TFM phase transitions.

α_{k-1}	α_k	α_{k+1}	ψ_{k+1}
1	1	1	πh
−1	−1	−1	$-\pi h$
1	−1	1	0
−1	1	−1	0
1	1	−1	$\pi h/2$
−1	1	1	$\pi h/2$
1	−1	−1	$-\pi h/2$
−1	−1	1	$-\pi h/2$

where η is the updating constant and the error signal e_k is defined by using the relation

$$\tilde{\psi}_{k+1} = \pi(\hat{h}_k + e_k)\left(\frac{1}{4}\alpha_{k-1} + \frac{1}{2}\alpha_k + \frac{1}{4}\alpha_{k+1}\right) \tag{26}$$

so that

$$e_k = \frac{\tilde{\psi}_{k+1} - \pi\hat{h}_k b_k}{\pi b_k} \tag{27}$$

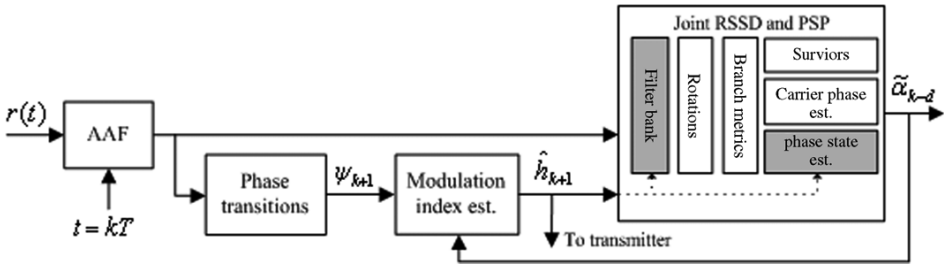

Fig. 7. TFM receiver with estimators.

and

$$b_k = \frac{1}{4}\alpha_{k-1} + \frac{1}{2}\alpha_k + \frac{1}{4}\alpha_{k+1}. \tag{28}$$

The calculation of (27) is neglected and the loop (25) is not updated if $b_k = 0$. When necessary, the bit decisions $\tilde{\alpha}_k$ (DD) can replace the known data bits α_k (DA). The updating constant η can be determined by using the normalized noise equivalent bandwidth $B_L T$ of the loop as

$$B_L T = \frac{\eta A}{2(2 - \eta A)} \tag{29}$$

where A denotes the slope of the S-curve at the origin [21].

Fig. 7 proposes the digital implementation for the joint RSSD and PSP receiver with a separate modulation index estimator. The received signal $r(t)$ is first fed to an anti-aliasing filter (AAF) (11) with phase equal to zero, and the filter outputs are sampled at symbol time $t = kT$. Timing synchronization is assumed to be ideal, and the samples are transferred to a discretized filter bank of Fig. 2. In the DD mode, the modulation index is estimated using bit decisions $\tilde{\alpha}_{k-d}$ from the RSDD and PSP carrier phase estimator, but there is no PSP principle in the modulation estimator itself. The estimated modulation index value $\hat{h}_k$ can be used for the controlling purposes in two ways. The receiver can, of course, send information on the current estimate to the transmitter, and based on that information the transmitter then adjusts the current index value towards the nominal one 0.5. On the other hand, or in addition, the estimated index value can be used for in the receiver itself. The ML receiver structure for TFM signaling in Section 2 is based on the nominal modulation index value: h is 0.5. However, we propose that the nominal value in the ML receiver is replaced with the current estimate $\hat{h}_k$. In more detail, and as shown in Fig. 7, the modulation index estimates are used to adapt the filter bank impulse responses (11) and phase states (3). The receiver is actually tried to be matched to the current modulation index value of the transmitter. Finally, the PSP carrier phase estimation can be used to compensate the residual error in the modulation index.

3.2. Simulation results with open loop

Let us next assume that there is no feedback between the receiver and the transmitter, and the iteration loop (25) is opened as

$$\hat{h}_k = \frac{\tilde{\psi}_{k+1}}{\pi b_k}. \tag{30}$$

The running average $\bar{h}_k$ can be expressed as

$$\bar{h}_k = \frac{1}{K}\sum_{j=1}^{K} \bar{h}_{k,j} \tag{31}$$

where the parameter K denotes the number of selected bit and AWGN sequence combinations and

$$\bar{h}_{k,j} = \frac{1}{1+k}\sum_{i=0}^{k} \hat{h}_{i,j}. \tag{32}$$

Finally, the standard deviation can be determined as

$$\sigma_k = \sqrt{\frac{1}{K-1}\sum_{j=1}^{K}(\bar{h}_{k,j} - \bar{h}_k)^2}. \tag{33}$$

Fig. 8 shows the simulation results for $\bar{h}_k$ and $\bar{h}_k - \sigma_k$ when $K = 5$ and SNR per bit is 11.5 dB. The bits a_k are also assumed to be known (DA) in the receiver. As the simulation results show, $\bar{h}_k$ approaches the current value of h, when the averaging time increases when $k \to \infty$. The memory of the open loop method is infinity. The drawback of this is that the error events of the estimation are also kept in the memory. At the end of the assumed preamble of 31 bits, Table 2 can be created for 95%, 99%, and 99.9% confidence limits. Finally, Fig. 9 shows the simulation results in a form of S-curve, and as the figure shows, very accurate results are achieved for the modulation index estimate.

3.3. Simulation results with closed loop

Let us next assume that the iteration loop (25) is now closed, and the error signal e_k is calculated as presented in (27). Using the normalized noise equivalent bandwidth of the loop $B_L T$ (29), the updating constant η can be determined. From Fig. 9 we can see that the slope A is 1 at the origin. Fig. 10 shows modulation index estimates $\hat{h}$ when $B_L T = 10^{-3}$ or $B_L T = 10^{-4}$ and SNR per bit is 11.5 dB. For convenience, all the bits α_k are assumed to be known (DA) in the receiver. The simulation results show that when the length of the transient state is increased, the jitter of the loop decreases and vice versa. The adjustable rate of change for the closed loop is very useful, especially in the case of time varying h. Also a possible initial value h_{init} of $\hat{h}$ can be efficiently used. In the presented simulations h_{init} is 0.5.

Table 2
Normal distribution confidence limits at the end of preamble 31 bits.

h	$\bar{h}_k$	$h - \bar{h}_k$	σ_k	$\sigma_{95} = 1.96\sigma_k$	$\sigma_{99} = 2.58\sigma_k$	$\sigma_{99.9} = 3.29\sigma_k$
0.55	0.57	−0.02	0.04	0.08	0.10	0.13
0.50	0.51	−0.01	0.03	0.06	0.08	0.10
0.45	0.44	+0.01	0.03	0.06	0.06	0.10

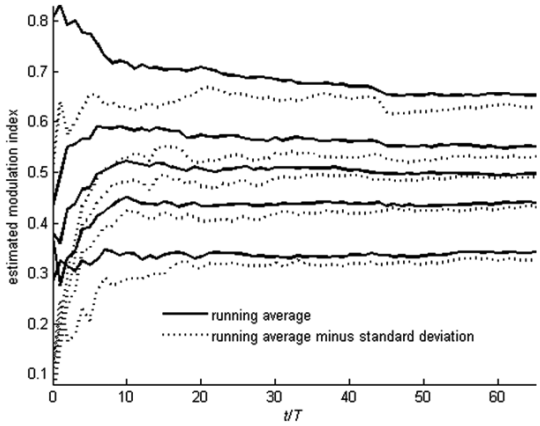

Fig. 8. Open loop modulation index estimate.

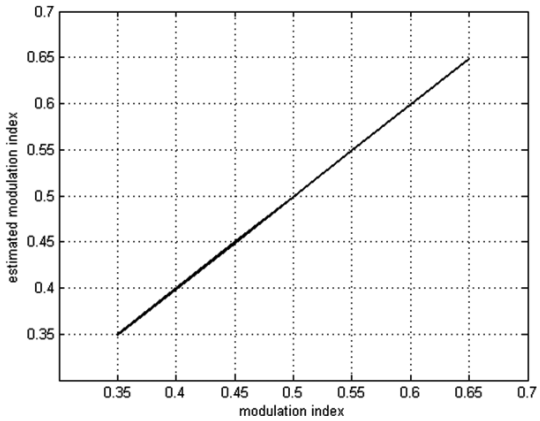

Fig. 9. S-curve for modulation index estimate.

Fig. 11 shows the closed loop performance results when the DA mode has been used only during the preamble of 31 bits, and right after that the BER is measured in the DD mode with a decision delay d of 9. The transmitter's deviated modulation index h' is 0.45 and the initial estimate h_{init} in the receiver is 0.5. The simulation results depend on the updating constant γ_θ in the PSP algorithm (16) and the value $B_L T$. In more detail, the PSP carrier phase estimation is used to compensate the residual error in the modulation index. For the simulations the value γ_θ is experimentally optimized at the SNR per bit value 11.5 dB so that $\gamma_\theta = 0.17$ when $B_L T = 10^{-3}$, $\gamma_\theta = 0.16$ when $B_L T = 10^{-4}$ and $\gamma_\theta = 0.25$ when $B_L T = 10^{-5}$.

As the figure illustrates, the performance degradation is less than 1.0 dB at BER 10^{-6} compared to the results when the index value 0.45 is known in the receiver, i.e., GTFM signaling with the modulation index 0.45. Especially at the low SNR, error propagation is causing additional bit errors. As Fig. 2 shows, the RSSD inherently includes the phase state estimation with a decision feedback. On the other hand, Fig. 7 illustrates that the modulation index estimation is based on the bit decisions in the DD mode. There is also an interaction between the two estimators, and the loops influence each other. The estimators' performance can be improved by increasing the length of the preamble in the DA mode, but on the other hand, the overall

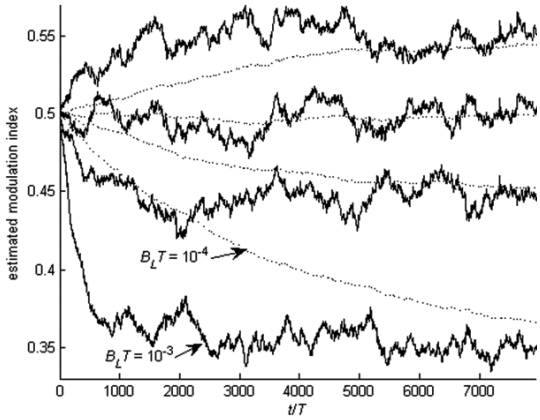

Fig. 10. DA closed loop modulation index estimates.

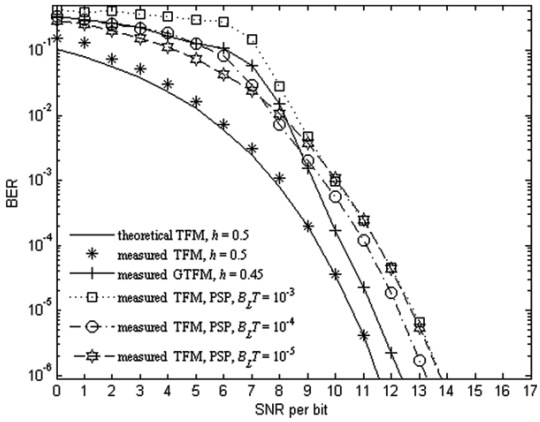

Fig. 11. DA and DD BER performances for modulation index estimation.

data throughput decreases since the ratio between the transmitted preamble data and the transmitted payload data is getting larger. Increasing the decision delay d increases the likelihood of correctly decoding the sequence, but at the same time incurs a greater delay in the decoded bits. With the presented compromise parameters values, the advantage of a separate modulation index estimator over exploiting only PSP carrier phase estimation is, however, evident. Based on Fig. 6, the performance gain is about 3.5 dB.

Related to Figs. 11 and 12 shows in more detail the closed loop modulation index estimates as a function of time. As the estimates show, the compromise between the length of the transient state and the loop jitter has to be made. If the transient state is lengthened, more bit errors can occur during that time, but the loop is less sensitive to AWGN. If the transient state is shortened, the loop is more sensitive to AWGN. On the other hand and clearly, the more accurately the modulation index is known in the receiver, the slower the estimation loop can operate with a smaller value of B_LT, and the better BER performance result can be expected.

Finally, even better BER performance results could be expected if a feedback between the receiver and the transmitter exists. In that case the receiver sends the information on the current estimate of the modulation index to the transmitter, and based on that information the transmitter adjusts the current index value toward the nominal value 0.5. This additional control would also adjust the bandwidth of the transmitted TFM signal toward the ideally expected one. The drawback is, however, the increased complexity of the transmitter.

4. Conclusions

We have presented algorithms and performance results to measure and control the modulation index of TFM especially in the coherent receiver. Since the optimal ML demodulation of a TFM signal involves a complex Viterbi algorithm, a receiver structure for the low complex RSSD was first introduced, and we showed that the simulated

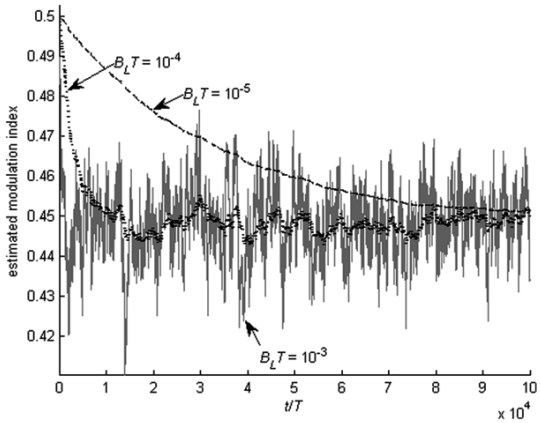

Fig. 12. DA and DD closed loop modulation index estimates.

performance results and the theoretical bit error probability meet well in a known AWGN channel. In simple FM transmitter implementation, the nominal modulation index value can drift due to the temperature variations of analog components, and the deviation generates time varying phase jitter causing substantial performance degradations. We illustrated with simulations that if the modulation index deviation is high enough, the earlier proposed mere PSP carrier phase estimation is not enough for the jitter compensation. A novel particular modulation index estimator was then presented, and it measures phase transitions in the receiver and derives the estimate by comparing the result to the coding rule of the TFM signal. The proposed estimator has acquisition and tracking ability, and the receiver actually tries to be matched with the current modulation index value of the transmitter. The proposed modulation index estimator is thus not valid only for TFM but for GTFM signaling, too. Finally, several steps were taken to optimize the performance of the RSSD and PSP receiver with the modulation index estimator, and we observed that the proposed method has less than 1 dB performance degradation compared to around 4.5 dB exploiting only the PSP carrier phase estimation. The performance could even be more improved by the use of coding techniques, but this task is left for further work.

Acknowledgments

The work was supported in part by the ONEFIT and AWARENESS projects funded by the European Union and VTT Technical Research Centre of Finland. The first author would also like to thank the Jenny and Antti Wihuri Foundation.

References

[1] Y.S. Wu, Constant capacity, DSP architecture—an historical prospective, in: V. Cappellini, A.G. Constantinides (Eds.), Digital Signal Processing, Elsevier Science Publishers BV, 1987, pp. 3–14.
[2] F. Jager, C.D. Dekker, Tamed frequency modulation: a novel method to achieve spectrum economy in digital transmission, IEEE Trans. Commun. 26 (5) (1978) 534–542.
[3] C.-E. Sundberg, Continuous phase modulation, IEEE Commun. Mag. 24 (4) (1986) 25–38.
[4] K. Chung, Generalized tamed frequency modulation and its application for mobile radio communications, IEEE J. Sel. Areas Commun. 2 (4) (1984) 484–494.
[5] J. Bao, Z. Yafeng, L. Jianhua, Concatenated eIRA codes for tamed frequency modulation communications, in: Proc. Int. Conf. Commun., Beijing, 2008, pp. 1886–1891.
[6] M. Kiviranta, A. Mämmelä, D. Cabric, D. Sobel, R.W. Brodersen, Constant envelope multicarrier modulation: performance evaluation in AWGN and fading channel, in: Proc. Military Commun. Conf., Atlantic City, 2005, pp. 807–813.
[7] T. Buzid, M. Huemer, S. Reinhardt, SC/FDE combined with MIMO: an improved out of band power and performance via tamed frequency modulation, in: Proc. Sarnoff Symposium, Princeton, 2007, pp. 1–5.
[8] P. Bianchi, P. Loubaton, F. Sirven, Non data-aided estimation of the modulation index of continuous phase modulations, IEEE Trans. Signal Process. 52 (10) (2004) 2847–2861.
[9] P. Bianchi, P. Loubaton, On the blind estimation of the parameters of continuous phase modulated signals, IEEE J. Sel. Areas Commun. 23 (5) (2005) 944–962.
[10] Z. Zhong, L. Zhang, H. Wu, S. Xia, Non prior knowledge estimation of modulation index for angle modulation signals, Procedia Eng. 23 (2011) 642–646.
[11] J.R. Fonollosa, J.A.R. Fonollosa, Estimation of the modulation index of CPM signals using higher-order statistics, in: Proc. Int. Conf. Acoustics, Speech, and Signal Processing, Minneapolis, 1993, pp. 268–271.
[12] J.R. Fonollosa, C.L. Nikias, Analysis of CPM signal using higher-order statistics, in: Proc. Military Commun. Conf., Boston, 1993, pp. 663–667.
[13] J.B. Anderson, T. Aulin, C.-E. Sundberg, Digital Phase Modulation, Plenum Press, New York, 1986.
[14] L. Lampe, R. Schober, M. Jain, Noncoherent sequence detection receiver for bluetooth systems, IEEE J. Sel. Areas Commun. 23 (9) (2005) 1718–1727.
[15] M.J. Miller, Detection of CPFSK signal using per survivor processing, in: Proc. Military Commun. Conf., Boston, 1993, pp. 524–528.
[16] R. Raheli, A. Polydoros, C.-K. Tzou, Per survivor processing: a general approach to MLSE in uncertain environments, IEEE Trans. Commun. 43 (2,3,4) (1995) 354–364.
[17] P. Moqvist, T.M. Aulin, Serially concatenated continuous phase modulation with iterative decoding, IEEE Trans. Commun. 49 (11) (2001) 1901–1915.
[18] S. Zarei, W. Gerstacker, G. Kilian, W. Koch, An iterative detection algorithm for coded CPFSK signals with irrational modulation index, in: Proc. European Signal Processing Conf., Bucharest, 2012, pp. 2541–2545.
[19] A. Svensson, Reduced state sequence detection of partial response continuous phase modulation, IEE Proc. 138 (4) (1991) 256–268.
[20] M. Kiviranta, Method for demodulating signal, US Patent 6597251, July 22, 2003.
[21] U. Mengali, A.N. D'Andrea, Synchronisation Techniques for Digital Receivers, Plenum Press, New York, 1997.
[22] T. Aulin, Continuous phase modulation—part II: partial response signalling, IEEE Trans. Commun. 29 (3) (1981) 210–225.

Markku Kiviranta received the degrees of M.Sc. (Tech.) and Lic.Sc. (Tech.) from the Department of Electrical Engineering, University of Oulu, Oulu, Finland, in 1994 and 2000, respectively. In 1993, he joined VTT and, until 1996, he was doing research and real time processing development work in the telecommunication field. In 1997–2002, he executed and managed customer R&D projects concentrating on algorithm development of digital signal processing (DSP) applications. During 2003–2011, he was leading the Digital Transceiver team in the Communication Platforms competence center. In 2005 he spent a year with the Berkeley Wireless Research Centre in the USA. Since 2011, he has been a principal scientist of Radio Systems.

Aarne Mämmelä received his D.Sc. (Tech.) degree (with honors) in the field of telecommunications from the University of Oulu, Oulu, Finland, in 1996. He was at the University of Oulu from 1982 to 1993. He visited the University of Kaiserslautern in Germany in 1990–1991 and the University of Canterbury in New Zealand in 1996–1997. In 1993 he joined VTT Technical Research Centre of Finland in Oulu. Since 1996 he has been a Research Professor of digital signal processing in wireless communications. His research interests are in adaptive and cognitive systems in telecommunications.

Physical Communication 17 (2015) 86–93

Contents lists available at ScienceDirect

Physical Communication

journal homepage: www.elsevier.com/locate/phycom

Full length article

Multiple trellis-coded modulation, per-survivor processing and Reed–Solomon coding in the presence of phase noise

Markku Kiviranta *, Aarne Mämmelä

VTT Technical Research Centre of Finland, P.O. Box 1000, FI-02044 VTT, Finland

ARTICLE INFO

Article history:
Received 6 June 2014
Accepted 21 August 2015
Available online 25 September 2015

Keywords:
Channel coding
Maximum likelihood estimation
Modulation
Phase noise
Tracking loops

ABSTRACT

The aim of this paper is to consider trellis coded modulation (TCM) in the presence of phase noise. The starting point is a two-dimensional 32 point cross (32-CR) signal set that has served as a benchmark for other power and bandwidth efficient modulation schemes. Per-survivor processing (PSP) is used for carrier phase estimation, and both the phase acquisition (transient state) and phase tracking (steady state) performances are considered in an additive white Gaussian noise (AWGN) channel, in which phase offset or time varying phase noise is introduced. Based on the theoretical and simulation results it can be said that the 32-CR constellation is itself more sensitive to a phase error rather than the PSP algorithm. Due to the phase error the TCM scheme becomes a catastrophic code. Possible solutions include stringent phase noise requirements for oscillators, multiple trellis-coded modulation (MTCM) and concatenated TCM and Reed–Solomon (RS) coding. Our simulation results show that a simple combined MTCM, PSP and RS scheme has around 3 dB advantage compared to the pure TCM and PSP in the presence of phase noise. A semianalytical approach is used for performance evaluation, and the method is a particularly convenient tool to determine the rate of RS coding in detail.

1. Introduction

According to the Shannon–Hartley law the basic resources of a transmission system are the transmitted power and the bandwidth. In general, the resources are tried to economize by using error control coding and modulation methods which have historically been treated as distinct subjects [1]. However, in his visionary paper of 1974 Massey [2] surmised that treating error control coding and modulation as an integrated entity would allow significant coding gains to be achieved over power and bandwidth limited systems. The first practical coded modulation scheme was proposed by Imai and Hirakawa 1977 [3], followed by Ungerboeck 1982 [4], who introduced first the term TCM. The original trellis codes based on one- and two-dimensional signal constellations and from the 1980s to the present numerous publications have appeared in the literature. Multidimensional trellis codes were first used by Wei [5] and Calderbank and Sloane [6]. The TCM schemes have applied for satellites, cellular and personal communications services (PCS), as well as for HF tropospheric long range and high speed short range communications among others. A recent paper [7] studies the TCM also for flash memories. In this work, we concentrate on a two-dimensional 32-CR TCM scheme that has the asymptotic coding gain of 4 dB compared to 16-quadrature amplitude modulation (16-QAM), and which is adopted by the ITU Telecommunication Standardization Sector (ITU-T) in the V.32 standard for high speed modems.

PSP provides a general framework for the approximation of maximum likelihood sequence estimation (MLSE) algorithms whenever the presence of unknown channel parameters prevents the precise use of the classical Viterbi

* Corresponding author. Tel.: +358 40 5890642; fax: +358 20 7222320.
E-mail addresses: markku.kiviranta@vtt.fi (M. Kiviranta), aarne.mammela@vtt.fi (A. Mämmelä).

http://dx.doi.org/10.1016/j.phycom.2015.08.004
1874-4907/

algorithm. In the classical PSP estimation, the symbol sequence associated to each survivor is used as the data-aided (DA) sequence [8]. In multiple survivor technique, aka joint data and channel estimation (JDCE) [9], each trellis state can have more than one survivor each having own estimator. The multiple state techniques [10] in turn, convey the idea that for every known channel state, there are several states in an expanded trellis. In contrast a reduced survivor technique at the cost of decreased performance is proposed in [11]. In this work we assume that the unknown channel parameter for the PSP estimation is carrier phase.

According to [12], TCM schemes are more sensitive to phase error than the corresponding uncoded modulations. At a given energy, the signal points in the constellation are close to each other as the alphabet size M for the transmitted symbols gets larger, which for a given phase perturbation is more likely to cause errors. In multiple trellis-coded modulation (MTCM) [13] different alphabet sizes M for the transmitted symbols are used, and the carrier phase estimation is obtained only from the smaller alphabet sizes symbols, which are less sensitive to phase error. The concatenation of TCM with outer RS coding has been studied, e.g., in [7]. Each incorrectly chosen path in the Viterbi algorithm produces an error burst, and the RS codes are well suited to handle these errors.

The novelty of this paper lies in a simple combined MTCM, PSP and RS scheme. According to our knowledge, this is the first paper which considers the performance of the fully integrated MTCM, PSP and RS system in the presence of phase noise. The starting point for the study is the 8-state 32-CR TCM modulation, and the analysis in an AWGN channel determines the performance boundaries. For comparison the results for a 16-state scheme is illustrated, too. When we introduce phase offset or time-varying phase noise to the system model, the latter type of noise is assumed to be slowly varying, and it is modeled as a zero mean, nonstationary, asymptotically infinite power Wiener process. Phase acquisition (transient state) and tracking (steady state) performances are studied. To get better results, the MTCM principle is then applied in a simple manner, and the method is complemented with the RS coding. For performance analysis of the combined MTCM, PSP and RS system a convenient semianalytical method is presented. Finally, the conclusions are drawn.

2. System model

2.1. General structure of a transmitter and receiver

In this work we concentrate on two-dimensional trellis codes. Assume that m information bits are to be TCM encoded per transmitted symbol $x_n = I_n + jQ_n$, in which symbols I_n and Q_n denote the real and imaginary part, respectively. In the encoder, $\tilde{m} \leq m$ bits are expanded by a rate $\tilde{m}/(\tilde{m}+1)$ binary convolutional encoder into $\tilde{m}+1$ coded bits. These coded bits are used to select one of $2^{\tilde{m}+1}$ subsets of a redundant 2^{m+1}-ary signal set. The remaining $m-\tilde{m}$ uncoded bits determine which of the $2^{m-\tilde{m}}$ signals in this subset is to be transmitted [12,14]. Since the V.32 standard serves as a benchmark for other power and bandwidth efficient schemes, it is a natural base for this paper, too. A rate-2/3 encoder has the constraint length $v = 3$ and the corresponding 8-state trellis code is used in conjunction with the 32-CR constellation. In fact, the trellis code of the V.32 is a variant of Ungerboeck's original one [4] so that Ungerboeck's trellis code is linear while the convolutional encoder in the V.32 modem is nonlinear [13]. With the linear trellis code, it is only possible to have either no or π rotational invariance. Since many carrier phase synchronization methods exhibit multiples of $\pi/2$ rad phase ambiguity in the recovered carrier phase, it is desirable to have fully rotationally invariant trellis codes [15,16].

If the transmitted pulse of unit energy is selected by using the Nyquist criterion [17], there is no intersymbol interference (ISI), and the time discrete model at symbol interval T at the output of the receiver matched filter can be expressed as

$$z_n = x_n + v_n \tag{1}$$

where v_n is a discrete time sample of AWGN. The Viterbi algorithm as an asymptotically optimum decoding technique for convolutional codes can be used to determine the coded sequence $\{\hat{x}_n\}$ closest to the received sequence $\{z_n\}$ provided that the generation of sequence $\{x_n\} \in \mathrm{C}$ follows the rules of a finite-state machine. In PSP, parameters are estimated by incorporating DA estimation techniques into the structure of the Viterbi algorithm. Each state has a separate estimator based on the survivor, and the estimators are updated without decision delay. Finally, a system model is shown in Fig. 1, and the combination of blocks marked with dotted lines emphasizes the novelty of this paper. The serially concatenated convolutional and RS codes are based on the assumption that in an inner convolutional code each incorrectly chosen path produces an error burst that is corrected by the RS. On the other hand, uncoded M-QAM symbols can be used for synchronization purposes, and in this work they are employed in the PSP carrier phase estimation when the MTCM is applied in the presence of phase noise.

2.2. Performance in AWGN channel

At high signal-to-noise ratios (SNRs), the bit error probability of linear trellis coding is generally well approximated [13] by

$$P_b \approx \frac{N_{\text{free}}}{m} Q\left(\sqrt{d_{f,n}^2 m E_b/2N_0}\right) \tag{2}$$

where N_0 is power spectral density of white Gaussian noise and N_{free} denotes the average number of nearest neighbor signal sequences with free distance d_{free} that diverge at any state from the transmitted signal sequence, and remerge with it after one or more transitions. The squared normalized free distance can be determined as

$$d_{f,n}^2 = \frac{d_{\text{free}}^2}{mE_b} \tag{3}$$

where E_b is average bit energy. For simplicity, we assume that (3) is 1, and according to [18], N_{free} is 16 which is also the limit of large two-dimensional signal "Z_2" sets of lattice

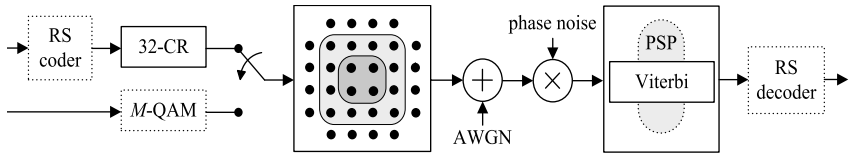

Fig. 1. System model for MTCM, PSP and RC coding.

type with 8-state trellis-code. As a comparison, an uncoded M-ary QAM, for which m is even, and Gray coded bits are used [17], is upper bounded at high SNR per bit (E_b/N_0) values as

$$P_b \approx \frac{1}{m}\left\{1-\left[1-2\left(1-1/\sqrt{2^m}\right)\times Q\left(\sqrt{3mE_b/N_0(2^m-1)}\right)\right]^2\right\}. \quad (4)$$

Theoretical asymptotic coding gain between 16-QAM and the linear 8-state 32-CR TCM approaches the value 4 dB [4]. It is also roughly speaking possible to gain nearly 5 dB with 16 states, and up to 6 dB with 128 or more states [18]. According to [19] the upper bound (2) error probability is not accurate for the nonlinear trellis codes such as V.32, and so called distance profile invariant transformations (DPIT) scheme is used to analyze performance. For simplicity and since the AWGN channel determines the performance boundaries for further study Fig. 2 presents simulation results for the nonlinear 8-state 32-CR TCM. At high SNR values the performances of nonlinear and linear trellis codes approach each other asymptotically, and the asymptotic coding gain 4 dB over the uncoded 16-QAM modulation can be achieved. Similar observations have been made in [19]. As a curiosity Fig. 2 shows also the simulated bit error rate (BER) for nonlinear 16-state trellis-coded 32-CR [20]. The code is also invariant to multiples of $\pi/2$ but it seems to be difficult to obtain the asymptotic coding gain 5 dB of the linear one. In the receiver, the decoding delay D for the Viterbi algorithm is five times the constraint length of the encoder v and the differential decoder is used.

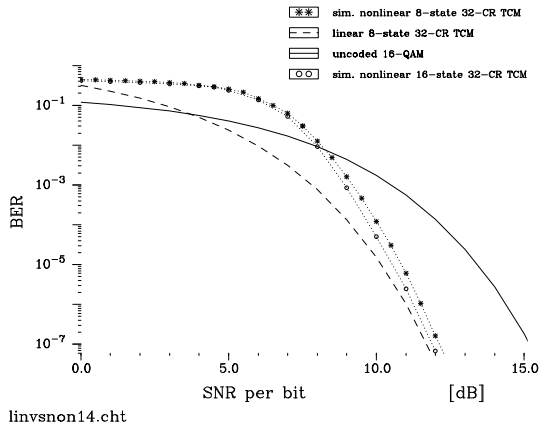

Fig. 2. Performances boundaries in an AWGN channel.

3. Joint decoding and carrier phase synchronization

The optimal MLSE receiver represents the optimum decoding strategy in a known linear band-limited AWGN channel [8]. Unfortunately, in many practical communication systems this ideal situation is not encountered, and a simplified receiver must be adopted to combat excessive complexity. We next consider the case where the carrier phase has to be estimated. According to (1), the time discrete model at the receiver can now be expressed as

$$z_n = x_n e^{j\theta_n} + v_n \quad (5)$$

where θ_n denotes the carrier phase that is assumed to change slowly during the symbol interval. The standard approach to approximate MLSE decoding in the presence of uncertainty is based on DA parameter estimation techniques using some known symbols. A decision-directed (DD) carrier phase synchronization loop uses tentative decisions from the Viterbi algorithm [4,8]. In this paper, we concentrate on joint TCM decoding and PSP carrier phase synchronization. Especially, we consider the phase acquisition (transient state) and tracking (steady state) performance of such an application.

For the formal description of the joint TCM decoding and PSP carrier phase synchronization, let us now denote the state in the trellis diagram by σ_n [8] at the nth epoch. Associated with the state transition $\sigma_n \rightarrow \sigma_{n+1}$ there is now a subset, which we denote as $X(\sigma_n \rightarrow \sigma_{n+1})$. The branch metrics are evaluated according to

$$\lambda(\sigma_n \rightarrow \sigma_{n+1}) = \min_{x_n \in X(\sigma_n \rightarrow \sigma_{n+1})} \left| z_n e^{-j\hat{\theta}(\sigma_n)} - x_n \right|^2 \quad (6)$$

where $\hat{\theta}(\sigma_n)$ denotes the per-survivor phase estimate. Denoting the survivor metrics with $\Gamma(\sigma_n)$, for all successor states σ_{n+1}, the accumulated metrics $\Gamma(\sigma_{n+1})$ are determined by performing a minimization over the current states σ_n

$$\Gamma(\sigma_{n+1}) = \min_{\sigma_n} \left[\Gamma(\sigma_n) + \lambda(\sigma_n \rightarrow \sigma_{n+1})\right]. \quad (7)$$

The survivors terminating in the current states are then extended by incorporating the transitions that comply with (7). Finally, per-survivor estimates $\hat{\theta}(\sigma_n)$ are updated for the transitions that extended the survivors according to

$$\hat{\theta}(\sigma_{n+1}) = \hat{\theta}(\sigma_n) + \eta \mathrm{Im}\left\{z_n x_n^* e^{-j\hat{\theta}(\sigma_n)}\right\} \quad (8)$$

where the symbol $x_n \in X(\sigma_n \rightarrow \sigma_{n+1})$ minimizing (6) is used and η is a suitable real valued constant.

3.1. The acquisition performance

First we will concentrate on the phase acquisition performance in the presence of phase offset. At high SNR, we assume [8,21] that the best surviving path at any given time is the correct path. As a result, the loop Eq. (8) can be expressed in the following compact form

$$\hat{\theta}_{n+1} = \hat{\theta}_n + \eta e_n \tag{9}$$

where

$$e_n = \mathrm{Im}\left\{ z_n x_n^* e^{-j\hat{\theta}_n} \right\}. \tag{10}$$

The error signal e_n provides a measure of the difference between the carrier phase θ_n and its current estimate $\hat{\theta}_n$. The error signal serves to steer the loop (9) and keeps the above mentioned difference as small as possible. The average of the error signal, conditioned on a fixed phase error $\phi \hat{=} \theta - \hat{\theta}$, is referred to as S-curve, i.e.,

$$S(\phi) \hat{=} \mathrm{E}\{e_n|\phi\} \tag{11}$$

where θ and $\hat{\theta}$ denote the phase offset and the phase offset estimate, respectively. In general, the S-curve provides information about loop acquisition capability. S-curves may have several stable points, separated by some fixed quantity from each other. According to literature the rectangular and cross shaped constellations in general have the periodicity of $\pi/2$. In general, this kind of phase ambiguity can be resolved with differential encoding and decoding. For TCM schemes, S-curves are usually derived by simulations since analytical methods are too complex [23]. Experimentally $S(\phi)$ is obtained by opening the loop (9) and measuring the time average of the error signal e_n in (10), so that $e^{-j\hat{\theta}_n} = 1$. The PSP algorithm is thus switched off, and it has no influence on the simulated results. Finally, Fig. 3 shows the S-curves of the nonlinear 8-state trellis-coded 32-CR with error signal (10). The figure confirms the $\pi/2$ periodicity, and between the stable points, the S-curves have extensive dead zones and spurious equilibria that cannot be resolved by differential encoding and decoding. If the initial phase error lies in a dead zone, there is no steering force to lead the loop (9) toward the nearby correct lock condition and the system will perform a long random walk before locking. In general these kinds of occurrences are called as hang-up phenomena, which occasionally occur during phase acquisitions. Due to the phase error the 32-CR TCM scheme becomes a catastrophic code [22]. Similar observations are presented in [23] where the S-curves for the linear trellis coded M-ary phase shift keying (PSK) are illustrated. The main difference is that the PSK constellations have a periodicity of $2\pi/M$.

From Fig. 3 we can observe that the two-sided operational range of the S-curve has roughly the value 0.4 rad, if no AWGN has been assumed. From Fig. 1 we can for one note that the minimum angle between two signal points, which have the same amplitude is also about 0.4 rad or 23°. As a conclusion, the phase error of about 0.2 rad or 11.5° can cause undesired results, as Fig. 3 shows. In the presence of noise, the situation can be even worse. In [23] it is mentioned that changes in the error signal e_n (10) are needed to prevent spurious equilibria, which may exhibit in the S-curves. For example, in [24–26] several error signals are proposed. However, after several simulations and analyses we can claim that the changes in the error signal do not give any better results.

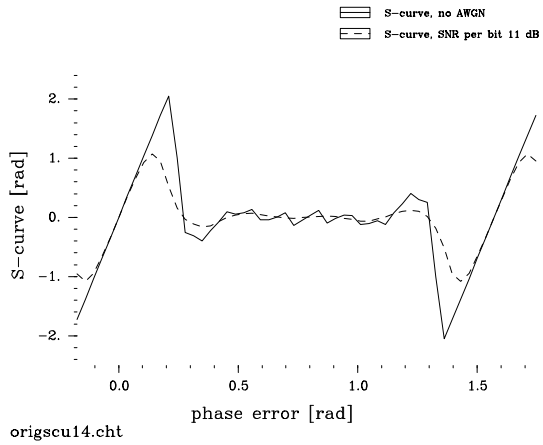

Fig. 3. The S-curve of the 32-CR TCM.

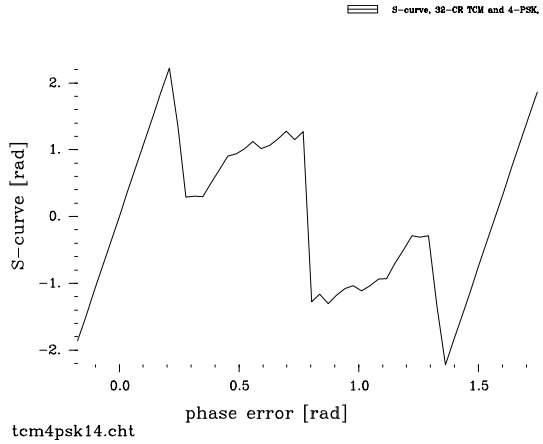

Fig. 4. The S-curve of the 32-CR MTCM.

Fig. 4 shows the S-curve when the earlier mentioned MTCM [13] principle is applied in such a way that every ninth symbol is a non-coded 4-QAM symbol, and the amplitude of the added symbols is equal to peak amplitude of the 32-CR in Fig. 1. As the S-curves show, we can avoid the problems of the extensive dead zones and spurious equilibria.

3.2. The tracking performance

We next consider the performance of the joint TCM decoding and carrier phase synchronization scheme in the presence of time varying phase noise. In order to determine the updating constant η for the phase tracking algorithm (9), let us determine the normalized noise equivalent

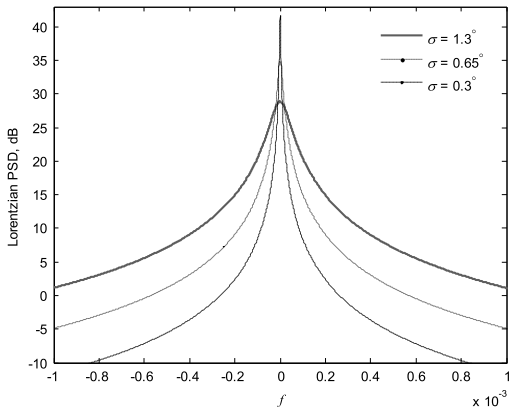

Fig. 5. The Lorentzian PSD with different standard deviation σ values.

bandwidth of the loop as

$$B_L T = \frac{\eta A}{2(2-\eta A)} \tag{12}$$

where A denotes the slope of the S-curve at the origin, and can be determined as follows: If we ignore the noise term v_n in (5) and assume that $e^{-j\hat{\theta}_n} = 1$ in (10), as in the case of S-curve simulations, we can rewrite the original error signal (10) as

$$e_n = \mathrm{Im}\left\{z_n x_n^* e^{j\theta}\right\} = \mathrm{Im}\left\{x_n x_n^* e^{j\theta}\right\} = \mathrm{Im}\left\{E_s e^{j\theta}\right\}. \tag{13}$$

By taking into account that $e^{j\theta} = \cos(\theta) + j\sin(\theta)$, we can express (13) as

$$e_n = E_s \sin(\theta). \tag{14}$$

The slope A can be finally determined at the origin of the S-curve as

$$A = \frac{d}{d\theta} E_s \sin(\theta) = E_s \cos(\theta) \approx E_s, \quad |\theta| \ll 1. \tag{15}$$

The phase noise is modeled as an asymptotically infinite power Wiener process

$$\theta_{n+1} = \theta_n + \varphi_n \tag{16}$$

where φ_n are independent and zero mean Gaussian random variables with the same standard deviation σ [23]. According to (5) the phase noise θ_n causes a disturbance $e^{j\theta_n}$ on the input signal [27]. When the phase noise is nonstationary Wiener process (16), the spectrum of $e^{j\theta_n}$ is Lorentzian

$$S(f) = \frac{2/\pi\beta_{\mathrm{PN}}}{1 + (2f/\beta_{\mathrm{PN}})^2} \tag{17}$$

where the normalized two sided 3-dB bandwidth or the phase noise rate is

$$\beta_{\mathrm{PN}} T = \sigma^2/2\pi. \tag{18}$$

As Eq. (18) and Fig. 5 show, the Lorentzian power spectral density (PSD) becomes wider or narrower with increasing or decreasing the value of the standard deviation σ in (16).

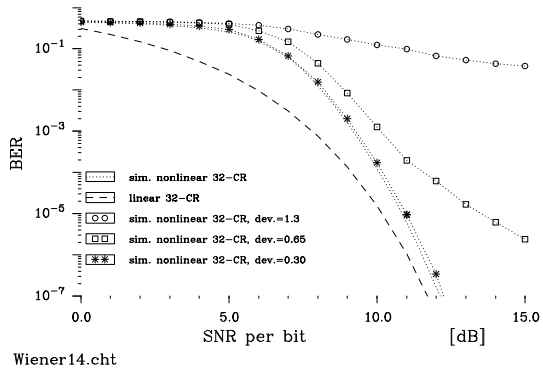

Fig. 6. The simulated BER for the nonlinear joint 32-CR TCM and PSP.

In the presence of phase noise, the performance of the PSP algorithm with linear 4- or 8-state trellis-coded 8-PSK [4] is considered in [23]. In those simulations the standard deviation is assumed to be $\sigma = 1.3°$ and the normalized noise equivalent bandwidth of the loop (9) is assumed to be $B_L T = 10^{-2}$, which corresponds a memory length of 100 symbols. These parameters are also the starting point for our nonlinear 8-state 32-CR TCM scheme and in the simulations the transient-state of the synchronization algorithm is assumed to be overtaken. The BER results in Fig. 6 show that the performance is bad when $\sigma = 1.3°$. If the standard deviation is halved, i.e., $\sigma = 0.65°$, somewhat better results are achieved, and the results are excellent when $\sigma = 0.3°$. As a rule of thumb we can also say that $\beta_{\mathrm{PN}} \ll \beta_L$, i.e., phase noise changes should be slow compared to the estimator memory length. In practice, the achieved results indicate stringent phase noise requirements for oscillators. On the other hand, we can conclude that 32-CR TCM is more sensitive to phase noise than the 8-PSK TCM in [4]. As stated earlier, this is obvious since for a given energy, the constellation density increases as the alphabet size M gets larger.

When the phase noise is strong, the reason for the bad performance results seems to be a phenomenon called cycle slipping [23]. Briefly, assume that the loop (9) is in the tracking mode and the estimate $\hat{\theta}_n$ is fluctuating around the true carrier phase θ_n. Fluctuations are usually small. If the phase error deviates enough from a stable point in the S-curve, $\hat{\theta}_n$ will be attracted toward some nearby equilibrium point. When this happens we say that a phase slip has occurred. A slip implies a net change of $\hat{\theta}_n$ by multiples of $\pi/2$ rad in the case of nonlinear 32-CR TCM (see Fig. 3). As a consequence of the phase slip, a burst of errors in the data detection process occurs. Cycle slips must be rare events in a well-designed loop.

Fig. 7 shows the phase noise θ_n (16) and the corresponding estimate $\hat{\theta}_n$ (9) as a function of symbol intervals, when σ is 1.3° in (16) and SNR per bit is 11 dB in an AWGN. As the figure illustrates the estimated phase noise $\hat{\theta}_n$ is first fluctuating around the phase noise θ_n, but then a very slow phase slips starts, and a net change of $\hat{\theta}_n$ by $\pi/2$ rad occurs. As a consequence of the slow phase slip, a long error burst is generated, as Fig. 8 shows. The length of burst appears

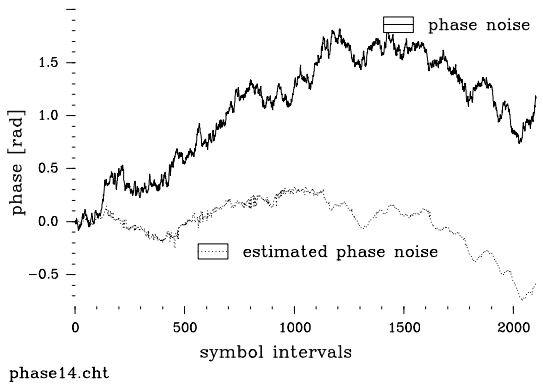

Fig. 7. The phase noise and the estimated phase as a function symbol intervals.

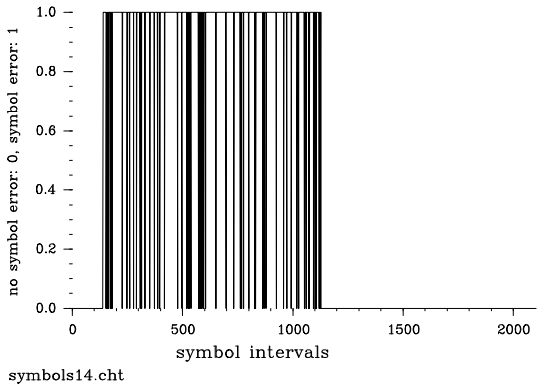

Fig. 8. TCM error burst caused by the cycle clipping.

to correspond to one order of magnitude longer than the estimator's memory.

In general, phase noise cannot be tracked fast enough if the estimator's loop bandwidth (12) is too small. On the other hand, a large bandwidth makes the loop more sensitive to noise. The PSP algorithm with the same simulation parameters is used for linear 8-PSK TCM in [23]. Both the theoretical and the simulation results show the superiority of the PSP algorithm. For example, the difference is 2–3 dB in the presence of phase noise with $\sigma = 1.3^{\circ}$. However, the problem of slow phase slips is enounced in [21]. In general, the PSP algorithm is useful to reduce the slip rates and to shorten the reacquisition when the loss of tracking has occurred [8]. Therefore, it is obvious that if the conventional carrier phase synchronization algorithm is used with the current nonlinear 32-CR TCM, even worse performance results are achieved.

3.3. Phase tracking with MTCM

Fig. 9 shows the TCM symbol errors when the MTCM [13] principle is applied so that the carrier phase tracking is obtained from both 32-CR TCM and 4-QAM symbols. As the results illustrate, significantly shorter error bursts are observed and thus, e.g., additional burst error

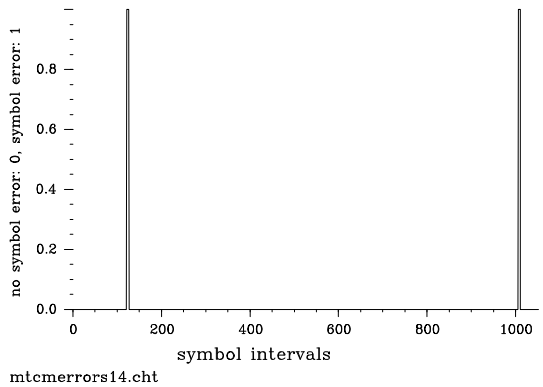

Fig. 9. Error burst in MTCM principle.

correction RS could be efficiently used. In the simulations, every ninth transmitted symbol is an uncoded 4-QAM symbol (see Fig. 1), and the corresponding acquisition S-curve is presented in Fig. 4. For each state σ_n of the trellis diagram in the receiver, the minimum squared Euclidean distances are now evaluated according to

$$\lambda(\sigma_n)_{4QAM} = \min_{p_n \in P_{4QAM}} \left| z_n e^{-j\hat{\theta}(\sigma_{n-L})} - p_n \right|^2. \tag{19}$$

After that per-survivor estimates $\hat{\theta}(\sigma_n)$ are updated according to

$$\hat{\theta}(\sigma_{n+1}) = \hat{\theta}(\sigma_{n-L}) + \eta Im\left\{ z_n p_n^* e^{-j\hat{\theta}(\sigma_{n-L})} \right\} \tag{20}$$

where symbol $p_n \in P_{4QAM}$ minimizing (19) is used. The suitable constant η equals with (8), but may also be unequal. When M-QAM symbols are added to the frame of symbols, the total number of information bits can be expressed as $(F-1)m + m_{\mathrm{QAM}}$ in which F is the total number of symbols in a frame and m_{QAM} is the number of information bits in one QAM symbol. In our simulations, the 4-QAM symbols are used only for phase tracking, and thus they increase the average energy for one information bit. In more detail, the average energy for one information bit can be given as

$$E_{b,\mathrm{inf}} = \frac{(F-1)E_s + E_{4-\mathrm{QAM}}}{(F-1)m} \tag{21}$$

where $E_{4-\mathrm{QAM}}$ is the energy of one 4-QAM symbol. When $E_{4-\mathrm{QAM}}$ is set to equal with the peak energy of 32-CR signal set, and (3) is 1, the decrease in SNR per information bit is $10\log_{10}\left(E_b/E_{b,\mathrm{inf}}\right) \approx 0.8$ dB.

3.4. Performance with outer RS coding

RS codes are well suited to correcting error bursts. Therefore, it is expected that MTCM scheme based on convolutional coding and RS code together will have a better performance in the presence of phase noise. The concatenated codes require also a symbol interleaver between them, and in the case of channels with memory we may be far from the ideal performance with all tolerable interleaver sizes.

According to [28] a very accurate approximation on the RS bit error probability can be given as

$$P_{b,\mathrm{RS}} \approx \frac{\gamma}{k} \sum_{i=t+1}^{l} \binom{l}{i} \frac{i}{l} P_{s,l}^{i} \left(1 - P_{s,l}\right)^{l-i} \tag{22}$$

where l is the length of RS(l, s) code word with k-bit information symbols s and $P_{s,l}$ is the symbol error probability at the RS decoder's input. The parameter γ refers to expected number of bit errors in an incorrect RS symbol at the inner decoder output. The unbiased estimate can be easily obtained by simulations as

$$\tilde{\gamma} \approx \frac{e_{b,l}}{e_{s,l}} \tag{23}$$

where $e_{b,l}$ and $e_{s,l}$ are the total numbers of occurring bit and symbol errors. Using (23), we can also write

$$P_{s,l} = \frac{k}{\ell} P_b. \tag{24}$$

For the linear 32-CR TCM, the theoretical P_b is determined by means of (2), but for the nonlinear modulations we can use the simulated BER in Fig. 2. The measured $\tilde{\gamma}$ varies with the changes of E_b/N_0, but as stated in [28], the variation is not large, and especially in the most interesting range of BER, it is almost a constant. According to our simulations $\tilde{\gamma}$ is approximately 2.08 in both AWGN channel and in the presence of phase noise.

Fig. 10 shows both the semianalytical (22) and measured BER for the combined MTCM, PSP and RS scheme. In general, the low redundancy high rate codes are the most attractive ones, and since the maximum code word length l for a RS code is $l = 2^k - 1$, the RS(15, 11) code is selected for simplicity as well as the ideal interleaver. As in the case of MTCM principle in Section 3.3, the RS coding has the similar decrease in SNR per information bit, and it can be expressed as $10 \log_{10}(s/l) \approx 1.3$ dB. The MTCM and RS cause also some increase in bandwidth, if we want to keep the information bit rate as a constant, and thus there is a trade-off in parameterization. Finally, as a summary, it can be said that the combined MTCM, PSP and RS scheme has around 3 dB advantage at the BER level of 10^{-7} compared to the pure TCM and PSP in the presence of phase noise. Since the measured results meet the semianalytical ones very well, the proposed approach can be used to determine the rate of RS coding in detail.

4. Conclusion

The starting point for the study was a 32-CR TCM scheme for which the theoretical performance analysis and simulations in an AWGN channel determined the performance boundaries. In the presence of phase error, both phase acquisition and phase tracking performances were studied. The open loop S-curve simulation results showed that there are spurious equilibria and extensive dead zones which may cause a long random walk for the estimator before locking. The PSP phase tracking was considered in the presence of a time varying phase noise, modeled as a Wiener process. In general, the phase noise changes should be slow compared to the estimator memory length. In practice, this would mean stringent phase noise requirements for oscillators. On the other hand, the results indicate that the 32-CR constellation is itself more sensitive to a phase error rather than the PSP algorithm. The MTCM principle was then proposed in a simple manner, and the method was complemented with the RS coding. Our simulation results show that the fully combined MTCM, PSP and RS scheme has around 3 dB advantage in the presence of phase noise. A semianalytical approach was used for performance evaluation, and the method is particularly convenient tool to determine the rate of RS coding in detail. Finally, the work can be extended to any two-dimensional constellations, and future research will cover the multidimensional trellis codes.

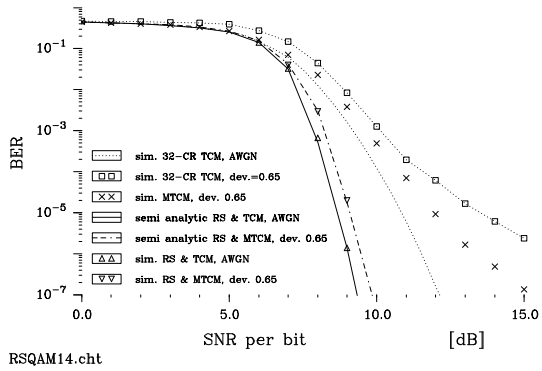

Fig. 10. Combined MTCM and PSP and RS coding in the presence of phase noise.

Acknowledgments

The work was partially done in the AWARENESS project funded by VTT Technical Research Centre of Finland and in the A-PLATE project funded by Tekes - the Finnish Funding Agency for Innovation (Grant number 40137/12) and VTT Technical Research Centre of Finland. The first author wishes also to thank the Jenny and Antti Wihuri as well as the Riitta and Jorma J. Takanen foundations.

References

[1] W. Web, L. Hanzo, Modern Quadrature Amplitude Modulation: Principles and Applications for Fixed and Wireless Channels, Pentech Press, London, 1994.
[2] J.L. Massey, Coding and modulation in digital communications, in: Proc. 1974 Int. Zurich Seminar on Digital Communications, 1974, pp. E2(1)–E2(4).
[3] H. Imai, S. Hirakawa, A new multilevel coding method using error-correcting codes, IEEE Trans. Inform. Theory 23 (1977) 371–377.
[4] G. Ungerboeck, Channel coding with multilevel/phase signals, IEEE Trans. Inform. Theory 28 (1982) 55–67.
[5] L.-F. Wei, Trellis-coded modulation with multidimensional constellations, IEEE Trans. Inform. Theory 3 (1987) 483–501.
[6] A.R. Calderbank, N.J.A. Sloane, An eight-dimensional trellis code, in: Proc. IEEE, 1986, pp. 757–759.
[7] J. Oh, J. Ha, J. Moon, G. Ungerboeck G, RS-enhanced TCM for multilevel flash memories, IEEE Trans. Commun. 61 (2013) 1674–1683.
[8] R. Raheli, A. Polydoros, C.-K. Tzou, Per survivor processing: A general approach to MLSE in uncertain environments, IEEE Trans. Commun. 43 (1995) 354–364. Feb./Mar./Apr..
[9] N. Seshadri, Joint data and channel estimation using blind trellis search techniques, IEEE Trans. Commun. 42 (1994) 1000–1011. Feb./Mar./Apr..
[10] K.M. Chugg, Blind acquisition characteristics of PSP-based sequence detectors, IEEE J. Sel. Areas Commun. 16 (1998) 1518–1529.

[11] N. Safari, A. Vahlin, Low complexity implementation of per-survivor processing for carrier-phase tracking in uncertain environments, in: Proc. Radio and Wireless Symposium, RWS, 2012, pp. 195–198.
[12] G. Ungerboeck, Trellis-coded modulation with redundant signal sets. Part II: State of the art, IEEE Commun. Mag. 25 (1987) 12–21.
[13] E. Biglieri, D. Divsalar, P.J. McLane, M.K. Simon, Introduction to Trellis-Coded Modulation with Applications, Macmillan Publishing, New York, 1991.
[14] G. Ungerboeck, The state of the art in trellis coded modulation, in: E. Biglieri, M. Luise (Eds.), Coded Modulation and Bandwidth-Efficient Transmission, Elsevier, Amsterdam, Netherlands, 1992, pp. 3–14.
[15] L.-F. Wei, Rotationally invariant convolutional channel coding with expanded signal space—Part II: Nonlinear codes, IEEE J. Sel. Areas Commun. 2 (1984) 672–686.
[16] U. Mengali, A. Sandri, A. Spalvieri, Phase ambiguity resolution in trellis-coded modulations, IEEE Trans. Commun. 38 (1990) 2087–2088.
[17] J.G. Proakis, Digital Communications, third ed., McGraw-Hill, New York, 1995.
[18] G. Ungerboeck, Trellis-coded modulation with redundant signal sets. Part I: Introduction, IEEE Commun. Mag. 25 (1987) 5–11.
[19] R. Buz, Uniformity of nonlinear trellis codes, in: E. Biglieri, M. Luise (Eds.), Coded Modulation and Bandwidth-Efficient Transmission, Elsevier, Amsterdam, The Netherlands, 1992, pp. 67–78.
[20] F. Maddens, Sixteen-state feedback convolutional encoder, IBM Tech. Discl. Bull. 28 (10) (1986) 4212–4213.
[21] E.S. Esteves, R. Sampaio-Neto, A per-survivor phase acquisition and tracking algorithm for detection of TCM signals with phase jitter and frequency error, IEEE Trans. Commun. 45 (1997) 1381–1384.
[22] A.J. Viterbi, J.K. Omura, Principles of Digital Communications and Coding, McGraw-Hill, New York, 1979.
[23] U. Mengali, A.N. D'Andrea, Synchronisation Techniques for Digital Receivers, Plenum Press, New York, 1997.
[24] A. Leclert, P. VanDamme, Universal carrier recovery loop for QASK and PSK signal sets, IEEE Trans. Commun. 31 (1983) 130–136.
[25] S. Moridi, H. Sari, Analysis of four decision–feedback carrier recovery loops in the presence of intersymbol interference, IEEE Trans. Commun. 33 (1985) 543–550.
[26] F.M. Gardner, Demodulator reference recovery techniques suited for digital implementation, Gardner Research Co., Palo Alto, CA, Final Rep. ESTEC Contract No. 6847/86/NL/DG, August 1988.
[27] L. Piazzo, P. Mandarini, Analysis of phase noise effects in OFDM modems, IEEE Trans. Commun. 50 (2002) 1696–1705.
[28] R. Nordman, A. Mämmelä, A semi-analytical approach for assessing the performance of a concatenated code, in: Proc. Communications Theory Mini-Conference, GLOBECOM, 1998, pp. 179–184.

Markku Kiviranta received the degrees of M.Sc. (Tech.) and Lic.Sc. (Tech.) from the Department of Electrical Engineering, University of Oulu, Oulu, Finland in 1994 and 2000, respectively. In 1993, he joined VTT and, until 1996, he was doing research and real time processing development work in the telecommunication field. In 1997–2002, he executed and managed customer R&D projects concentrating on algorithm development of digital signal processing (DSP) applications. During 2003–2011, he was leading the Digital Transceiver team. In 2005 he spent a year with the Berkeley Wireless Research Centre in the USA. Since 2011, he has been a principal scientist of radio access systems.

Aarne Mämmelä received his D.Sc. (Tech.) degree (with honors) in the field of telecommunications from the University of Oulu, Oulu, Finland in 1996. He was at the University of Oulu from 1982 to 1993. He visited the University of Kaiserslautern in Germany in 1990–1991 and the University of Canterbury in New Zealand in 1996–1997. In 1993 he joined VTT Technical Research Centre of Finland in Oulu. Since 1996 he has been a Research Professor of digital signal processing in wireless communications. His research interests are in adaptive and cognitive systems in telecommunications.

TRANSACTIONS ON EMERGING TELECOMMUNICATIONS TECHNOLOGIES
Trans. Emerging Tel. Tech. (2016)
Published online in Wiley Online Library (wileyonlinelibrary.com). DOI: 10.1002/ett.3068

SPECIAL ISSUE ARTICLE

Power efficiency, phase noise, and DC offset in constant envelope OFDM transceivers

Markku Kiviranta*, Aarne Mämmelä and Olli Apilo

VTT Technical Research Centre Of Finland Ltd, P.O. Box 1100, FI-90571 Oulu, Finland

ABSTRACT

This paper considers constant envelope orthogonal frequency-division multiplexing (CE-OFDM) that is an attractive candidate for the future Long Term Evolution over satellite and device-to-device communications in merging public safety and commercial networks. The constant envelope modulation allows power amplifier (PA) to operate near saturation levels thus maximizing power efficiency. Because the phase noise transforms just into an additive noise term after the phase detector, the CE-OFDM has significant advantage compared with phase noise sensitive OFDM. The transceiver power efficiency is evaluated by measuring the bit error rate as a function of average PA input signal-to-noise ratio so that the effects of the PA nonlinearities are taken into account in the performance evaluation. Our simulation results show that with a typical nonlinear satellite amplifier, the CE-OFDM has up to 6.0 dB gain compared with the OFDM. This is beneficial especially in a channel having high attenuation. The consistent gains for the ideally linearized amplifier and common terrestrial three-way Doherty amplifiers are 2.2 and 2.5 dB, respectively. The enhanced PA efficiency enables battery to be smaller or last longer in mobiles devices. For CE-OFDM implementation, a simple transmitter and receiver structure with novel direct current offset removal is presented by keeping in mind that the key factor for the rapid uptake of the future fifth generation systems is the maximization of technology commonalities with existing systems. Copyright © 2016 John Wiley & Sons, Ltd.

***Correspondence**
M. Kiviranta, VTT Technical Research Centre Of Finland Ltd, P.O. Box 1100, FI-90571 Oulu, Finland.
E-mail: markku.kiviranta@vtt.fi

Received 3 November 2015; Revised 4 March 2016; Accepted 9 June 2016

1. INTRODUCTION

The spectrally efficient multicarrier orthogonal frequency-division multiplexing (OFDM) is the modulation method in most of the new wireless standards such as the terrestrial Long Term Evolution (LTE) downlink. The convergence of commercial and public safety communications is ongoing. Device-to-device (D2D)-enabled LTE devices may act as a fallback for rescuer. LTE over satellites will have an emerging role whenever there is a need for a long-lasting local area network and no other communication channels are available. The OFDM is very resistant to frequency selective fading, but, as a stand-alone high peak-to-average power ratio (PAPR) modulation, it may be overkill for the relatively benign line of sight satellite channels and long battery life D2D communications. The vulnerability of OFDM to nonlinear distortions increases the power consumption in terminals and satellites. In any case, the key factor for the rapid uptake of the LTE D2D and LTE over satellite systems is the maximization of the technology commonalities. Although commercially launched LTE over satellite networks exist (e.g. from LEMKO Corp.), they are not yet mature and practical. The low (LEO) and geostationary (GEO) earth orbit satellites have problems of stability and attenuation, respectively. Single carrier frequency division multiple access (SC-FDMA) is a low PAPR variant of OFDM that is used in the LTE uplink and it is adopted for the digital video broadcasting (DVB) - next generation handheld (NGH) satellite standard, too. The constant envelope (CE) OFDM is another candidate where the frequency modulation (FM) or phase modulation (PM) creates a fully CE, and compared with the SC-FDMA, it maximizes PA efficiency. The OFDM-FM was originally [1] proposed for mobile radios to retrofit inexpensively and simply existing FM systems, and nowadays, it has potential for the LTE D2D and LTE over satellite. The D2D was first limited to critical applications, but it will have an emerging role in the fifth generation (5G) millimetre wave communication [2]. The CE-OFDM was studied for the digital TV over satellite in Japan [3], and in general, the LTE broadcasting will enable authority information to citizens in the future.

In general, the FM can be viewed also as PM, and the spectrum of wideband FM and PM is known to be Gaus-

sian shaped [4]. Digital narrowband FM signals without memory have a spectral peak at the carrier [5, 6]. The spectral peak vanishes when memory is added via continuous phase modulation at the cost of complex maximum likelihood Viterbi receiver, but for simplicity, we are focusing on the memoryless coherent receiver. The spectral peaks may create co-channel interference with other signals [7], and the spectral flatness is one quality parameter in the LTE. In OFDM, frequency domain equalization is used, and the estimation is accomplished by transmitting known pilots with both flat spectrum and CE [8]. The CE-OFDM has a CE, but there is strong peak at the carrier. High-pass filtering of the peak distorts the CE nature of the transmitted signal and introduces intersymbol interference [7]. Because the direct current (DC) offset is a mean value, it can be subtracted [9] from the transmitted signal, but the subtraction distorts again the CE property. According to our knowledge, this is the first paper in the literature to present a dedicated DC offset removal technique for the CE-OFDM signals at all, and especially at the transmitter. The proposed novel method is verified via spectrum and performance simulations.

While the subcarrier data modulation in the terrestrial OFDM systems is usually quadrature amplitude modulation, the satellite standard supports also binary data modulation. For example, binary phase shift keying (BPSK) is a modulation used typically when the signal-to-noise ratio (SNR) is low and when the robustness is more important than the high data rate. The recent DVB forward link second generation extension (S2X) proposes BPSK for the very low signal-to-noise ratio GEO scenarios. Because the BPSK does not belong to the terrestrial LTE family, our aim is to consider and propose a simple way to add it, and retrofit existing FM satellite systems for the LTE over satellite. Recently, the BPSK is seen as also a modulation candidate for the 5G air interfaces [10], and thus, the binary modulated CE-OFDM can be investigated for the public safety and commercial D2D communication.

As a major novelty, we are discussing the CE-OFDM power consumption in the transmitter and the effects of the phase noise in the receiver. The transceiver power efficiency is evaluated by measuring the bit error rate (BER) as a function of average PA input SNR so that the effects of the PA nonlinearities are taken into account in the performance evaluation. Typical nonlinear models for both satellite and terrestrial PAs are used. We demonstrate with analysis, block diagrams, and simulations that CE-OFDM allows for a significant advantage compared with the OFDM, which is well known to be very phase noise sensitive and requires a highly linear PA.

The paper is organized as follows. First, simple transmitter and receiver structures for the CE-OFDM system are proposed, after which performance is verified in an additive white Gaussian noise (AWGN) channel with the LTE parameters. Then spectral peak caused by the DC offset is discussed, and a novel removal method is illustrated with simulation results. Power consumption in CE-OFDM and OFDM is analysed and simulated using typical models for both satellite and terrestrial amplifiers. Before conclusions, the advantage of CE-OFDM structure compared with the OFDM structure is shown in the presence of phase noise.

2. SYSTEM MODEL AND PARAMETERS

The system model for the LTE OFDM over satellite is shown in Figure 1. During an OFDM symbol period $0 \leqslant t \leqslant T$, discrete time multicarrier signal can be given using the N-point inverse fast Fourier transform (IFFT) as

$$x_n = \frac{1}{N}\sum_{k=0}^{N-1} X_k e^{j2\pi kn/N}, n = 0, 1, \ldots, N-1 \qquad (1)$$

where n and k are discrete time and subcarrier indices, respectively, N is the number of subcarriers and X_k are either uncorrelated frequency-domain M-ary data carriers of which number is N_d or virtual zero carriers ($X_k = 0$). Because real OFDM signalling is required at the input of the phase modulator, the frequency-domain OFDM symbols have to satisfy the Hermitian symmetry property by assuming that N is an even number and by making the transformation

$$\begin{aligned} \dot{X}_0 &= Re\,(X_0) \\ \dot{X}_k &= X_k, k = 1, 2, \ldots, N/2-1 \\ \dot{X}_N/2 &= Im\,(X_0) \\ \dot{X}_{N-k} &= X_k^*, k = 1, 2, \ldots, N/2-1 \end{aligned} \qquad (2)$$

The symmetry means that the spectral efficiency is halved, but if the binary data modulation is assumed [11], the Hermitian symmetry can be used at the receiver through maximum-ratio combiner (MRC). The discrete cosine transforms [12] and the fast Hartley transforms (FHT) [13] are also used to furnish a real OFDM signal. FHT can be simply implemented and expressed as

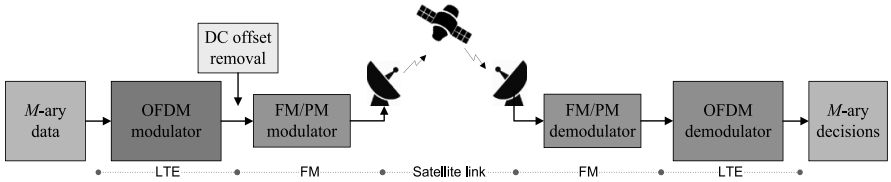

Figure 1. Long Term Evolution over satellite via constant envelope orthogonal frequency-division multiplexing.

DOI: 10.1002/ett

$$X_k^{FHT} = \text{Real}\{X_k\} - \text{Imag}\{X_k\} \quad (3)$$

and the FHT has the property of being its own inverse. The discrete cosine transforms and the FHT have no symmetry requirement, but only real constellations such as BPSK and ASK can be used as in this work.

In PM, the angle is varied linearly with x_n as

$$\phi_n = \pi \boldsymbol{h} \boldsymbol{x_n} \quad (4)$$

where h is the modulation index, and thus, the resulting continuous time domain t carrier wave at frequency ω_c can be given as

$$r_{PM}(t) = cos\left[\omega_c t + \pi h x(t)\right] \quad (5)$$

Correspondingly, the FM wave can be expressed as

$$r_{FM}(t) = cos\left[\omega_c t + h\int_{-\infty}^{t} x(\alpha)d\alpha\right] \quad (6)$$

and it is apparent that PM and FM are inseparable as demonstrated in Figure 2, and PM modulator can be implemented also via FM. In the receiver, the PM wave can be detected by an FM discriminator followed by an integrator.

By adjusting the modulation index value, there is a trade-off between detection performance and spectral spreading. The need and content of the DC offset removal block (Figure 1) is presented in detail in the next section of this paper. In a fading channel, a frequency domain equalizer is needed prior to phase or frequency demodulation [8], and the demodulator makes decisions $\tilde{\phi}_n$ at the data rate, and those time domain samples are the input for N-point OFDM demodulator. For the constant phase error, the frequency transform generates just a DC value to be ignored. Finally, the system parameters, similar to the values of the LTE uplink, are shown in Table I.

2.1. Complexity consideration

Single carrier frequency division multiple access is known to have similar performance compared with OFDM [14]. Because of its inherent single carrier structure, it has lower PAPR, and it is adopted in the uplink of the LTE. The main complexity impact in SC-FDMA is the need of additional FFT and IFFT at the transmitter and the receiver, respectively. In OFDM, each data symbol occupies a single subcarrier, while in SC-FDMA, the energy of each data symbol is spread over several subcarriers. In CE-OFDM, there is no additional FFT in the transmitter, but an additional FFT and IFFT are needed for the frequency domain equalization in the receiver. FHT-based implementation requires an extra OFDM symbol addition operation (3) in the transmitter. Compared with the SC-FDMA, the complexity is thus moved from the transmitter to the receiver. However, depending on the channel condition such as the line of sight in the satellite communications, the equalization might not be required at all, therefore reducing the receiver complexity.

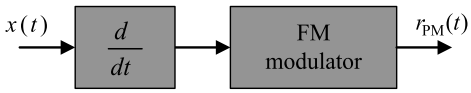

Figure 2. Phase modulation modulator via frequency modulation.

Table I. LTE system parameters for 10-MHz channel bandwidth.

Carrier spacing, Δf (kHz)	15	Sampling rate (MHz)	15.36
Number of data carriers, N_d	600	Length of FFT and IFFT, N	1024

LTE, Long Term Evolution; FFT, fast Fourier transform; IFFT, inverse fast Fourier transform.

2.2. Performance consideration

Theoretically, the single carrier data modulation and the corresponding multicarrier OFDM signal have an equivalent performance in an AWGN channel. Binary BPSK and 2-ASK are identical, and they have about 4-dB gain over 4-ASK [15]. For CE-OFDM, the error probability is, however, more difficult to derive because of the presence of nonlinear phase operation [6], and Figure 3 shows the simulated BER as a function of SNR per bit for OFDM-PM. The modulation index values are experimentally optimized by searching the minimum BER at level 10^{-4}. As the figure shows, there is < 0.5 dB performance degradation compared with the OFDM in the case of the binary subcarrier modulation, and the performance is reduced much more for the 4-ASK. The number of CE-OFDM constellation points depends on the parameters M and N_d of data modulation as 2^{MN_d}, and thus, the increased constellation deteriorates the performance. At higher and lower modulation indices, the phase wrapping at $\pm\pi$ [16] and not evenly spaced constellation [11] degrade the performance. From now on, we will focus on the binary data-modulated

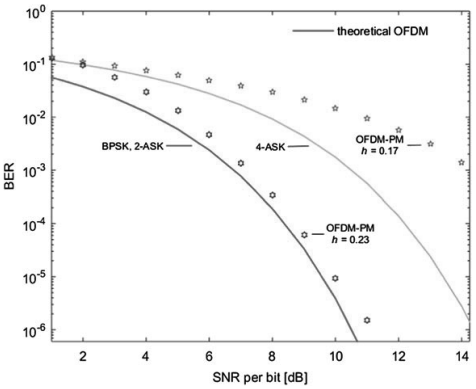

Figure 3. Bit error rate for OFDM-PM with optimized modulation index values.

OFDM-PM. FFT and FHT implementations have no difference in the BER performance.

3. SPECTRUM AND ELIMINATION OF DC OFFSET

Figure 4 shows the phase modulator output signal (Figure 1) mapped onto a unit circle and histogram for the real axis when the earlier (Figure 3) optimized modulation index value h is 0.23 is used. As the left-hand side subfigure shows, the constellation is not symmetric with respect to the origin. Furthermore, the points in the constellation are not all equally probable because the large values correspond OFDM signal peak values with low probability and vice versa. Because the mean value of the signal is not 0, the DC offset is appearing as a peak in the spectrum as demonstrated at the left-hand side of Figure 5. In general, the DC offset Δ_{DC} is the mean of phase modulator output signal, that is,

$$\Delta_{DC} = E[s_n] \tag{7}$$

As discussed in the introduction, the high-pass filtering and subtraction of the mean of the signal distort the CE nature of the transmission. We next present a novel DC offset removal technique for CE-OFDM signals. The method is based on the assumption that when the constellation is symmetrical, it generates signal with 0 mean, and the DC offset is disappearing. The requirement is fulfilled when every second CE-OFDM symbol is rotated 180° as

$$s'_{n,i} = s^{e}_{n,i}{}^{j\pi \bullet \mathrm{mod}(i,2)}, n = 1, 2, \ldots N, i = 1, 2, \ldots \tag{8}$$

where mod(i, 2) is the modulo operation and i is the index of the transmitted symbol. In order to better retrofit the existing FM and PM systems, we can place the DC offset removal block prior to phase modulator, and

$$\phi'_{n,i} = \phi_{n,i} + \pi \bullet \mathrm{mod}\,(i, 2)\,, n = 1, 2, \ldots N, i = 1, 2, \ldots \tag{9}$$

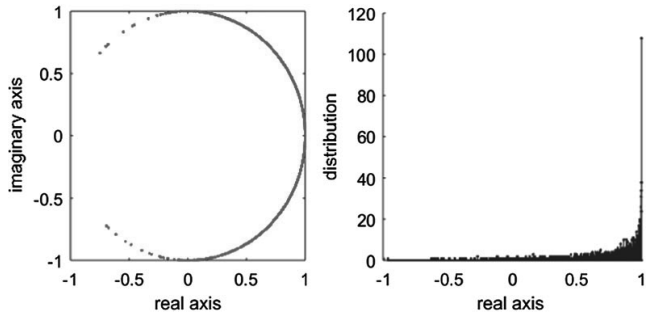

Figure 4. Constellation (left) and histogram (right) at the output of phase modulator.

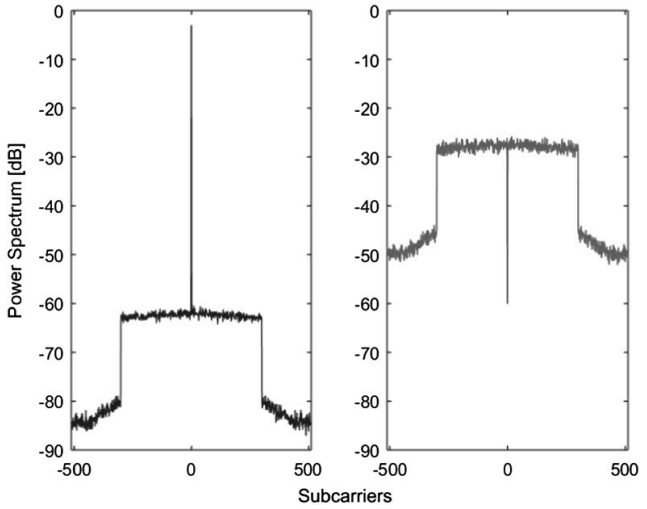

Figure 5. CE-OFDM spectrum with the peak and with the DC offset removal.

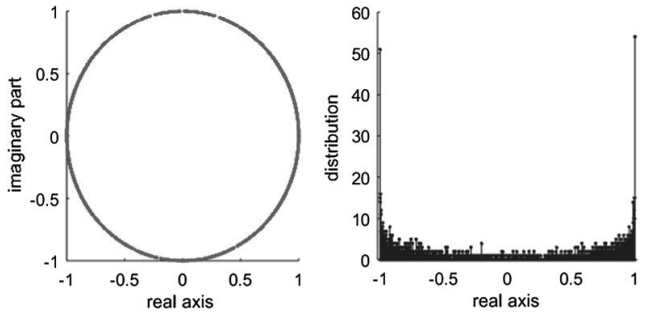

Figure 6. Constellation (left) and histogram (right) after rotation.

An inverse constellation rotation is accomplished at the receiver before the phase demodulation. Equation (8) can be also interpreted as the use of a short DC balanced code sequence $[+1 - 1]$ containing an equal number of minus and plus ones. In contrast, long pseudonoise sequences would cause increased averaging time for the transmitted symbols to achieve the 0 mean.

The signal after constellation rotation is presented in the left hand subfigure of Figure 6, and constellation mirroring in the unit circle preserves the CE property, too. As the right hand subfigure histogram shows, the signal points are not uniformly distributed, but because of symmetry property, the mean value is 0. Finally, the spectrum for CE-OFDM with the DC offset removal is presented in the right-hand side of Figure 5, and as the subfigure shows, the peak energy is distributed smoothly over the subcarriers.

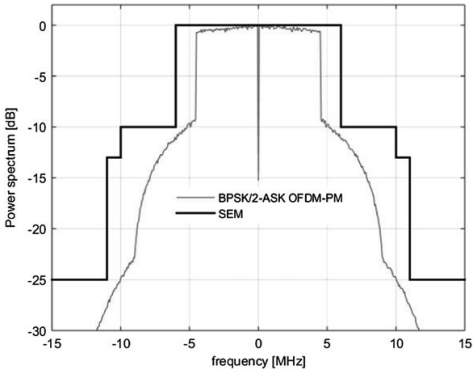

Figure 7. OFDM-PM spectrum and uplink spectrum emission mask.

Figure 7 shows the LTE spectrum emission mask (SEM) example defining the out of band emission limit. As the figure shows, the BER optimized modulation index value $h = 0.23$ for the binary modulated CE-OFDM (Figure 3) meets also the spectrum mask. A smaller index value means lower side lobes and vice versa. Because the PM is a nonlinear operation, it generates also in-band distortions.

3.1. Impact of DC offset on channel estimation

Without equalization, the DC offset has no effect on the BER performance in an AWGN channel because every second CE-OFDM symbol is just rotated 180° in (8) in the transmitter and an inverse operation is performed in the receiver. When an equalizer is needed, it has to be placed in front of the nonlinear phase detector in Figure 1. If binary modulated CE-OFDM and symmetry property in (2) are assumed, the MRC can be applied [11] as shown in Figure 8.

In the figure, H_k, $k = 1, 2, \ldots, N/2 - 1$, denotes the N-point FFT of the discrete channel impulse response, and V_k

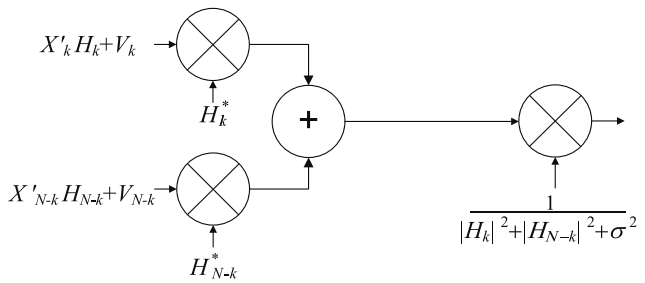

Figure 8. Frequency domain equalizer with maximum-ratio combiner for subcarrier k.

is the frequency domain AWGN sample with variance σ^2. The minimum mean square error equalizer minimizes the combined effect of intersymbol interference and the additive noise. If the noise variance term σ^2 is ignored, zero forcing equalizer is achieved. The zero forcing equalizer-type equalizer is simply the inverse of channel response that leads to infinite noise enhancement at frequencies corresponding spectral nulls.

When the channel coefficients are not known in advance and are changing over time in a time-varying channel, the channel estimation prior to equalization is needed for coherent detection. The estimation can be accomplished by transmitting known pilot symbols whose structure influences the quality of the channel estimate. It is desirable to have pilots with a flat spectrum over the frequency band and a CE in the time domain [8]. By assuming that the signals are wide-sense stationary, a tool to evaluate channel estimation is mean-square error (MSE)

$$\mathrm{MSE} = E\left\{|H_{k,i} - \hat{H}_{k,i}|^2\right\} \tag{10}$$

where $\hat{H}_{k,i} k = 0, 1, \ldots, N-1$ is the channel estimate at the kth subcarrier of the ith symbol. The simple least squares estimate is commonly used as an initial estimate, and it is obtained by dividing the received symbols by the known reference symbols D_k, that is,

$$\hat{H}_k = H_k + D_k^{-1} V_k \tag{11}$$

Figure 9 shows the measured MSE results for OFDM-PM channel estimation with or without the proposed DC offset removal (8). In the simulations, the parameters in Table I are used, and the observation interval for channel estimation is 120 symbols, and the interval is divided into eight segments with 50% overlap, and each section is windowed with a Hamming window. As the figure shows, the DC offset removal yields superior results, and the gain is around 2.1 dB. Without removing the DC offset, the effect of additive noise V_k in (11) is minimum at the channel estimate corresponding the strong power carrier and more severe for those subcarriers around the dominating one. When the DC offset is removed, the signal peak power is smoothly spreading out over the entire frequency range of subcarriers. The increased accuracy of channel estimates inherently leads to a better detection performance and error rate. When there is equal disturbance of additive noise samples over subcarriers, we can also assume that applying bit and power loading with water filling becomes more favourable.

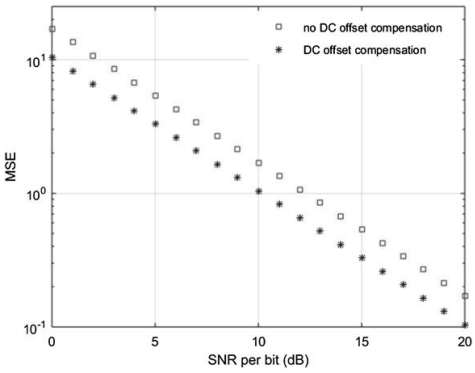

Figure 9. Mean-square error (MSE) with or without DC offset compensation.

4. NONLINEAR POWER AMPLIFIER AND POWER CONSUMPTION

The PA is one of the most power-consuming analogue component in the transmitter, and as discussed in [17], power consumption can be approximated when the knowledge of PAs efficiency, distribution of input signal envelope and the amount of input back-off (IBO) are known. From the central limit theorem, it follows that for large values N, the OFDM signal becomes Gaussian distributed, and the amplitude of the signal has therefore Rayleigh distribution with average power

$$E\left[|x_n|^2\right] = \frac{1}{N^2} \sum_{k=0}^{N-1} |X_k|^2 \tag{12}$$

and the PAPR

$$P_{\mathrm{PAPR}} = 10\log_{10}\left(\frac{\max(|x_n|^2)}{E\left[|x_n|^2\right]}\right) \tag{13}$$

If a binary data modulation is assumed and by choosing $X_k = \pm\sqrt{N}$, the variance (12) and the PAPR (13) are equal to 1 and $10\log_{10}(N)$ dB, respectively. In practice, the IBO is less than the PAPR because the OFDM peak values have low probability. On the other hand, the CE systems do not require any IBO, and thus, they have the capability to transmit roughly IBO decibels more energy into the channel for a given PA. This is beneficial especially in the very low signal-to-noise ratio channel and if the increase in transmit power is allowed by the standard. The CE-OFDM can also reduce the power consumption of the PA. The average PA efficiency determines the PAs ability to convert DC power P_{DC} from supply into alternating current output power P_{RF} as

$$\eta = \frac{E\left[P_{\mathrm{RF}}\right]}{E\left[P_{\mathrm{DC}}\right]} \tag{14}$$

The power $(1-\eta)P_{\mathrm{DC}}$ not converted to the radio frequency (RF) signal is wasted as heat. In general, common PAs can be classified into A, B, AB and C classes, and the class B amplifiers have higher maximum efficiency of 78.5% than the class A amplifiers of 25–50% efficiency and better linearity than the class C amplifiers that have 99% efficiency. In practice, there is an interconnection between the PA input signal envelope and PA efficiency, and in [17], the average efficiencies for linearized and nonlinear travelling-wave tube (TWT) amplifiers have been drawn in the presence of OFDM signal. In general, the

TWT amplifiers are commonly used in satellite communications, and for them, the class B average efficiency can be expressed as

$$\eta_{\mathrm{TWT}} = \frac{\sqrt{\pi\xi}\left\{(1+4\xi)\,e^{4\xi}\mathcal{M}\,(4\xi)-1\right\}}{1-2\sqrt{\pi\xi}e^{4\xi}\mathrm{erfc}\left(2\sqrt{\xi}\right)} \tag{15}$$

where ξ is the required IBO and

$$\mathcal{M} = \int_1^{\infty} e^{-4\xi t/t} dt \tag{16}$$

The corresponding average efficiency for the ideally linearized PA model is

$$\eta_{\mathrm{lin}} = \frac{\sqrt{\pi}}{2}\frac{1-e^{-\xi}}{\sqrt{\xi}\mathrm{erf}\left(\sqrt{\xi}\right)} \tag{17}$$

Finally, Table II shows the IBO requirements for the binary data-modulated OFDM to obtain the same BER below 10^{-4} as the corresponding OFDM-PM with modulation index value h is 0.23 in Figure 3. In general, nonlinear operation generates both in-band and out-of-band distortions, and in this work, we have confirmed that both the OFDM and the OFDM-PM signals for Table II meet the SEM of the LTE uplink shown in Figure 7. The power consumption differences P_Δ are defined as the ratios between the amplifier's maximum $\eta_{\max}$ and the average (15)–(17) power efficiencies

$$P_\Delta = 10\log_{10}\left(\frac{\eta_{\max}}{\eta}\right) \tag{18}$$

For the simulations, amplitude modulation (AM–AM) and AM–PM curves for the nonlinear TWT amplifier are illustrated in Figure 10, and they are based on the well-known Saleh model [18]:

$$F_{\mathrm{AM/AM}}(x) = \frac{\alpha_1 x}{1+\beta_1 x^2} \tag{19}$$

$$F_{\mathrm{AM/PM}}(x) = \frac{\alpha_2 x^2}{1+\beta_2 x^2} \tag{20}$$

where the coefficient values α_1, α_2, β_1 and β_2 are found by fitting these equations to the experimental data through a minimum MSE procedure.

If the aim is a multi-standard architecture with a common class B amplifier, we can summarize from Table II that with the CE-OFDM, we can save in the power consumption. This is beneficial in a mobile device or in the satellite enabling a battery to be smaller or last for a longer time. On the other hand, if the aim is, for example, the LTE over satellite retrofitting existing FM systems, the CE-OFDM would also allow using the very nonlinear but very power-efficient class C amplifiers. The modulation index value has no effect on the CE property of the signal, and if the index value is not the optimized $h = 0.23$, the BER performance just decreases, and the OFDM needs also less IBO to meet that poorer performance (Figure 3). As a consequence, the corresponding power consumption differences in Table II decrease and in that sense the measured values in Table II correspond to the maximum values. As discussed in Section 3, adjusting the modulation index is also affecting the spectrum (Figure 7).

There are also many other common PA architectures that have a potential for significant improvement of efficiency

Table II. Average efficiency and power consumption difference for linearized and nonlinear PAs.

		Linearized PA	Nonlinear TWT
OFDM	ξ [dB]	2.5	11.0
	η %	59	24
CE-OFDM (class B*) versus OFDM (class B)	P_Δ [dB]	1.2	5.0
CE-OFDM (class C**) versus OFDM (class B)	P_Δ [dB]	2.2	6.0

*Class B:$\eta_{\max} = 78.5\%$.
**Class C:$\eta_{\max} = 99\%$.
PA, power amplifier; TWT, travelling-wave tube; OFDM, orthogonal frequency-division multiplexing; CE-OFDM, constant envelope orthogonal frequency-division multiplexing.

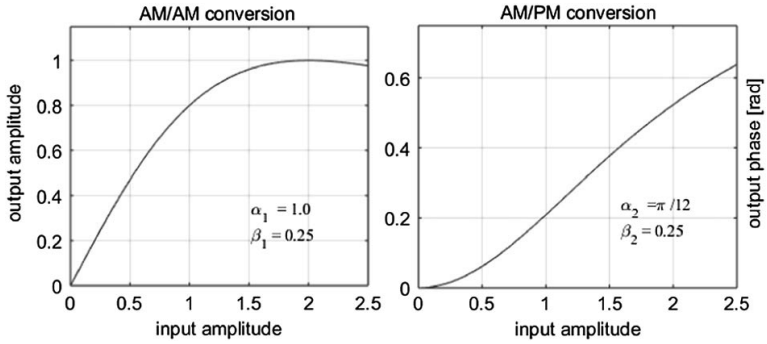

Figure 10. The AM/AM and AM/PM conversions for Saleh's nonlinear amplifier [18].

but in turn at the cost of increasing other analogue and digital circuit complexity. For example, a very popular Doherty PA is examined in [19] for the terrestrial LTE, and with our parameters, the instantaneous DC power is

$$P_{\mathrm{DC}} = \frac{4}{b\pi} \begin{cases} \sqrt{|x_n|^2/\xi}, & 0 \leqslant |x_n|^2 \leqslant \xi |x_n|^2/b^2 \\ (b+1)\sqrt{|x_n|^2/\xi} - 1, & \xi |x_n|^2/b^2 \leqslant |x_n|^2 \leqslant \xi |x_n|^2 \end{cases} \tag{21}$$

where b is a positive integer determining that there is one carrier amplifier and b-1 peaking amplifiers in parallel. This is a simple approach to acquire b times larger-sized peaking amplifier compared with the carrier amplifier. The average PA efficiency can be determined using (14). When the power efficient Doherty technology is applied, a distortion compensation circuit is still necessary to correct its nonlinearity. Assuming a solid state power amplifier implementation, AM to PM conversion is not so large, and Rapp's model can be used for AM to AM characteristic as

$$F_{\mathrm{AM/AM}}(x) = \frac{x}{\left(1 + (x)^{2\rho}\right)^{1/2\rho}} \tag{22}$$

where the smoothness of the transition from the linear region to limiting region is controlled by the positive parameter ρ. The Rapp model is commonly used in the case of the OFDM, and in our simulations, the AM–AM curve of Figure 11 is used. As earlier, Table III shows the measured IBO requirement and PA efficiency for the OFDM-PM as well as the power consumption benefit compared with the OFDM. Recently, Doherty amplifiers have gained attention especially in the millimetre wave communications [20], and therefore, the CE-OFDM is attractive for both commercial and public safety LTE D2D communication.

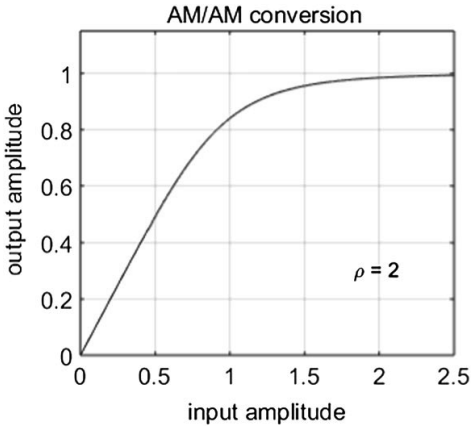

Figure 11. The AM/AM conversion for Rapp's nonlinear amplifier.

So far, the transmitter energy efficiency is evaluated using the average PA efficiency, and as presented in Figure 3, the BER performances of the OFDM and CE-OFDM are compared in an AWGN channel as a function of the average SNR at the receiver. The transmitted and received powers are equal if the channel attenuation is normalized to unit. We next evaluate the transceiver energy efficiency using the BER as a function of average PA input SNR [21] so that the effect of the PA efficiency is taken into account in the performance evaluation. For this task, the BER curves need to be shifted by $10\log_{10}(\eta)$ decibels in order to take into account the loss in the PA efficiency. Then Tables II and III show the measured efficiency values for the OFDM, and for the CE-OFDM, the 99% efficiency of the class C amplifier can be used. Finally, the BER results as a function of the PA input SNR are shown in Figure 12, and the figure confirms that the CE-OFDM outperforms the OFDM by the amount of the last row values

Table III. PA efficiency and power consumption difference for the three-way Doherty PA.

		Doherty PA
OFDM	ξ [dB]	4
	η%	56
CE-OFDM (class C **) versus OFDM (Doherty)	P_Δ [dB]	2.5

**class C:$\eta_{\max} = 99\%$.
PA, power amplifier; OFDM, orthogonal frequency-division multiplexing; CE-OFDM, constant envelope orthogonal frequency-division multiplexing.

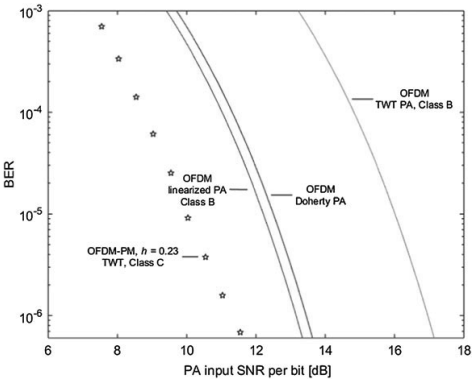

Figure 12. Transceiver efficiencies as bit error rate (BER) for orthogonal frequency-division multiplexing (OFDM) and constant envelope (CE)-OFDM.

in Tables II and III. The performance gain decreases when the PA linearity increases and vice versa. However, the linearization is achieved at the cost of increasing other circuit complexity, and roughly speaking, the power consumption is moved from one place to another. In any case, the presented performance gains for the CE-OFDM could not have been seen with traditional SNR metrics because they do not take into account the efficiency of the PA. The average transmitted power is equivalent to the average PA input power only when the PA has ideal 100% efficiency over its whole output power range.

5. EFFECTS OF PHASE NOISE

As commonly known in the literature, for example, in [22], oscillator's phase noise has a very large impact on OFDM, and similar conclusions are also drawn for SC-FDMA, for example, in [23]. When we assume that the discrete time domain OFDM signal (1) is only affected by phase noise θ_n, the received signal can be expressed as

$$r_n = x_n e^{j\theta_n} \tag{23}$$

If θ_n is assumed to be sufficiently small for all n [22], we can write

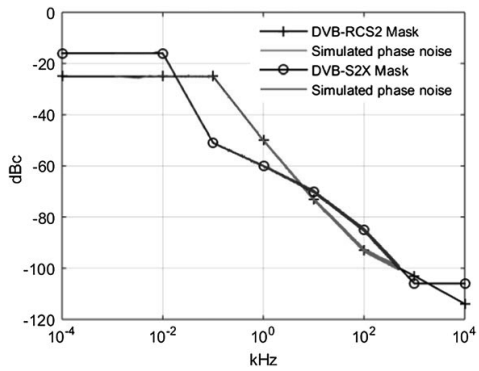

Figure 13. The DVB-RCS2 phase noise mask.

$$e^{j\theta_n} \approx 1 + j\theta_n \tag{24}$$

After the FFT in the receiver, the discrete frequency domain signal can be given as

$$R_k \approx X_k + j\sum_{r=0}^{N-1} X_r \sum_{n=0}^{N-1} \theta_n e^{j(2\pi/N)(r-k)n} \tag{25}$$

When $r=k$, the latter sum term in (25) corresponds to a multiplicative common phase error for each subcarrier. In more detail, the error is an average of phase noise samples, and it can be corrected by some phase rotation. If $r \neq k$, the second term in (25) is the sum of the information in other N-1 subcarriers each multiplied with the average of phase noise with a spectral shift. In general, the additive error is known as loss of orthogonality or intercarrier interference (ICI). When the ratio of 3 dB phase noise bandwidth B_{3dB} and subcarrier spacing Δf is small, the common phase error dominates over ICI and vice versa. In the literature, a common conclusion, for example, in [24], for the OFDM signal phase noise tolerance is that the subcarrier constellations up 64-quadrature amplitude modulation can be supported as long as

$$B_{3dB} \ll \Delta f \tag{26}$$

As a concrete example, Figure 13 shows both theoretical and simulated finite power phase noise masks for the DVB-RCS2 and DVB-S2X standards for which the SC-FDMA is a modulation candidate. In the figure, the mask is expressed in decibels relative to the carrier, and it represents the phase noise power relative to the carrier signal power. In the simulations, experimentally obtained autoregressive moving average model [25] of phase noise is used. Because the 3-dB-phase noise bandwidth is around 15 and 150 Hz for the RCS2 and S2X standards, the effect of ICI is severe with the presented LTE parameters, and a separate compensation method is needed. The ICI is even worse when the minimum bit rate requirements of 8 kbps are targeted in the RCS2.

Figure 14 demonstrates that the impact of phase noise is different in OFDM-PM from the one in OFDM. In both systems, the phase noise is multiplied with the transmitted signal, but as illustrated in the lower subfigure, the

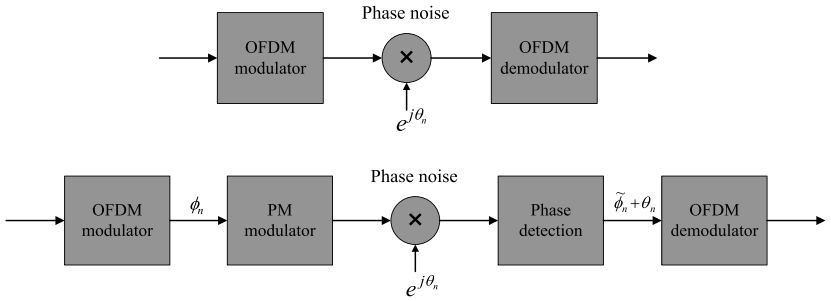

Figure 14. Impact of phase noise in orthogonal frequency-division multiplexing (OFDM) (upper) and OFDM-(PM) phase modulation (lower) systems.

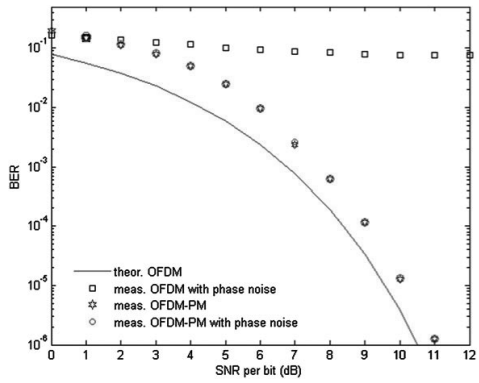

Figure 15. Bit error rate (BER) performance of orthogonal frequency-division multiplexing (OFDM) and OFDM-(PM) phase modulation in the presence of phase noise.

phase noise transforms just into an additive noise term after the phase detector. For example, in Figure 13, the phase noise mask is negative in terms of decibels relative to the carrier, and it represents the number of decibels the phase noise power is below the carrier power. As a consequence, when the phase noise θ_n is sufficiently below the signal (Figure 14), the phase noise has no notable effect to the BER performance. This phenomenon is illustrated in Figure 15 where the OFDM-PM is simulated in an AWGN channel with or without the presented phase noise mask for the DVB-RCS2. When phase noise varies fast compared with the OFDM symbol rate, it makes generally tracking and compensation more difficult. As in the case of AWGN, channel coding could be used to obtain better performance results in the presence of disruptive additive phase noise. When the phase noise mask covers only the small part of the OFDM bandwidth, only the subcarriers at low frequencies are interfered by the phase noise. If these distorted subcarriers are removed, the CE-OFDM signaling would not need a separate phase noise correction. When there is a constant phase error during the OFDM symbol, the FFT generates just a DC value, and by avoiding the zero carriers, there is no degradation in the BER performance at all.

6. CONCLUSIONS

In this paper, we have considered the binary data-modulated CE-OFDM that is an attractive candidate for the future LTE over satellite and D2D communications, especially when the SNR is low and when the robustness is a more important design criteria than the high data rate. A simple transmitter and receiver structure for the CE-OFDM is presented by keeping in mind that the practical key factor for the rapid uptake of the LTE enabled public safety and commercial 5G systems is the maximization of the technology commonalities. We have presented a novel method for removing the DC offset in the CE-OFDM. The DC offset generates a spectral peak at carrier, causing a harmful interference and reduces the performance of channel estimation at the receiver. The proposed simple technique spreads out the peak power over the entire frequency band and preserves the CE nature of the signal. The simulation results show that the proposed technique can provide several decibels of improvement in channel estimation. We have compared the power consumption in the CE-OFDM and OFDM using typical models for both satellite and terrestrial amplifiers. The CE-OFDM allows the use of more power-efficient class C amplifiers, while the class B amplifiers are typical for the OFDM. We have measured the transceiver energy efficiency using the BER as a function of average PA input SNR so that the effect of the PA efficiency is taken into account in the performance evaluation. With the nonlinear TWT amplifier, the CE-OFDM has up to 6.0 dB gain compared with the OFDM (Figure 12). This is beneficial especially in the VL-SNR satellite channel. The corresponding gains for the ideally linearized PA and three-way Doherty amplifiers are 2.2 and 2.5 dB, respectively. The linearization and more power-efficient Doherty implementation are achieved at the cost of increasing other circuit complexity. Finally, we have illustrated with block diagrams that the structure of the CE-OFDM system fundamentally allows for a significant advantage compared with the very phase noise-sensitive OFDM. The phase noise has no notable effect to the BER performance of CE-OFDM because the phase noise transforms just into an additive noise term in the phase detector. The next step of work will be the real implementation of complete transmitter–receiver chain using the CE-OFDM.

ACKNOWLEDGEMENTS

The work was performed in the CONCARI and AWARENESS projects funded by Tekes – the Finnish Funding Agency for Technology and Innovation and VTT Technical Research Centre of Finland Ltd. The first author wishes also to thank the Jenny and Antti Wihuri Foundation as well as Mika Lasanen at VTT Technical Research Centre of Finland Ltd.

REFERENCES

1. Casas EF, Leung C. OFDM for data communication over mobile radio FM channels – Part I: Analysis and experimental results. *IEEE Transactions on Communications* 1991; **39**: 783–793.
2. Qiao J, Shen X, Mark JW, Shen Q, He Y, Lei L. Enabling device-to-device communications in millimeter-wave 5G cellular networks. *IEEE Communications Magazine* 2015; **53**: 209–215.
3. Anwar K, Hara T, Okada M, Yamamoto H. Digital terrestrial television transmission over OFDM/FM using satellite communications system. *Electronics and Communications in Japan,* Part 2 2007; **90**: 74–84.

4. Schwartz M, Bennett WR, Stein S. *Communication Systems and Techniques*. McGraw-Hill: New York, 1966.
5. Anderson RR, Salz J. Spectra of digital FM. *Bell System Technical Journal* 1965; **44**: 1165–1189.
6. Thompson SC, Ahmed AU, Proakis JG, Zeidler JR. Constant envelope OFDM phase modulation: spectral containment, signal space properties and performance. In *Proceedings MILCOM*, Monterey, California, USA, 2004.
7. Spilker JJ. *Digital Communications by Satellite*. NJ: Prentice-Hall: Englewood Cliffs, 1977.
8. Ahmed AU, Thompson SC, Zeidler JR. Channel estimation and equalization for CE-OFDM in multipath fading channel. In *Proceedings MILCOM*, San Diego, California, USA, 2008.
9. Razavi B, Bateman A, Haines DM, Wilkinson RJ. Linear transceiver architectures. In *Proc. VTC*, Philadelphia, Pennsylvania, USA, 1988.
10. Cudak M. *5G What to expect and where to start*, 2015. Available: http://www.rle.mit.edu/ncrc/wp.../Phil_5G-Day-at-MIT-5-8-2015_Nokia.pdf. [Accessed: 16- Sep- 2015].
11. Kiviranta M, Mämmelä A, Cabric D, Sobel D, Brodersen RW. Constant envelope multicarrier modulation: performance evaluation in AWGN and fading channel. In *Proceedings MILCOM*, Atlantic City, New Jersey, USA, 2005.
12. Thompson SC, Ahsen AU, Proakis JG, Zeidler JR, Geile MJ. Constant envelope OFDM. *IEEE Transactions on Communications* 2008; **56**: 1300–1312.
13. Fabrega JM, Moreolo MS, Chochol M, Junyent G. Impact of modulator driving on constant envelope optical OFDM based on Hartley transform. *IEEE Photonics Technology Letters* 2013; **25**: 598–601.
14. Myung HG, Goodman D. *Single Carrier FDMA: A New Air Interface for Long Term Evolution*. John Wiley & Sons: New York, 2008.
15. Xiong F. M-ary amplitude shift keying OFDM system. *IEEE Transactions on Communications* 2003; **51**: 1638–1642.
16. Ahmed U, Thompson SC, Zeidler JR. Threshold extending receiver structures for CE-OFDM. In *Proceedings MILCOM*, Orlando, Florida, USA, 2007.
17. Ochiai H. An analysis of band-limited communication systems from amplifier efficiency and distortion perspective. *IEEE Transactions on Communications* 2013; **61**: 1460–1472.
18. Saleh AAM. Frequency-independent and frequency-dependent nonlinear models of TWT amplifiers. *IEEE Transactions on Communications* 1981; **29**: 1715–1720.
19. Apilo O, Lasanen M, Mämmela A. Energy-efficient dynamic point selection and scheduling method for intra-cell CoMP in LTE-A. *Wireless Personal Communications* 2016; **86**(2): 705–726.
20. Camarchia V, Pirola M, Quaglia R, Jee S, Cho Y, Kim B. The Doherty power amplifier: review of recent solutions and trends. *IEEE Transactions on Microwave Theory and Techniques* 2015; **63**: 559–571.
21. Apilo O, Lasanen M, Boumard S, Mämmelä A. Energy efficiency of power-adaptive spatial diversity methods. *IEEE Transactions on Wireless Communications* 2013; **12**: 4246–4257.
22. Armada AG. Understanding the effects of phase noise in orthogonal frequency division multiplexing (OFDM). *IEEE Transactions on Broadcasting* 2001; **47**: 153–159.
23. Syrjälä V. Modelling and practical iterative mitigation of phase noise in SC-FDMA. In *Proceedings PIMRC*, Sydney, Australia, 2012.
24. Pollet T, Van Bladel M, Moeneclaey M. BER sensitivity of OFDM systems to carrier frequency offset and Wiener phase noise. *IEEE Transactions on Communications* 1995; **50**: 191–193.
25. Piazzo L, Mandarini P. Analysis of phase noise effects in OFDM modems. *IEEE Transactions on Communications* 2002; **50**: 1696–1705.

Aalto-DD 56/2017
VTT SCIENCE 149

ISBN 978-952-60-7356-9 (printed)
ISBN 978-952-60-7355-2 (pdf)
ISSN-L 1799-4934
ISSN 1799-4934 (printed)
ISSN 1799-4942 (pdf)

978-951-38-8526-7 (printed)
978-951-38-8525-0 (pdf)
2242-119X
2242-119X (printed)
2242-1203 (pdf)

Aalto University
School of Electrical Engineering
Department of Signal Processing and Acoustics
www.aalto.fi

BUSINESS + ECONOMY

ART + DESIGN + ARCHITECTURE

SCIENCE + TECHNOLOGY

CROSSOVER

DOCTORAL DISSERTATIONS